GEOMETRIC CONTROL AND MOTION PLANNING FOR THREE-DIMENSIONAL BIPEDAL LOCOMOTION

BY

ROBERT DE MOSS GREGG IV

DISSERTATION

Submitted in partial fulfillment of the requirements
for the degree of Doctor of Philosophy in Electrical and Computer Engineering
in the Graduate College of the
University of Illinois at Urbana-Champaign, 2010

Urbana, Illinois

Doctoral Committee:

Professor Mark W. Spong, Chair
Assistant Professor Timothy W. Bretl
Professor Seth A. Hutchinson
Associate Professor Daniel M. Liberzon
Assistant Professor Prashant G. Mehta

ABSTRACT

This thesis presents a hierarchical geometric control approach for *fast* and *energetically efficient* bipedal dynamic walking in three-dimensional (3-D) space to enable motion planning applications that have previously been limited to inefficient quasi-static walkers. In order to produce exponentially stable hybrid limit cycles, we exploit system energetics, symmetry, and passivity through the energy-shaping method of *controlled geometric reduction*. This decouples a subsystem corresponding to a lower-dimensional robot through a passivity-based feedback transformation of the system Lagrangian into a special form of controlled Lagrangian with broken symmetry, which corresponds to an equivalent closed-loop Hamiltonian system with upper-triangular form. The first control term reduces to mechanically-realizable passive feedback that establishes a *functional* momentum conservation law that controls the "divided" cyclic variables to set-points or periodic orbits. We then prove extensive symmetries in the class of open kinematic chains to present the multistage application of controlled reduction. A *reduction-based control law* is derived to construct straight-ahead and turning gaits for a 4-DOF and 5-DOF hipped biped in 3-D space, based on the existence of stable hybrid limit cycles in the sagittal plane-of-motion. Given such a set of *asymptotically stable gait primitives*, a dynamic walker can be controlled as a discrete-time switched system that sequentially composes gait primitives from step to step. We derive "funneling" rules by which a walking path that is a sequence of these gaits may be stably followed by the robot. The primitive set generates a tree exploring the action space for feasible walking paths, where each primitive corresponds to walking along a nominal arc of constant curvature. Therefore, dynamically stable motion planning for dynamic walkers reduces to a discrete search problem, which we demonstrate for 3-D compass-gait bipeds. After reflecting on several connections to human biomechanics, we propose extensions of this energy-shaping control paradigm to robot-assisted locomotor rehabilitation. This work aims to offer a systematic design methodology for assistive control strategies that are amenable to sequential composition for novel progressive training therapies.

To my parents, Robert D. Gregg III and Leslie A. Gregg, for their love and support

ACKNOWLEDGMENTS

I am forever grateful for my experiences at the Coordinated Science Laboratory (CSL) and Department of Electrical and Computer Engineering at the University of Illinois at Urbana-Champaign. I would first like to thank my adviser, Mark W. Spong, for his unwavering support, advice, and encouragement in my research pursuits over the past four years. During both his time at CSL and more recently at the University of Texas at Dallas, he offered me the perfect balance of guidance and autonomy that effectively taught me to be a controls researcher. I am very fortunate to have had the opportunity to work with him.

I would also like to thank the other members of my committee, Timothy W. Bretl, Seth Hutchinson, Daniel Liberzon, and Prashant G. Mehta, who served as a network of support and inspiration at CSL. In particular, Prashant Mehta challenged me to understand the symmetry and symmetry-breaking aspects of controlled geometric reduction. The multiple courses I took with him and Daniel Liberzon contributed greatly to my understanding of control theory. I enjoyed the motivating and sometimes philosophical conversations with Tim Bretl, who pushed me to see connections to motion planning and human rehabilitation during the later years of my studies. He and Seth Hutchinson kindly welcomed me to their research group meetings after my adviser's departure to UT Dallas, which encouraged collaborations and ideas that I might otherwise have missed.

Of course, many other members of the Decision and Control group at CSL deserve recognition. Dusan Stipanovic welcomed me to CSL with friendly conversations and reflections on our experiences in California's Bay Area. Sean Meyn and Todd Coleman offered endless encouragement in my pursuit of various research topics and ultimately post-doctoral positions. Several Ph.D. candidates provided invaluable mentoring during my early years as a graduate student. For this, I am indebted to Peter Hokayem, Silvia Mastellone, Jonathan Holm, Shankar Rao, and Shreyas Sundaram. I might not have weathered the adjustment to Urbana-Champaign and academia at large were it not for them. The support staff of the Decision and Control group, Ronda Rigdon, Becky

Lonberger, and Jana Lenz, deserve great thanks. Their warm conversations and administrative expertise made my time at CSL all the more memorable. I would also like to thank Robert McCabe and Nikolaos Freris for the late conversations at CSL and for refreshing my less-than-perfect memory on real analysis. Recognition is due to my undergraduate assistant, Adam Tilton, for his outstanding work on the planned walking simulations in this thesis. The project reached this higher level thanks to his programming contributions and the helpful advice of Sal Candido.

My colleagues and friends around CSL and the University made all the difference in my experience at the University of Illinois. To name a few not already mentioned: Nikhil Chopra, Aneel Tanwani, Yoav Sharon, Stephan Trenn, Dayu Huang, Neera Jain, Kira Barton, Alex Shorter, David Hoelzle, Miles Johnson, Jeremy Kemmerer, Ashlee Ford, Erick Rodriguez-Seda, Jae-Sung Moon, Adam Cushman, Melody Bonham, Shreyas Prasad, Jeff Lee, Nitin Navale, Bill Eisenhower, Greg Lucas, Roger Serwy, Sundeep Kartan, Mike King, Scott Jobling, Megan Haselschwerdt, Patrick Lynch, Lance Kingston, and Carey Ash. I also greatly enjoyed the many ice hockey seasons with CSL colleagues Spencer Brady, Jared McNew, and John Sartori.

I would like to recognize Jessy W. Grizzle, Ambarish Goswami, and Romeo Ortega for their many helpful comments on my papers and the inspiration they provided through their own work. I also thank Aaron D. Ames and S. Shankar Sastry for advising and training me as an undergraduate researcher during my time at the University of California, Berkeley. Our work served as the foundation for this thesis project. My fellow student and friend at UC Berkeley, Eric D.B. Wendel, also deserves recognition for coding the early version of our Matlab simulation package.

I am most grateful for the support of my family in California, Rob, Leslie, and Joseph Gregg; my surrogate family in Urbana-Champaign, Joe, Bea, and Nick Pavia; and my loving partner Kristin Drogos. They have stood by me through the good times and the very difficult times. Wayne and Kay Carter mentored me from my childhood, and to this day provide a source of inspiration and pride. I also enjoyed the company of my dog, Oskee, while writing this thesis.

In closing, I kindly thank my many colleagues in the IFAC American Automatic Control Council for the unexpected support and motivation they provided for this line of work. The past four years of research would not have been possible without the financial support of National Science Foundation grants CMS-0510119 and CMMI-0856368.

TABLE OF CONTENTS

LIST OF ABBREVIATIONS

ZMP	Zero moment point.
CoP	Center of pressure.
FRI	Foot rotation indicator.
IDA	Interconnection and damping assignment.
RLC	Resistor/capacitor/inductor.
2-D	Two-dimensional space (planar).
3-D	Three-dimensional space.
DOF	Degree(s) of freedom.
4D	4-DOF biped.
5D	5-DOF biped.
A	Assumption.
E-L	Euler-Lagrange.
AS	Asymptotically stable.
GAS	Globally asymptotically stable.
ES	Exponentially stable.
LES	Locally exponentially stable.
GES	Globally exponentially stable.
CICS	Convergent-input convergent-state.
BoA	Basin of attraction.
LTI	Linear time-invariant.
LTV	Linear time-varying.
PD	Proportional-derivative.

ACH	Almost-cyclic Hamiltonian.
ACL	Almost-cyclic Lagrangian.
k-ACL	k-almost-cyclic Lagrangian.
GRF	Ground reaction force(s).
CW	Clockwise.
CCW	Counter-clockwise.
S	Straight.
LQR	Linear quadratic regulator.
CoM	Center of mass.
EMG	Electromyography.
RoM	Range of motion.
AFO	Ankle-foot orthosis.

LIST OF SYMBOLS

∇	Gradient operator, i.e., vectorized partial derivative operator.
L	Lie derivative operator, i.e., change of a function along the flow of a vector field.
$\mathcal{K}$	Kinetic energy.
$\mathcal{V}$	Potential energy.
$\mathcal{H}$	Hamiltonian function, i.e., total energy.
$\mathcal{L}$	Lagrangian function.
$\mathcal{R}$	Routhian function.
M	Inertia/mass matrix.
C	Coriolis matrix.
Q	Gyroscopic matrix.
N	Potential torque vector.
B	Control input to torque map.
u	Control input.
v	Auxiliary control input.
f	Vector field.
g	Control input vector fields.
$\mathscr{HC}$	Hybrid control system.
$\mathscr{H}$	Hybrid system.
P	Poincaré map.
Δ	Impact map.
G	Guard/switching surface.
$\mathcal{O}$	Periodic orbit.

$\mathcal{J}$	Momentum map.
J_c	Constraint Jacobian.
J	Optimality performance index.
$\mathrm{SO}(n)$	Special orthogonal group of dimension n.
$\mathrm{SE}(n)$	Special Euclidean group of dimension n.
$\mathbb{S}^1$	Unit circle group.
$\mathbb{R}^n$	n-dimensional real numbers group.
$\mathbb{T}^n$	n-dimensional torus group.
$\mathcal{Q}$	Configuration space.
S	Shape space, i.e., reduced configuration space.
$\mathbb{G}$	Symmetry group.
$T\mathcal{Q}$	Tangent bundle of $\mathcal{Q}$, i.e., the phase space.
$T^*\mathcal{Q}$	Cotangent bundle of $\mathcal{Q}$, i.e., the phase space.
TS	Tangent bundle of S, i.e., the reduced phase space.
$\mathcal{Z}$	Invariant surface in $T\mathcal{Q}$.
$\mathcal{D}$	Invariant surface in $T^*\mathbb{S}^1$.
q	Generalized configuration vector.
p	Generalized momentum vector.
x	Phase state vector, i.e., $(q, \dot{q}) \in T\mathcal{Q}$.
λ	Conserved momentum function.
ψ	Biped yaw (heading) angle.
φ	Biped roll (lean) angle.
θ_{s}	Biped stance pitch angle.
θ_{t}	Biped torso pitch angle.
θ_{ns}	Biped nonstance (swing) pitch angle.
s	Step cycle steering angle.
$\mathcal{G}$	Asymptotically stable gait primitive.
$\mathcal{P}$	Set of asymptotically stable gait primitives.
$\mathcal{T}$	Gait transition.
$\mathcal{E}$	Walking path execution.
$\mathcal{S}$	Sequence of steering angles (output of planner).

CHAPTER 1

INTRODUCTION

The step-level control and high-level motion planning of humanoid walking have been active areas of research over the past decades. Robotic technology is proving essential to alleviating the intensive labor required by physical therapists in locomotor rehabilitation, restoring mobility in lower-extremity amputees with powered prosthesis, and providing gait assistance to the disabled or elderly. The incredible efficiency of bipedalism, which allows humans to outwalk quadrupeds over long distances [1, 2], also motivates its use on autonomous locomotive mechanisms. In fact, researchers have demonstrated "passive" walking down shallow slopes for simple planar bipeds without any actuation whatsoever [3, 4].

This energy-efficient form of locomotion is known as *dynamic walking*. During every step cycle, the body's center of mass (CoM) engages in a controlled fall along a pendular arc until foot-ground impact redirects this motion into the next cycle. The joint trajectories thus evolve according to both continuous and discrete dynamics in a *hybrid system*, producing periodic orbits in the system state called *hybrid limit cycles* (as opposed to equilibrium configurations).

1.1 Hybrid Systems

Hybrid systems are dynamical systems containing both continuous and discrete dynamics. Bipedal walkers are often represented as simple hybrid systems with one continuous phase, so we adopt the definition of a "system with impulse effects" as in [5, 6].

Definition 1. A *hybrid control system* has the form

$$\mathscr{HC} : \begin{cases} \dot{x} = f(x) + g(x)u & x \in D \backslash G \\ x^+ = \Delta(x^-) & x^- \in G \end{cases}$$

where $G \subset D$ is called the *guard* and $\Delta : G \to D$ is the *reset map*. The system state x is in domain

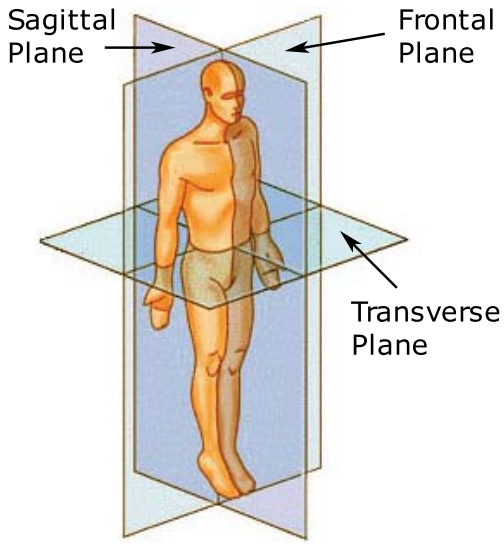

Figure 1.1: The transverse (or axial), frontal (or lateral), and sagittal planes-of-motion of the human body [7]. These correspond to the yaw/heading, lean/roll, and pitch degrees-of-freedom, respectively, at the ankle.

D, and control input u is in control space U. An uncontrolled or closed-loop system is represented as a *hybrid system* without an explicit control input:

$$\mathscr{H} : \begin{cases} \dot{x} = f(x) & x \in D \backslash G \\ x^+ = \Delta(x^-) & x^- \in G \end{cases}$$

In the case of an n-degree-of-freedom (DOF) robotic system, the state $x = (q^T, \dot{q}^T)^T \in \mathbb{R}^{2n}$ is composed of the configuration vector $q \in \mathbb{R}^n$ of joint positions and its tangent vector $\dot{q} \in \mathbb{R}^n$ of joint velocities. We now discuss solution (or integral) curves of hybrid systems in order to define hybrid limit cycles, our mathematical representation of bipedal walking gaits.

1.1.1 Solutions of hybrid systems

Bipedal walking gaits correspond to periodic solutions of hybrid systems. In particular, bipedal walking gaits are 2-step periodic (with skew-symmetry between steps) due to bilateral symmetry seen in the frontal and transverse planes-of-motion in Fig. 1.1.

A solution curve $x(t)$ to a hybrid system $\mathscr{H}$ is called a *hybrid flow*. This is *h-periodic* if $x(t) = x(t + \sum_{i=1}^{h} T_i)$, for all $t \geq 0$, where T_i is the fixed *time-to-impact* between the $(i-1)^{\text{th}}$ and i^{th}

discrete events. The image of a periodic hybrid flow in the phase space is an invariant set[1] called the *h-periodic hybrid orbit*

$$\mathcal{O} \quad = \quad \left\{ x \in D \mid x = x(t), t \in [0, \sum_{i=1}^{h} T_i] \right\}. \tag{1.1}$$

If a periodic hybrid orbit is isolated, rather than one in a continuum of orbital solutions, it is called a *hybrid limit cycle* of $\mathscr{H}$.

1.1.2 Orbital stability

We must consider orbital stability of hybrid limit cycles in order to account for perturbations in bipedal locomotion. An h-periodic hybrid orbit $\mathcal{O}$ is said to be *(locally) asymptotically stable* if all hybrid flows initiated in a neighborhood of $\mathcal{O}$ asymptotically approach the orbit. To be precise, we define a stronger sense of stability: an h-periodic hybrid orbit $\mathcal{O}$ is *(locally) exponentially stable* if there exist constants $k, \alpha, \gamma > 0$ such that for all hybrid flows $x(t)$ with $d(x(t_0), \mathcal{O}) < \gamma$,

$$d(x(t), \mathcal{O}) \quad \leq \quad k e^{-\alpha(t-t_0)} d(x(t_0), \mathcal{O}) \tag{1.2}$$

for all $t \geq t_0$. The distance function from vector x to set $\mathcal{O}$ in Euclidean metric space $(\mathbb{R}^{2n}, d)$ is defined as $d(x, \mathcal{O}) := \inf_{y \in \mathcal{O}} ||x - y||$.

The stability of periodic hybrid orbits is determined using the method of *Poincaré sections* [6], which analyzes the *Poincaré map* $P : G \to G$ associated with hybrid system $\mathscr{H}$. This is a discrete map defined on the Poincaré section, naturally chosen to be guard G, which characterizes the evolution of a hybrid flow between intersections with G. In particular, the h-composition of this map sends state $x_j \in G$ ahead h impact events by the discrete system $x_{j+h} = P^h(x_j)$. In the case of an h-periodic hybrid orbit $\mathcal{O}$, we have an *h-fixed point* $x^* \in G \cap \mathcal{O}$ such that $x^* = P^h(x^*)$. We then know that periodic hybrid orbit $\mathcal{O}$ is locally exponentially stable (LES) if and only if the associated fixed point x^* is LES in the discrete-time system defined by Poincaré map P.

Although we cannot analytically calculate this nonlinear map to determine its stability about x^*, we can numerically approximate it through simulation. This allows us to locally analyze orbital stability as a linear discrete system by the map's linearization, δP^h, where exponential stability is equivalent to the eigenvalue magnitudes of δP^h being strictly within the unit circle. The local

[1] In the analogous case of continuous-time systems, this would be a compact set defined by a closed trajectory [8].

stability region about h-fixed point x^*, known as the *basin of attraction*, is defined as

$$BoA(x^*) \quad = \quad \left\{ x \in G \ \text{ s.t. } \lim_{z \to \infty} P^{hz}(x) = x^* \right\}. \tag{1.3}$$

We defer the numerical details of simulation-based Poincaré analysis to [4, 9].

This mathematical representation of walking gaits applies to multiple forms of bipedal locomotion. In order to provide context and motivation for studying dynamic locomotion, we first distinguish this mode of transportation from quasi-static walking.

1.2 Quasi-Static Walking

Many sophisticated humanoid robots, such as HRP-2 [10] and Honda ASIMO [11], have demonstrated robotic bipedal walking that is *not* dynamic. Rather, the motion of these robots is constrained by "quasi-static" equilibrium conditions related to the *zero moment point* (ZMP).

A walking mechanism resists gravity by applying force against the ground, resulting in an equal and opposite reaction force acting at a point called the *center of pressure* (CoP) inside the support polygon/footprint, i.e., the convex hull of the ground contact area(s). In order for the biped to remain statically balanced (i.e., no foot rotation), there must be zero net moment at the CoP:

$$M + R \times F \quad = \quad 0, \tag{1.4}$$

where the walking mechanism contributes (linear) force vector F and moment vector M at the ankle, and R is the vector defined from the CoP to the center of the ankle.

The nominal point at which condition (1.4) holds is called the *foot rotation indicator* (FRI) [12]. This point coincides with the CoP when inside the biped's support polygon. In this case, the ZMP is said to exist and the foot remains flat on the ground. When the FRI exits the support polygon, the ZMP disappears and the biped rotates about a new passive DOF at a point or edge on the boundary of the support polygon. This falling scenario is always avoided by ZMP trajectory planners, whereas dynamic gaits are largely composed of such pendular falling states.

Definition 2. A *quasi-static* walking gait is a hybrid limit cycle in which condition (1.4) always holds. A *dynamic* walking gait is a hybrid limit cycle in which condition (1.4) is violated for some portion of the cycle.

However, satisfying ZMP condition (1.4) does not necessarily imply *stability* of the hybrid limit cycle associated with a quasi-static gait [6, Section 10.8]. This form of locomotion also requires large actuators to track constrained reference joint angles/velocities while actively supporting the body weight with flexed knees during the entirety of each step cycle [13, 14]. This results in unnatural shuffling motion that is up to an order of magnitude *less efficient* than dynamic walking in terms of specific energetic cost of transport (energy consumed per unit weight per unit distance) [15]. Arguably, ZMP gaits may have a closer resemblance to the inefficient postural attributes of chimpanzee bipedalism – these hunched gaits similarly have flexed knees that never pass beneath the hip joint, preventing the pendular falling motion of dynamic walking gaits [16].

However, ZMP control strategies have dominated humanoid applications requiring motion planning, such as locomotion with obstacle avoidance in three-dimensional (3-D) space [17,18], interaction with complex environments [19,20], and walking and climbing on rough terrain [21,22]. These practical applications have historically proven more difficult to achieve with dynamic walkers, which we wish to address in this thesis.

1.3 Dynamic Walking

In principle, dynamic walking embraces ballistic momentum and gravitational potential energy for speed and energetic efficiency (in fact, gravity provides the only power source in passive walking down shallow slopes [3]). This has been exploited by active robot control strategies that shape the potential energy into different forms, such as rotating the gravity vector to enable pseudo-passive dynamic walking on arbitrary slopes (i.e., uphill "feels like" downhill) [23, 24]. These stable gaits do not track reference patterns, but naturally appear from the system nonlinearities, including the potential energy.

1.3.1 Planar bipeds

Early work on dynamic walking began with simple serial-chain models, such as the two-link "compass-gait" biped of Fig. 1.2, constrained to the sagittal plane-of-motion to roughly approximate human dynamic motion (Fig. 1.1). In the pioneering work on passive walking [3], McGeer discovered the existence of stable hybrid limit cycles down shallow slopes between about 3° and 5°, the range of slope angles for which the potential energy introduced by gravity after each step is

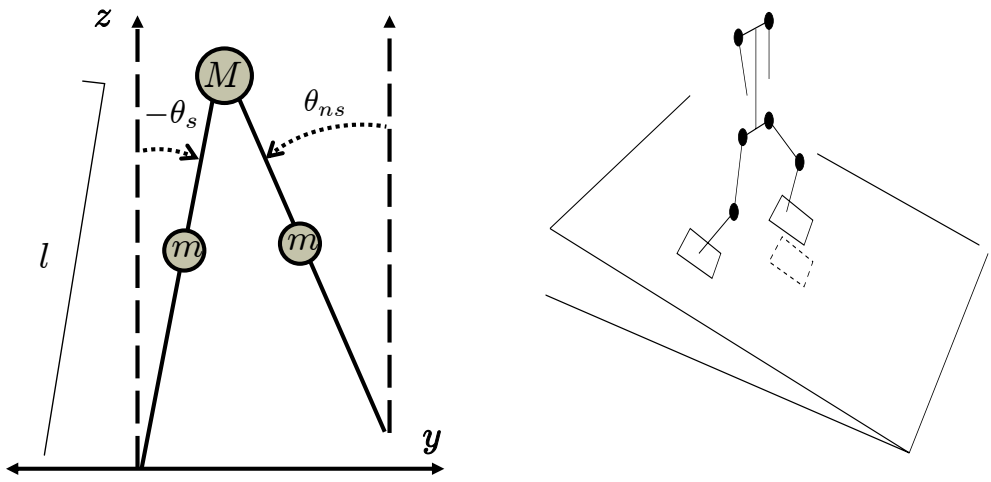

Figure 1.2: The two-link "compass-gait" biped constrained to the sagittal plane-of-motion (left) and a general 3-D biped (right).

matched by the energy dissipated at foot impact with ground. Gravity-powered passive walking was further studied in [4], showing period-doubling (flip) bifurcations in the gait as model parameters such as slope angle are varied beyond some stability region.

Underactuated planar walking on flat ground was achieved with the method of *hybrid zero dynamics* [5,6,25], using output linearization to zero hybrid-invariant output functions (i.e., virtual constraints) describing some desired gait. This theory was applied to the compass-gait biped with rigid legs as well as compliant legs to incorporate a nontrivial double-support phase [6,26]. In fact, hybrid zero dynamics was successfully implemented on the planar RABBIT bipedal robot at the Laboratoire Automatique de Grenoble in France [27] and more recently on the planar MABEL biped at the University of Michigan [28].

Terrain uncertainty was confronted in [29] by discretizing the state space and dynamics of the planar compass-gait biped, so as to analyze the stochastic "metastability" of the resulting controlled Markov chain. However, the mesh state space expands exponentially with the robot's dimensionality, bringing into question this method's practicality for high-DOF bipeds in three dimensions.

1.3.2 Three-dimensional walking

Although these various concepts have been successful with regard to planar dynamic walkers, there has been scattered success in extending these ideas to 3-D space, where robot dynamics become quite complex with highly-coupled DOFs in three planes-of-motion (Fig. 1.1). Passive dynamic

walking was extended to a spatially 3-D biped (modeling pitch and lean without yaw) in [30], requiring direct control over the leg splay angle and an assumption that the continuous dynamics are invariant under this actuation. The carefully tuned walking mechanism of [31] demonstrated 3-D passive walking down a particular fixed slope from a specific initial configuration, but its gait was incredibly sensitive to perturbations and thus prone to falls.

Stochastic reinforcement learning was used to separately compute control policies for the frontal- and sagittal-plane modes of a simple 3-D biped in [32]. Spatial 3-D walking was similarly achieved in [33] with a decoupling assumption between the planes-of-motion to separately define virtual constraints for hybrid zero dynamics. However, we argue that these planes-of-motion are strongly coupled, especially in the case of significant swaying and steering motions, requiring a more sophisticated method of decomposing a biped's dynamics. This philosophy was embraced in [34, 35], where hybrid zero dynamics was rigorously extended to 3-D bipeds by employing optimization instead of manual inspection to define the complicated virtual constraints.

The aforementioned energy-shaping methods of [23, 24, 36], known as controlled symmetries and passivity-based control, exploit the geometric structure inherent in robot dynamics of arbitrary dimensionality. Specifically, the first method maps passive limit cycles down shallow slopes to pseudo-passive limit cycles on arbitrary slopes (with trajectory time-scaling in [37–39]). Passivity-based energy tracking then expands the small basin of attraction associated with passive limit cycles to enable stable walking on uneven terrain. However, these tools necessarily require the existence of stable passive limit cycles, which is usually not the case for complex 3-D bipedal walkers (e.g., right side of Fig. 1.2). This has limited the primary application of these energy-shaping approaches to sagittal-plane walkers such as the compass-gait biped. We wish to extend these satisfying results to general 3-D walkers.

1.3.3 Motion planning

Some of the biggest challenges in dynamic locomotion concern stable motion planning in complex or uncertain environments. A rigorous framework for controlling the planned flight trajectories of planar dynamics runners was developed in [40]. Step-level planning over irregular terrain was applied to planar dynamic walkers in [41, 42]. However, these methods have not yet scaled to high-DOF models in 3-D space.

Hybrid zero dynamics has proven successful in constructing LES walking gaits capable of steering

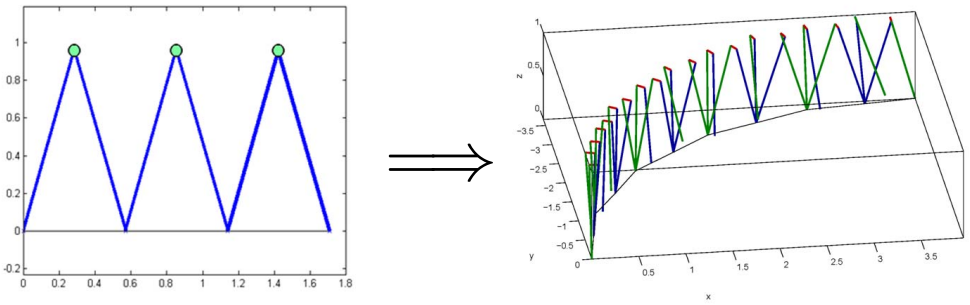

Sagittal-plane (2D) walking gait Three-dimensional walking gait

Figure 1.3: Controlled geometric reduction: building a 3-D walking gait (right) from a sagittal-plane walking gait (left).

to nearby headings in 3-D space [35]. In particular, LES implies local input-to-state stability (LISS): sufficiently small changes in heading result in small changes in state between impact events. Unfortunately, it is difficult to find the bounds for this form of stability over arbitrary curved paths (i.e., what range of initial states will recover from some bounded sequence of steering angles).

In fact, we are unaware of any *path planning* results for directional dynamic walking in 3-D space, aside from the work [43] to be revisited in this thesis. The lack of related work is likely due to challenges in creating dynamic gaits for fully 3-D bipedal robots, where additional yaw dynamics must be controlled to variable headings with some sense of stability.

1.4 Contributions of the Thesis

Despite the minute class of 3-D bipeds that can stably exploit passive dynamics, symmetry- and passivity-based methods remain appealing due to the natural and efficient dynamic gaits they produce for planar robots. The existence problem of passive limit cycles for 3-D bipeds was addressed with a controlled form of symmetry-based geometric reduction in [44–46]. In particular, energy-shaping control was used to decouple a spatially 3-D biped's sagittal plane-of-motion, which is well studied with known limit cycles, and from this build pseudo-passive walking gaits for the full-order system. We generalize these *reduction-based control* results throughout this thesis to consider fully 3-D bipeds and curved walking paths as in Fig. 1.3.

1.4.1 Reduction-based control

We present the energy-based method of controlled geometric reduction, which is fundamentally related to the geometric properties of symmetry and passivity. Given a mechanical system characterized by its Lagrangian function $\mathcal{L} = \mathcal{K} - \mathcal{V}$ or Hamiltonian function $\mathcal{H} = \mathcal{K} + \mathcal{V}$ (for kinetic energy $\mathcal{K}$ and potential energy $\mathcal{V}$), we consider symmetries in the form of *cyclic* variables q_1, which do not explicitly appear in the Lagrangian or Hamiltonian functions:

$$\frac{\partial \mathcal{L}}{\partial q_1} \;=\; 0 \quad \Longleftrightarrow \quad \frac{\partial \mathcal{H}}{\partial q_1} \;=\; 0. \tag{1.5}$$

Passive feedback in an energy-shaping control law establishes a *functional* momentum conservation law that optimally controls cyclic variables to set-points or limit cycles. This nonholonomic constraint (an invariant) defines a lower-dimensional zero dynamics corresponding to the original robot with the first DOF fixed.

We show that a stabilizing controlled reduction can be designed based on a passivity-based feedback transformation of $\mathcal{L}$ into a special form of controlled Lagrangian with broken symmetry:

$$\mathcal{L}_\lambda(q, \dot{q}) \;\;=\;\; \mathcal{K}_\lambda(q, \dot{q}) + Q_\lambda(q)\dot{q} - \mathcal{V}_\lambda(q), \tag{1.6}$$

depending on some desirable function λ of the cyclic variables. This *almost-cyclic* Lagrangian system in closed loop corresponds to an equivalent Hamiltonian system with upper-triangular form, showing that full-order stability is provided in a manner analogous to backstepping (specifically, *forwarding* control) [8,47]. By choosing the biped's sagittal plane as the desired zero dynamics, we can exploit the minimum phase property provided by the existence of passive limit cycles.

We then generalize this theory for recursive decoupling of subsystems as in [48, 49], allowing application to completely 3-D bipeds with both yaw and lean modes (respectively in the frontal and transverse planes of Fig. 1.1). This method exploits symmetries inherent in serial kinematic chains, but human morphology involves a significantly more complex branching tree structure (i.e., a branched chain). Therefore, multistage controlled reduction is extended to the class of open kinematic chains [50], such as robots with torsos and articulated arms (e.g., right side of Fig. 1.2). This simplifies the search for full-order hybrid limit cycles and significantly expands the class of 3-D bipeds that can achieve pseudo-passive dynamic walking.

1.4.2 Path planning

We will use reduction-based control to construct straight-ahead walking gaits corresponding to LES hybrid limit cycles [48, 49], which can be steered toward arbitrary headings as illustrated in Fig. 1.3. These results will be extended to show that constant-curvature steering between steps induces LES hybrid limit cycles (modulo yaw) corresponding to circular turning [50, 51]:

$$x^{*\mathrm{tu}(s)} + \begin{pmatrix} s & 0_{2n-1} \end{pmatrix}^T \quad = \quad P^h_{\mathrm{tu}(s)} \left(x^{*\mathrm{tu}(s)} \right), \tag{1.7}$$

where s is the constant steering angle resulting in h-fixed point $x^{*\mathrm{tu}(s)}$ for an n-DOF robot walker. However, walking paths can entail an *arbitrary* sequence of turning motions that may accumulate perturbations and lead to instability.

In order to build bipedal robots that can quickly and efficiently navigate through real-world environments, the stability of dynamic walking must be considered when *planning* walking paths with significant steering. This is no trivial task, as turning motion inherently deviates from known hybrid limit cycles associated with straight-ahead walking [51]. Unlike ZMP methods, the robot state cannot be checked against closed-form balance conditions like (1.4). The hybrid nonlinear dynamics of a dynamic walker make it difficult to analytically assure stability[2] – the fate of a walking trajectory from given initial conditions is usually computed in simulation [4, 9].

Therefore, we present a hierarchical control and planning framework for 3-D dynamic locomotion. Given a low-level controller that produces a set of *asymptotically stable gait primitives*, a dynamic walker can be controlled as a discrete-time switched system that sequentially composes gait primitives from step to step [43]. Each gait primitive is a pair $\mathcal{G} = (P^h_{\mathrm{cl}}, x^*)$, where x^* is an asymptotically stable h-fixed-point (modulo yaw) of the closed-loop Poincaré map P_{cl} for some walking strategy. Motivated by the controller composition method of Lyapunov funneling [52], we derive rules by which a planned walking path that is a sequence of these primitives (e.g., Fig. 1.4) may be stably followed by the robot.

The continuously parameterized set of primitives $\mathcal{P}^s = \{\mathcal{G}^{\mathrm{st}}, \mathcal{G}^{\mathrm{tu}(s)}, \mathcal{G}^{\mathrm{tu}(-s)}\}$ is associated with a nominal set of constant-curvature arcs on the walking surface, growing a discrete tree with branching factor three. Hence, dynamically stable path planning reduces to a discrete tree search that explores the action space of primitive arcs. This result enables motion planning for fast and efficient dynamic walkers in a similar manner to what is already possible for quasi-static walkers.

[2] This challenge is not limited to dynamic walking – ZMP condition (1.4) does not necessarily imply stability [6].

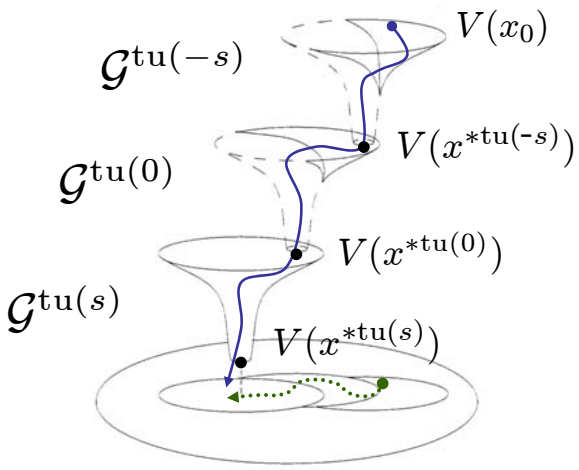

Figure 1.4: Sequential composition of Lyapunov funnels, each being the graph of a Lyapunov function over its state space (illustrated as circular neighborhoods in a planar global space). The funneled state trajectory (dotted green) corresponds to the trajectory of the funneled Lyapunov functions (solid blue). Original figure from [52] reproduced with permission of the publisher.

1.5 Organization of the Thesis

We begin the thesis with a background review of the geometric notions of passivity, symmetry, and reduction in Chapter 2. This leads to our Lagrangian and Hamiltonian formulations of controlled geometric reduction in Chapter 3, by which we establish unifying connections to passivity and symmetry. We present the multistage application of controlled reduction to mechanical systems in Chapter 4, identifying symmetries to control the large class of open kinematic chains as lower-dimensional subsystems. We then introduce the primary application of the thesis in Chapter 5: the 4-DOF and 5-DOF bipedal walkers, their general control law, and simulation results of straight-ahead walking and turning in 3-D space. This motivates the sequential composition theory of asymptotically stable gait primitives in Chapter 6, including planned walking results for the hipless 4-DOF and 5-DOF compass-gait bipeds. We compare these results to human biomechanics and propose extensions of the energy-shaping control paradigm to robot-assisted locomotor rehabilitation in Chapter 7. We conclude in Chapter 8 with remarks on the significance of this material and the future work it motivates.

CHAPTER 2

PASSIVITY AND SYMMETRY IN MECHANICAL SYSTEMS

Although mechanical systems often have complex nonlinear dynamics, they are rich with geometric structure that can be exploited for control and analysis independent of specific dynamic models. For example, the notion of passivity allows an energetic interpretation of system dynamics using common Lyapunov and $\mathscr{L}_2$-gain methods [8, 53–55]. In other words, a complex nonlinear system can be studied much like an RLC circuit or spring-damper system. Nonlinear passivity-based control methods provide stability with larger basins of attraction and better robustness to model uncertainty [56–59] than that possible with linear methods. This has enabled oscillatory pattern generation for locomotion [36, 37] and synchronization [60]. It has also been shown that optimal feedback control is directly related to passive outputs [61], demonstrating the importance of this structural property for both linear and nonlinear systems.

Geometric reduction is another classical tool, used to analytically decompose the calculation of integral curves of a physical system with symmetries. These systems are characterized by Lagrangian or Hamiltonian functions that are invariant under the action of a symmetry group on the configuration space [62–64]. For example, in the case of *Routhian* reduction, a Lagrangian function has no dependence on so-called *cyclic* variables, so the system is invariant under the action of rotating these variables. By dividing out the coordinates corresponding to such symmetry groups, integral curves can be solved in a lower-dimensional space that uniquely characterize the full-order solution. Complex symmetry groups can also be decomposed into subgroups for dynamical reduction *by stages* as discussed in [63, 64].

A topological perspective was used in [65] to show a lower bound on dynamic model reduction of serial kinematic chains based on kinematic models, by which reduced adaptive control algorithms are designed. A similar concept not directly related to symmetry is *differential flatness*, describing nonlinear (control) systems whose integral curves are in smooth one-to-one correspondence with arbitrary curves of a lower-dimensional space [66]. The full-order space is mapped to the

lower-dimensional space by so-called flat outputs, which are functions of the system state and their derivatives. From these outputs and their derivatives, the full-order state can be solved without integration. Although this property is not necessarily based on symmetries, [67] shows its application to a special class of mechanical systems with symmetry and one degree of underactuation (e.g., underwater vehicles). This method is helpful for simplified trajectory planning [68], but in general, differential flatness is difficult to determine and characterize with appropriate outputs.

The properties of symmetry and passivity are easy to identify and provide model-independent structure, motivating analysis and control methods like controlled geometric reduction. Therefore, this chapter offers a background discussion to define these geometric properties. We begin with two important formulations of the dynamics of mechanical systems: Lagrangian and Hamiltonian mechanics. The resulting dynamics are equivalent, but each method offers a different perspective that will prove useful for exploiting passivity and symmetry.

2.1 Lagrangian Mechanics

An n-DOF mechanical system with configuration space $\mathcal{Q}$ is described by elements $(q, \dot{q})$ of tangent bundle[1] $T\mathcal{Q}$ and Lagrangian function $\mathcal{L} : T\mathcal{Q} \to \mathbb{R}$, given in coordinates by

$$\begin{aligned} \mathcal{L}(q, \dot{q}) &= \mathcal{K}(q, \dot{q}) - \mathcal{V}(q) \\ &= \frac{1}{2}\dot{q}^T M(q)\dot{q} - \mathcal{V}(q), \end{aligned} \tag{2.1}$$

where $\mathcal{K}(q, \dot{q})$ is the kinetic energy, $\mathcal{V}(q)$ is the potential energy, and $n \times n$ symmetric, positive-definite $M(q)$ is the generalized mass/inertia matrix. By the least action principle [62], system integral curves necessarily satisfy the *Euler-Lagrange* (E-L) equations

$$\mathscr{E}\mathscr{L}_q\{\mathcal{L}\} := \frac{d}{dt}\nabla_{\dot{q}}\mathcal{L} - \nabla_q\mathcal{L} = \tau, \tag{2.2}$$

where n-dimensional vector τ contains the external joint torques. This system of second-order ordinary differential equations directly gives the dynamics for the actuated mechanism in phase space $T\mathcal{Q}$. These equations have the special structure

$$M(q)\ddot{q} + C(q, \dot{q})\dot{q} + N(q) = Bu, \tag{2.3}$$

[1]The space of configurations and their tangential velocities.

where $n \times n$-matrix $C(q, \dot{q})$ contains the Coriolis/centrifugal terms, vector $N(q) = \nabla_q \mathcal{V}(q)$ contains the potential torques, and $n \times m$-matrix B (full row rank) maps actuator input vector $u \in \mathbb{R}^m$ to joint torques $\tau = Bu \in \mathbb{R}^n$ for $m \leq n$. We initially consider the case of full actuation ($m = n$ implying that B is invertible), so we take B to be identity without loss of generality.

These dynamics yield control system (f, g) on $T\mathcal{Q}$:

$$\begin{pmatrix} \dot{q} \\ \ddot{q} \end{pmatrix} = f(q, \dot{q}) + g(q)u, \tag{2.4}$$

with vector field f and matrix g of control vector fields:

$$\begin{aligned} f(q, \dot{q}) &= \begin{pmatrix} \dot{q} \\ M(q)^{-1}\left(-C(q, \dot{q})\dot{q} - N(q)\right) \end{pmatrix} \\ g(q) &= \begin{pmatrix} 0_{n \times n} \\ M(q)^{-1} \end{pmatrix}. \end{aligned}$$

Defining state $x = (q^T, \dot{q}^T)^T \in T\mathcal{Q}$, this takes the form of a first-order differential control system. For the analytical results in Chapters 2-4, we make the standard assumption of local Lipschitz continuity. We later present numerical results for hybrid systems with Lipschitz continuous phases in Chapters 5 and 6 – analytical results are possible in this context with a special case of controlled reduction as seen in [45].

2.2 Hamiltonian Mechanics

The Hamiltonian formulation begins with the Hamiltonian function, representing the system's mechanical energy:

$$\mathcal{H} = \mathcal{K} + \mathcal{V} = \mathcal{L} + 2\mathcal{V}.$$

This quantity is more useful when expressed in terms of the system's generalized momentum, defined as

$$\begin{aligned} p = \mathcal{J}(q, \dot{q}) &:= \nabla_{\dot{q}} \mathcal{L}(q, \dot{q}), \\ &= M(q)\dot{q} \end{aligned} \tag{2.5}$$

where momentum map $\mathcal{J}$ expresses p in terms of Lagrangian coordinates $(q, \dot{q})$. The phase space of the system can then be expressed in canonical coordinates (q, p) of the cotangent bundle[2] $T^*\mathcal{Q}$. In these coordinates, Hamiltonian $\mathcal{H} : T^*\mathcal{Q} \to \mathbb{R}$ is obtained from a Lagrangian $\mathcal{L}$ by a Legendre transformation:

$$\begin{aligned} \mathcal{H}(q,p) &= \left[p^T\dot{q} - \mathcal{L}(q,\dot{q})\right]\Big|_{p=\mathcal{J}(q,\dot{q})} \\ &= \frac{1}{2}p^T M^{-1}(q)p + \mathcal{V}(q). \end{aligned} \tag{2.6}$$

Note that the sign of the Hamiltonian function (and thus the Legendre transformation) is merely a convention, and in some cases it is convenient to use the opposite sign.

The controlled dynamics are given by *Hamilton's* equations, two first-order partial differential equations (PDEs):

$$\begin{pmatrix} \dot{q} \\ \dot{p} \end{pmatrix} = \begin{pmatrix} 0_{n\times n} & I_{n\times n} \\ -I_{n\times n} & 0_{n\times n} \end{pmatrix} \begin{pmatrix} \nabla_q \mathcal{H} \\ \nabla_p \mathcal{H} \end{pmatrix} + \begin{pmatrix} 0_{n\times 1} \\ u \end{pmatrix} \tag{2.7}$$

where control u enters into the derivative of the generalized momentum, known as the Newtonian forces (or torques). Note that direct calculation gives $\nabla_p \mathcal{H} = M^{-1}(q)p$, and the right-hand side of (2.7) defines the *covector field* on $\mathcal{Q}$.

2.3 Passivity

Given either mechanics formulation, we can define a first-order control system with an output:

$$\begin{aligned} \dot{x} &= f(x) + g(x)u \\ y &= h(x), \end{aligned} \tag{2.8}$$

where $x \in \mathbb{R}^{2n}$ and $u, y \in \mathbb{R}^n$. In this context, the notion of passivity offers an energetic perspective based on common Lyapunov methods [36].

Definition 3. Control system (2.8) is (input/output) *passive* if there exists a differentiable non-negative scalar function $S : \mathbb{R}^{2n} \to \mathbb{R}$, called the storage function, such that $\dot{S} \leq y^T u$.

[2]The space of configurations and their conjugate momenta.

Lemma 1. Suppose (2.8) is passive with storage function S. Given output feedback control $u = \gamma(y)$, where γ is any continuous function satisfying $y^T\gamma(y) \leq 0$, the origin is *stable in the sense of Lyapunov*, i.e., for every $\epsilon > 0$ there exists a $\gamma > 0$ such that if $||x(0)|| < \gamma$ then $||x(t)|| < \epsilon$ for all $t > 0$. Moreover, the zero level-set $\{x|\gamma(h(x)) = 0\}$ is asymptotically attractive.

This classical result is proven in [8,54]. It is important to note that this offers no further stability guarantees on the attractive zero level-set, and these so-called zero dynamics are a common topic of study, e.g., [5,6,36,45].

Passivity also has interesting connections with optimal control discussed in [61]. Given performance index

$$J(x_0) \;=\; \frac{1}{2}\int_0^\infty (l(x)^T l(x) + u^T u)d\tau, \tag{2.9}$$

if a differentiable optimal function $V(x) = \min_{u(\cdot)} J(x)$ exists, then the optimal feedback control has the form [54]

$$u \;=\; -L_g V(x) \;:=\; -\nabla_x V g(x), \tag{2.10}$$

where $L_g V$ is the *Lie derivative* of function V with respect to vector field g. It is shown in [61] that the optimal system has a passivity property with respect to output $y = h(x) = L_g V(x)$. Conversely, given a feedback control law $u^* = -k(x)$, a pair $\{V(\cdot), l(\cdot)\}$ for which (2.9) is minimized by u^* is known as the solution to the *inverse* optimal control problem. This is similarly related to passivity [61]:

Theorem 1. A necessary/sufficient condition for the existence of a solution to the inverse optimal control problem of system (2.8) with $u^* = -k(x)$ subject to (2.9) is that the following system is passive with respect to input v:

$$\begin{aligned} \dot{x} &= f(x) - g(x)k(x) + g(x)v \\ y &= k(x). \end{aligned} \tag{2.11}$$

Given state $x = (q^T, \dot{q}^T)^T \in T\mathcal{Q}$, a structural property of robots shows input/output passivity for $y = \dot{q}$, since the Hamiltonian $\mathcal{H}$ (i.e., total energy) acts as a storage function: $\dot{\mathcal{H}} = \dot{q}^T u$ for vector u of input torques [55]. For any nonpositive passive feedback law $\gamma(\dot{q}) \leq 0$, we have $\dot{\mathcal{H}} = \dot{q}^T\gamma(\dot{q}) \leq 0$

providing Lyapunov stability by Lemma 1. If this law is negative-definite, then this further shows asymptotic dissipation of joint velocities: $\dot{q} \to 0$. In fact, we find that linear γ is optimal by Theorem 1:

Proposition 1. Linear output feedback $u = -\dot{q}$ is the optimally stabilizing control (in the sense of Lyapunov) of a robot with respect to (2.9) for $l(x) = \dot{q}$.

Proof. Hamiltonian $\mathcal{H}$ is our value function. Using the robot passivity property, [61, Theorem 1] tells us that $k(x) = L_g\mathcal{H} = \dot{q}$ and $l^T(x)l(x) = -L_f\mathcal{H} + L_{gk}\mathcal{H} = \dot{q}^T\dot{q}$ since $L_f\mathcal{H} = 0$ (conservation of energy). Based on candidate optimal feedback law $k(x) = \dot{q}$, we can define $v = \bar{u} + \dot{q}$ for system (2.11):

$$\begin{aligned} \dot{x} &= f(x) - g(x)k(x) + g(x)v \\ &= f(x) + g(x)\bar{u}. \end{aligned}$$

This is the original robot system with input $\bar{u}$ and output $y = \dot{q}$, so $\dot{\mathcal{H}} = \dot{q}^T\bar{u} = \dot{q}^Tv - \dot{q}^T\dot{q}$, implying $\dot{\mathcal{H}} \leq \dot{q}^Tv$ and satisfying passivity for (2.11). Hence, $u^* = -k(x)$ is stabilizing by Lemma 1 and optimal by Theorem 1. □

Note that this passive feedback can be implemented mechanically with a rotary (or linear) damper. We now discuss the notion of symmetry in order to connect these properties to symmetry-breaking control.

2.4 Symmetry

We introduce the notion of symmetry with some basic concepts from differential geometry (cf. [62, 69–71]), starting with formalisms from group theory.

Definition 4. A set $\mathbb{G}$ together with a binary operation $\circ$ defined on elements of $\mathbb{G}$ is called a *group* if it satisfies the following four axioms:

1. *Closure*: If $g_1, g_2 \in \mathbb{G}$, then $g_1 \circ g_2 \in \mathbb{G}$.
2. *Identity*: There exists an identity element, $e \in \mathbb{G}$, such that $e \circ g = g$ for every $g \in \mathbb{G}$.
3. *Inverse*: For each $g \in \mathbb{G}$, there exists a unique inverse, $g^{-1} \in \mathbb{G}$, such that $g \circ g^{-1} = g^{-1} \circ g = e$.

4. *Associativity*: If $g_1, g_2, g_3 \in \mathbb{G}$, then $(g_1 \circ g_2) \circ g_3 = g_1 \circ (g_2 \circ g_3)$.

Groups define actions on sets (which may also be groups), such as rotations in a configuration space. Since we are interested in differential systems, we also show how these group actions induce maps on tangent spaces [24].

Definition 5. A group $\mathbb{G}$ is said to *act* on another set $\mathcal{Q}$ (through a *group action*) if each element $g \in \mathbb{G}$ defines a bijective mapping $\Phi : \mathbb{G} \times \mathcal{Q} \to \mathcal{Q}$ taking a pair (g, q) to $\Phi(g, q) = \Phi_g(q)$ and satisfying for all $q \in \mathcal{Q}$:

1. $\Phi_e(q) = q$, where e is the identity element of $\mathbb{G}$.

2. $\Phi_{g_1}(\Phi_{g_2}(q)) = \Phi_{g_1 g_2}(q)$.

Definition 6. Let $T_q\mathcal{Q}$ be the linear space of tangent vectors at q, and let $T\mathcal{Q} = \bigcup_q T_q\mathcal{Q}$ be the tangent bundle of $\mathcal{Q}$. Letting $g \in \mathbb{G}$, we then denote $T_q\Phi_g$ as the tangent function to Φ_g mapping $T_q\mathcal{Q}$ onto $T_{\Phi_{g(q)}}Q$. This defines the *lifted action* $T\Phi : \mathbb{G} \times T\mathcal{Q} \to T\mathcal{Q}$.

In the context of differential calculus, we consider continuous Lie groups, which are smooth manifolds (cf. [62, 69]). Common examples are $\mathrm{SO}(n)$, the group of orthogonal orientations (or rotations) in n dimensions with matrix multiplication as the group operation; $\mathbb{S}^1$, the group of rotations about the unit circle with scalar addition; and $\mathbb{R}^k$, the group of Euclidian translations with vector addition. Such a group $\mathbb{G}$ is called a *symmetry group* if a function is invariant under its action:

Definition 7. Let $F : M \to N$ be a smooth mapping between manifolds M and N and let $\Phi : \mathbb{G} \times M \to M$ be an action of the Lie group $\mathbb{G}$ on M. Then, we say that F is *invariant* under the group action if $F \circ \Phi = F$, i.e., if for all $g \in \mathbb{G}$ and $m \in M$, $(F \circ \Phi_g)(m) = F(m)$.

For a smooth vector field[3] X mapping $\mathcal{Q}$ to $T\mathcal{Q}$, this definition of invariance corresponds to

$$X(\Phi_g(q)) \;=\; T_q\Phi_g(X(q)) \;=\; X(q),$$

for all $g \in \mathbb{G}$, $q \in \mathcal{Q}$. I.e., lifted action $T_q\Phi_g$ is the identity map. In the Hamiltonian framework, this is similarly the case for a covector field Y on $\mathcal{Q}$, where $T_q^*\Phi_g = I$. This definition can be

[3]Given a configuration space $\mathcal{Q}$, Lagrangian mechanics define $T\mathcal{Q}$ as the state space, so vector fields map $T\mathcal{Q}$ to a 2nd-order tangent space. The definitions of invariance in this section apply to Lagrangian mechanics if we relabel this state space to be set $\mathcal{Q}$.

relaxed to the case of *equivariance* where $T_q\Phi_g$ is not always identity. However, this thesis will only consider group actions Φ that are commutative on $\mathcal{Q}$, implying that the lifted action is indeed identity. An important implication of invariance is the following:

Lemma 2. Let vector field X be Φ-invariant, and let $\gamma : [0, T] \to \mathcal{Q}$ be an integral curve of X. Then, for all $g \in \mathbb{G}$, $\Phi_g \circ \gamma$ is also an integral curve of X.

Uniqueness of solutions to X tells us that, if γ has initial condition $\gamma(0)$, then $\Phi_g \circ \gamma$ is the integral curve from initial condition $\Phi_g(\gamma(0))$. Hence, X has no isolated stable solutions in full-order space. Rather, we may find infinitely many fixed-points or periodic orbits. We will revisit this implication shortly.

2.5 Geometric Reduction

Geometric reduction requires the existence of symmetry in a mechanical system's dynamics, which induces an invariant submanifold[4] in phase space $T\mathcal{Q}$. Symmetries are often found in the form of *conservation laws*, where a physical quantity of the system is conserved by the dynamics [70]. Therefore, these conservation laws can be expressed as nonholonomic constraints of the first-order form $J_c(q)\dot{q} = b(q)$ or second-order form $J_c(q)\ddot{q} = b(q, \dot{q})$. If constraint Jacobian J_c has row rank k in the former case, then the system dynamics restricted to the invariant surface

$$\mathcal{Z} \quad = \quad \{(q, \dot{q}) | J_c(q)\dot{q} = b(q)\} \tag{2.12}$$

give a reduced-order system of dimension $n - k$. The constraints then uniquely describe the "divided" coordinates, $q_c \in \mathbb{R}^k$, based on the reduced coordinates, $q_r \in \mathbb{R}^{n-k}$, where $q = (q_c^T, q_r^T)^T$.

In classical Routhian reduction [62], a Lagrangian $\mathcal{L}$ has configuration space $\mathcal{Q} = \mathbb{G} \times S$ (say, an n-torus), where $\mathbb{G} = \mathbb{T}^k = \mathbb{S}^1 \times \ldots \times \mathbb{S}^1$ is the configuration symmetry group and $S \cong \mathcal{Q} \backslash \mathbb{G} = \mathbb{T}^{n-k}$ is the *shape space*. Symmetries of $\mathcal{L}$ are characterized by *cyclic* variables $q_c \in \mathbb{G}$, such that

$$\nabla_{q_c}\mathcal{L} \quad = \quad 0. \tag{2.13}$$

[4] A submanifold of manifold $T\mathcal{Q}$ is a subset which itself has the structure of a manifold. Any system trajectory initialized in an invariant submanifold will remain in the submanifold for all time.

The symmetry group $\mathbb{G}$ acts on $\mathcal{Q}$ by rotating the cyclic coordinates, i.e.,

$$\Phi_g(q) \quad = \quad (q_1 + g_1, \ldots, q_k + g_k; q_{k+1}, \ldots, q_n)^T \tag{2.14}$$

for $g \in \mathbb{G}$ and $q \in \mathcal{Q}$. The lifted action induced on $T\mathcal{Q}$ is the identity map $T_q\Phi_g(\dot{q}) = \dot{q}$. Then, the Lagrangian is invariant under this rotating action:

$$\begin{aligned} (\mathcal{L} \circ \Phi_g)(q, \dot{q}) &= \mathcal{L}(\Phi_g(q), T_q\Phi_g(\dot{q})) \\ &= \mathcal{L}(\Phi_g(q), \dot{q}) \\ &= \mathcal{L}(q, \dot{q}) \end{aligned} \tag{2.15}$$

for all $g \in \mathbb{G}$ and $(q, \dot{q}) \in T\mathcal{Q}$. The second equality follows from identity of the lifted action. Recalling that Lagrangian $\mathcal{L}$ has no dependence on q_c by (2.13), the last equality follows from the group action (2.14) rotating only these cyclic variables. A similar statement can be made about invariance of the corresponding vector field.

If the Lagrangian has cyclic variables that are free from external forces (e.g., no actuation), we can decompose the dynamics with Routhian reduction. Equation (2.13) implies that momentum vector p_c conjugate to the cyclic coordinates is equal to some constant vector μ. The dynamics then evolve on invariant level-set $\mathcal{Z}$ of these conserved momentum quantities, where $J_c = [I_{k\times k} \quad 0_{k\times n-k}]M$ and $b(q) = \mu$ in (2.12). Based on these constraints, we can directly relate full-order integral curves on phase space $T\mathcal{Q}$ to reduced-order integral curves on phase space TS, and vice versa. In other words, we divide out group $\mathbb{G}$ by projecting $T\mathcal{Q}$ onto reduced space TS. However, stability in $T\mathcal{Q}$ modulo $\mathbb{G}$ allows arbitrary drift along orbits of $\mathbb{G}$ by Lemma 2, and these divided coordinates often correspond to unstable modes.

Control can break the symmetry of group $\mathbb{G}$ and stabilize orbits of $T\mathbb{G}$, as applied to wave equations in [72]. The energy of underwater vehicles is shaped with symmetry-breaking potentials to obtain stability in [73]. Similarly, controlled reduction shapes system energy to stabilize bipedal walking gaits in three-dimensional space [44–46, 48–51]. We revisit controlled reduction by first developing a passive-feedback control law to generate new invariants that control cyclic coordinates to set-points or periodic orbits. We then show that this corresponds to a form of symmetry-breaking that preserves the projection map for dividing out group $\mathbb{G}$ of "almost-cyclic" variables.

CHAPTER 3

CONTROLLED GEOMETRIC REDUCTION

Geometric control methods exploiting passivity, symmetry, and system energetics have been widely studied in the literature. In many cases, symmetry groups correspond to the coordinates of unstable and/or unactuated modes (e.g., rotation at the contact between a biped's toe and ground). Symmetry-based reduction was elegantly applied to geometric motion planning of underactuated mechanical systems in [74, 75], using the reduced system to produce motion along unactuated coordinates corresponding to the symmetry group (but without considering stability). From the dynamics perspective, a class of planar systems with unactuated cyclic variables were shown to have relative degree three, allowing asymptotic stabilization and tracking of these variables [40].

In the energetic approach of [58, 59], *interconnection and damping assignment* (IDA) passivity-based control shapes an underactuated system's Hamiltonian function and injects damping via passive feedback to achieve asymptotic stability. Closely related work [76] uses energy-shaping control to obtain *controlled Lagrangian* systems to guarantee stability modulo the symmetry group (i.e., in a reduced phase space). Reduction theory for controlled Lagrangian or Hamiltonian systems with symmetry was developed in [77], and potential shaping was used in [73,78] to break symmetry in order to stabilize the divided coordinates in addition to the reduced phase space.

We are interested in the controlled form of geometric reduction, termed *functional Routhian reduction*, which was developed in [44–46, 48–51, 79] to build stable limit cycles for bipedal walking robots based on stable limit cycles in the sagittal plane-of-motion. This chapter revisits controlled reduction to establish connections to passivity, inverse optimality, and symmetry discussed in the previous chapter.We first offer a Hamilton-Lagrange perspective to show that passive feedback establishes a *functional* momentum conservation law that optimally controls cyclic variables. Based on this conservation law, we define the controlled reduction from a full-order system to its reduced-order subsystem. This allows the desired properties of a controlled reduction to be specifically designed and achieved through a passivity-based feedback transformation of the system

Lagrangian into a controlled Lagrangian with broken symmetry, known as an *almost-cyclic Lagrangian*. This uniquely corresponds to an *almost-cyclic Hamiltonian*, by which we establish a new passivity property and connections to IDA passivity-based control [58, 59]. A change of canonical coordinates results in upper-triangular form in this closed-loop Hamiltonian system, showing that full-order stability is provided in a manner analogous to *forwarding* control [8, 47].

3.1 Control of Cyclic Variables

In this section, we use mechanically-realizable passive feedback to control a scalar cyclic variable in systems with symmetry (the vectorized case follows analogously and the *recursively cyclic* case is considered in [80]). To begin, we define an n-DOF robot's configuration space $\mathcal{Q} = \mathbb{T}^n$ with configuration vector $q = (q_1, q_2^T)^T$, where scalar q_1 is the first coordinate and vector $q_2 \in \mathbb{T}^{n-1}$ contains the remaining $n-1$ coordinates. Assuming that q_1 is a cyclic coordinate, we have Lagrangian invariance under the group action of $\mathbb{S}^1$ for rotating the cyclic variable: $\mathcal{L}(q, \dot{q}) = \mathcal{L}(\Phi_g(q), T_q\Phi_g(\dot{q}))$ for all $g \in \mathbb{S}^1$, $(q, \dot{q}) \in T\mathcal{Q}$, where $\Phi_g(q) = (q_1 + g, q_2^T)^T$ and $T_q\Phi_g = I$.

This further implies that the inertia matrix is cyclic and can be expressed as

$$M(q_2) \;=\; \begin{pmatrix} m_1(q_2) & M_{12}(q_2) \\ M_{12}^T(q_2) & M_2(q_2) \end{pmatrix}. \tag{3.1}$$

Here, $m_1(\cdot)$ is the scalar self-induced inertia term of coordinate q_1, and $M_{12}(\cdot) \in \mathbb{R}^{n-1}$ is the row vector of inertial cross-coupling terms between q_1 and coordinates q_2. Moreover, $M_2(\cdot) \in \mathbb{R}^{(n-1)\times(n-1)}$ is the symmetric positive-definite inertia submatrix of coordinates q_2. From the properties of inertia matrices [55], we know that inertia term m_1 is bounded above and below:

$$\underline{m}_1 \;<\; m_1(\cdot) \;<\; \overline{m}_1, \tag{3.2}$$

implying that

$$\frac{1}{\overline{m}_1} \;<\; \frac{1}{m_1(\cdot)} \;<\; \frac{1}{\underline{m}_1}, \tag{3.3}$$

for some constants such that $0 < \underline{m}_1 < \overline{m}_1 < \infty$.

Based on the definition (2.5), the first pair of canonical coordinates, (q_1, p_1), is related to the

Lagrangian coordinates by the momentum map:

$$\begin{aligned} p_1 &= \mathcal{J}_1(q,\dot{q}) := \begin{pmatrix} 1 & 0_{n-1} \end{pmatrix} M(q_2)\dot{q} \\ &= m_1(q_2)\dot{q}_1 + M_{12}(q_2)\dot{q}_2. \end{aligned} \tag{3.4}$$

Rearranging terms, this is equivalent to the first-order expression

$$\dot{q}_1 = \frac{1}{m_1(q_2)}(p_1 - M_{12}(q_2)\dot{q}_2). \tag{3.5}$$

The right-hand side of (3.5) is invariant under rotations of q_1. Moreover, (2.2) and (2.13) show that the rate of change in momentum p_1 is equal to the first control torque:

$$\frac{d}{dt}\frac{\partial \mathcal{L}}{\partial \dot{q}_1} = \frac{d}{dt}p_1 = u_1.$$

From the Hamiltonian perspective, $\partial \mathcal{H}/\partial q_1 = 0$ in (2.7) implies $\dot{p}_1 = u_1$. When control $u_1 = 0$, this establishes a momentum conservation law (p_1 is constant). Therefore, q_1 naturally evolves by (3.5) in one of infinitely many invariant sets $\{(q,\dot{q}) | \mathcal{J}_1(q,\dot{q}) = \mu\}$, depending on momentum constant μ.

Many systems have unactuated cyclic variables and actuated shape variables, such as the Acrobot [81, 82] constrained to the transverse plane (orthogonal to gravity) and bipedal runners in flight phase [40]. These underactuated systems similarly conserve an angular momentum quantity. This was exploited in [40] to construct a reduced system and derive conditions for the existence of a set of outputs yielding an empty zero dynamics. The authors further showed that a dynamic extension renders these underactuated systems feedback linearizable to provide controllability of the reduced system. A rotary spring attached between the fixed base and first link then breaks the momentum conservation law to stabilize the full-order system about an equilibrium. In the next section, we consider a slightly different approach, using passive *damping* in input u_1 to control the cyclic coordinate by replacing the existing conservation law with a new *functional* momentum law.

3.1.1 Passive-feedback control

Starting with some scalar linear function of the cyclic variable, $\lambda(q_1) = -c(q_1 - \tilde{q}_1)$ with $\tilde{q}_1$ and $c > 0$ constant, consider the passive-feedback control

$$u_1 \;=\; \frac{d}{dt}\lambda(q_1) \;=\; -c\dot{q}_1, \tag{3.6}$$

where $\frac{\partial \lambda}{\partial q_1} = -c$, implying that

$$\dot{p}_1 \;=\; -c\dot{q}_1. \tag{3.7}$$

Recall that (3.6) is the first term of feedback law $\gamma(\dot{q}) = -c\dot{q}$, which is associated with a scaled inverse-optimal solution. This non-zero u_1 violates conservation of angular momentum p_1.

At first glance, we see that this implies instantaneous mechanical power

$$\dot{\mathcal{H}} \;=\; \dot{q}^T\begin{pmatrix} -c\dot{q}_1 & 0_{n-1} \end{pmatrix} \;=\; -c(\dot{q}_1)^2 \;\leq\; 0, \tag{3.8}$$

so the system is trivially stable in the sense of Lyapunov and $\dot{q}_1$ converges to zero by Lemma 1. Further analysis shows that the generalized momentum now evolves according to

$$\begin{aligned} p_1(t) &= p_1(t_0) + \int_{t_0}^{t} \frac{\partial \lambda}{\partial q_1}\dot{q}_1(\tau)d\tau \\ &= p_1(t_0) + \frac{\partial \lambda}{\partial q_1}(q_1(t) - q_1(t_0)) \end{aligned}$$

by the fundamental theorem of calculus. Given initial boundary condition

$$p_1(t_0) \;=\; \lambda(q_1(t_0)), \tag{3.9}$$

it follows that

$$p_1(t) \;=\; \lambda(q_1(t)) \tag{3.10}$$

for all $t \geq t_0$.

Hence, passive control (3.6) produces the functional conservation law

$$\mathcal{J}_1(q,\dot{q}) \;=\; -c(q_1-\tilde{q}_1) \tag{3.11}$$

in phase space $T\mathcal{Q}$ for some choice of $\tilde{q}_1$ satisfying the initial boundary condition (3.9). Every initial condition has an associated conservation law, so we have generated infinitely many invariant submanifolds parameterized by $\tilde{q}_1$:

$$\mathcal{Z}_{\tilde{q}_1} \;=\; \{(q,\dot{q})|\mathcal{J}_1(q,\dot{q})+c(q_1-\tilde{q}_1)=0\}\,. \tag{3.12}$$

This is known as a *foliation* of the manifold $T\mathcal{Q}$ [83]. Given initial conditions in some $\mathcal{Z}_{\tilde{q}_1}$, (3.4)-(3.5) show that trajectories satisfy the constraint equation

$$\dot{q}_1 \;=\; \frac{-c}{m_1(q_2)}(q_1-\tilde{q}_1)-\frac{1}{m_1(q_2)}M_{12}(q_2)\dot{q}_2, \tag{3.13}$$

depending on *almost-cyclic* variable q_1. This constraint is not invariant under the rotating action of the cyclic coordinate group – the new conservation law does not possess the symmetry. This will be related to the typical notion of breaking Lagrangian invariance in Section 3.2.

Integral curves $(q_1(t),\dot{q}_1(t))$ and $(q_2(t),\dot{q}_2(t))$ typically must be solved simultaneously in system (2.3), so constraint equation (3.13) is nonholonomic (non-integrable). However, given some assumptions on reduced coordinate pair $(q_2,\dot{q}_2)$, e.g., properties provided by reduction, we can show several stability results for the first DOF based on negative-gain linearity in constraint equation (3.13). It will be convenient to express these results in terms of the first canonical pair (q_1,p_1) in the phase space $T^*\mathcal{Q}$ projected onto $T^*\mathbb{S}^1$, where we can define invariant surface $\mathcal{D}_{\tilde{q}_1}=\{(q_1,p_1)\mid p_1+c(q_1-\tilde{q}_1)=0\}$ from (3.11). Since $\mathcal{D}_{\tilde{q}_1}$ defines a bijective mapping between canonical coordinates q_1 and p_1, (3.13) is equivalent to constraint equation

$$\dot{p}_1 \;=\; \frac{-c}{m_1(q_2)}p_1+\frac{c}{m_1(q_2)}M_{12}(q_2)\dot{q}_2. \tag{3.14}$$

3.1.2 Special case without inertial cross-coupling

When $M_{12}(\cdot)\equiv 0$, some immediate properties of these subsystems follow:

Lemma 3. Given $M_{12}(\cdot)\equiv 0$, $q_1=\tilde{q}_1$ is the unique equilibrium point of (3.13). Equivalently,

$p_1 = 0$ is the unique equilibrium point of (3.14). Moreover, $(\tilde{q}_1, 0) \in \mathcal{D}_{\tilde{q}_1}$.

Proof. The LTV gains of (3.13)-(3.14) are strictly bounded away from zero by (3.3), so it is clear that $q_1 = \tilde{q}_1$, $p_1 = 0$ are the unique equilibrium points for their respective systems. The equivalence implication is provided by the bijective mapping of $p_1 = \lambda(q_1) = -c(q_1 - \tilde{q}_1)$. Finally, $\lambda(\tilde{q}_1) = 0$ shows the last claim. □

Standard results for LTV systems (cf. [8]) show that subsystems (3.13)-(3.14) are stable about their respective equilibrium points:

Theorem 2. Given $M_{12}(\cdot) \equiv 0$, (3.13) is asymptotically stable (AS) about $q_1 = \tilde{q}_1$ and (3.14) is AS about $p_1 = 0$, i.e., $\lim_{t\to\infty}(q_1(t), p_1(t)) = (\tilde{q}_1, 0)$ for any $(q_1(t_0), p_1(t_0)) \in \mathcal{D}_{\tilde{q}_1}$. Moreover, these coordinates converge exponentially fast; i.e., there exist constants $k, \alpha > 0$ such that

$$\begin{aligned} |q_1(t) - \tilde{q}_1| &\leq k e^{-\alpha(t-t_0)} |q_1(t_0) - \tilde{q}_1| \\ |p_1(t)| &\leq k e^{-\alpha(t-t_0)} |p_1(t_0)| \end{aligned}$$

for all $t \geq t_0$.

Proof. When $\dot{q}_1 \equiv 0$ and $M_{12}(\cdot) \equiv 0$, (3.5) $\iff$ $p_1 = \mathcal{J}_1(q, \dot{q}) = 0$. The set

$$\{(q, \dot{q}) \mid \mathcal{J}_1(q, \dot{q}) = 0, \dot{q}_1 = 0\}$$

is attractive by Lemma 1 and LaSalle's invariance principle [8, 54]. Moreover, in set $\mathcal{D}_{\tilde{q}_1}$ we have $p_1 = 0 \iff q_1 = \tilde{q}_1$ by Lemma 3, so (3.13)-(3.14) must be AS about these points.

In order to prove exponential convergence, we first set $\tilde{q}_1 = 0$ without loss of generality. Although $\frac{c}{m_1(q_2(t))}$ is time-varying, we can bound it within $(\frac{c}{\overline{m}_1}, \frac{c}{\underline{m}_1})$. Thus, we can bound solutions of LTV system

$$\dot{q}_1(t) = -\frac{c}{m_1(q_2(t))} q_1(t), \quad q_1(t_0) = q_0 \tag{3.15}$$

above by solutions of LTI system

$$\dot{\overline{q}}_1(t) = -\frac{c}{\overline{m}_1} \overline{q}_1(t), \quad \overline{q}_1(t_0) = q_0. \tag{3.16}$$

Since (3.16) is globally exponentially stable (GES), we have $|q_1(t)| \leq |\overline{q}_1(t)| = e^{-(c/\overline{m}_1)(t-t_0)}|q_0|$. Hence, $q_1(t) \to 0$ exponentially fast as $t \to \infty$. The same proof applies for ES of (3.14) about $p_1 = 0$. □

Note that each system is separately GES, but the solution of one system uniquely implies the solution to the other by (3.10). Thus, this canonical pair is ES in domain $\mathcal{D}_{\tilde{q}_1}$, i.e., GES *conditionally to* $\mathcal{D}_{\tilde{q}_1}$ in terms of [54].

3.1.3 General case with inertial cross-coupling

The case with inertial cross-coupling $M_{12}(\cdot)$ does not have trivial equilibrium points as in the special case of Lemma 3, so we will need certain behavior in the reduced subsystem to prove stability for the cyclic coordinate. If we apply passive feedback $u = -c\dot{q}$ to the overall system, noting that (3.6) is the first control term, we can show more than the classical results of Lyapunov stability and $\dot{q} \to 0$.

Theorem 3. Given q_1 cyclic and overall control law $u = -c\dot{q}$ for system (2.3), subsystem (3.13) is AS about $q_1 = \tilde{q}_1$ and subsystem (3.14) is AS about $p_1 = 0$ for any $(q_1(t_0), p_1(t_0)) \in \mathcal{D}_{\tilde{q}_1}$.

Proof. Asymptotic stability is equivalent to stability in the sense of Lyapunov plus asymptotic convergence. The cross-coupling term in (3.13) can be interpreted as a disturbance to the LTV system (3.15), which is ES by Theorem 2. The passive feedback law provides $\dot{q}_2 \to 0$, implying that disturbance $d(t) = -\frac{1}{m_1(q_2(t))} M_{12}(q_2(t))\dot{q}_2(t)$ converges to zero asymptotically (M_{12} is bounded for revolute q_2). Moreover, asymptotically stable LTV systems satisfy the convergent-input convergent-state (CICS) property, i.e., $d(t) \to 0 \implies q_1(t) \to 0$. This, coupled with Lyapunov stability from Lemma 1, proves AS of (3.13) about $q_1 = \tilde{q}_1$, and the same proof applies for subsystem (3.14). □

Conversely, we can determine the infinite-horizon end condition for any given initial condition without integration by $q_1(t_\infty) = \frac{-1}{c} p_1(t_0) + q_1(t_0)$. Hence, the geometric structure provided by symmetry allows passive feedback to (optimally) control cyclic variables to set-points, which are known *a priori*. We can use this fact to globally stabilize set-points by making desired $\mathcal{Z}_{\tilde{q}_1}$ globally attractive in Section 4.4.

3.1.4 Creating limit cycles

If the objective is instead to produce periodic limit cycles, such as gait patterns for locomotion, we must have different behavior in the reduced-order subsystem (e.g., $\dot{q}_2$ does not converge to zero). We again choose $u_1 = -c\dot{q}_1$ but leave u_2 free. This latter input may break the negative-definite power inequality (3.8) that provides $\dot{q}_1 \to 0$, allowing us to create periodic trajectories. We now assume a special property associated with geometric reduction:

Assumption 1. There exists a reduced solution operator $\Psi_2^t\left(q_2(0), \dot{q}_2(0)\right) = \left(q_2(t), \dot{q}_2(t)\right)$. I.e., reduced integral curves can be solved independent of coordinates $(q_1, \dot{q}_1)$.

This implies that constraint equations (3.13)-(3.14) of the first DOF are now *integrable* (by first solving the reduced subsystem curves). Therefore, these equations become first-order LTV systems that can be controlled based on our choice of λ-function. If the time-varying disturbance introduced by cross-coupling is periodic, we will find closed orbits in neighborhoods around $q_1 = \tilde{q}_1$ and $p_1 = 0$.

Assumption 2. Reduced coordinates are T-periodic, i.e., $q_2(t+T) = q_2(t)$ and $\dot{q}_2(t+T) = \dot{q}_2(t)$, $\forall t \geq t_0$.

Theorem 4. Given A1 and A2, system (3.13) has a unique T-periodic solution $q_1^*(t)$ and system (3.14) has a unique T-periodic solution $p_1^*(t)$. Moreover, these solutions are exponentially stable in $\mathcal{D}_{\tilde{q}_1}$; i.e., there exist constants $k, \alpha > 0$ such that for any $(q_1(t_0), p_1(t_0)) \in \mathcal{D}_{\tilde{q}_1}$,

$$\begin{aligned} |q_1(t) - q_1^*(t)| &\leq k e^{-\alpha(t-t_0)} |q_1(t_0) - q_1^*(t_0)| \\ |p_1(t) - p_1^*(t)| &\leq k e^{-\alpha(t-t_0)} |p_1(t_0) - p_1^*(t_0)| \end{aligned}$$

for all $t \geq t_0$.

Proof. We first set $\tilde{q}_1 = 0$ without loss of generality. A1-A2 allow us to consider (3.15) as a homogenous linear differential equation with T-periodic coefficients. Since (3.15) admits a unique equilibrium point solution, it is well-known that system (3.13), having an additional T-periodic disturbance, admits a unique T-periodic solution $q_1^*(t)$ [84]. We can then easily verify that $e(t) = q_1(t) - q_1^*(t)$ is a solution to homogenous (3.15), from which Theorem 2 implies $e(t)$ is GES about zero. Conditionally to $\mathcal{D}_{\tilde{q}_1}$, the bijective mapping of (3.10) gives the unique, ES, and T-periodic solution $p_1^*(t)$ to (3.14). □

Note that any periodic solution evolves in an invariant compact subset of the phase space called a periodic orbit. We will consider orbital stability as defined in Section 1.1.2 when constructing bipedal walking gaits in Chapter 5.

Theorem 4 shows that periodicity (or equilibrium) in reduced-order phase space $T\mathcal{Q}$ mod $T\mathbb{S}^1$ implies periodicity (or equilibrium) in $(q_1, p_1) \in T^*\mathbb{S}^1$. In terms of the Lagrangian formulation, we can say the following:

Proposition 2. Given A1 and A2, if the first canonical coordinate pair of (2.7) has a unique T-periodic solution $(q_1^*(t), p_1^*(t))$, then the first Lagrangian coordinate pair of (2.4) has a unique T-periodic solution $(q_1^*(t), \dot{q}_1^*(t))$.

This immediately follows from the periodicity of the right-hand-side of (3.5). Hence, we can produce periodic (or equilibrium) solutions in full-order phase space $T\mathcal{Q}$ or, equivalently, $T^*\mathcal{Q}$.

Proposition 3. There exists a unique T-periodic solution $(q^*(t), p^*(t))$ of (2.7) if and only if there exists a unique T-periodic solution $(q^*(t), \dot{q}^*(t))$ of (2.4).

Proof. By definition, we have $p = M(q)\dot{q} \iff \dot{q} = M(q)^{-1}p$. Recalling that $M(q)$ is positive-definite (and in this case, T-periodic), the claim immediately follows. □

In fact, we can refine A2 to account for transient behavior in the subsystem, where the coordinates are instead convergent to periodic trajectories:

Assumption 3. Reduced coordinates are asymptotically convergent to T-periodic, bounded solution $(q_2^*(t), \dot{q}_2^*(t))$.

Lemma 4. Given A1 and A3, system (3.14) is asymptotically convergent to unique, T-periodic, and bounded solution $p_1^*(t)$. Equivalently, (3.13) is asymptotically convergent to unique, T-periodic, and bounded solution $q_1^*(t)$.

Proof. T-periodic solution $(q_2^*(t), \dot{q}_2^*(t))$ yields T-periodic parameters in system (3.14) and thus a T-periodic solution $p_1^*(t)$ by Theorem 4. We can rewrite this nominal system as $\dot{z}^*(t) = -A^*(t)z^*(t) + B^*(t)$, where state $z^*(t) = p_1^*(t)$ and $A^*(t) > 0$, $B^*(t)$ are T-periodic and bounded. However, given transient trajectories $(q_2(t), \dot{q}_2(t))$, system (3.14) will not immediately have periodic dynamics or a periodic solution. Defining state $z(t) = p_1(t)$, this system can be rewritten as $\dot{z}(t) = -A(t)z(t) + B(t)$, for transient parameters $A(t) > 0$ and $B(t)$, where A3 implies that $A(t) \to A^*(t)$ and

$B(t) \to B^*(t)$ as $t \to \infty$. If we define the error from the nominal solution as $e(t) = z^*(t) - z(t)$, we have the error dynamics

$$\begin{aligned}
\dot{e}(t) &= -A^*(t)z^*(t) + B^*(t) + A(t)z(t) - B(t) \\
&= -A^*(t)z^*(t) + A(t)z^*(t) - A(t)e(t) + B^*(t) - B(t) \\
&= -A(t)e(t) + (A(t) - A^*(t))z^*(t) + (B^*(t) - B(t)) \\
&= -A(t)e(t) + v(t),
\end{aligned}$$

where input $v(t)$ converges asymptotically to zero by A3 (note that $z^*(t)$ is bounded by Theorem 4). We know that $A(t)$ is positive-definite and bounded by (3.2), so this is a zero-input GES LTV system. By the CICS property we have $v(t) \to 0 \implies e(t) \to 0$, implying that $p_1(t) \to p_1^*(t)$, or equivalently, $q_1(t) \to q_1^*(t)$. □

Theorem 5. Given A1 and subsystem control (3.6), asymptotic stability about a T-periodic solution $(q_2^*(t), \dot{q}_2^*(t))$ in reduced-order phase space $T\mathcal{Q}$ mod $T\mathbb{S}^1$ implies asymptotic stability about a T-periodic solution $(q^*(t), \dot{q}^*(t))$ in phase space $T\mathcal{Q}$ conditionally to $\mathcal{Z}_{\tilde{q}_1}$.

Proof. We know that control (3.6) provides Lyapunov stability by Lemma 1. Also, A1 and asymptotic stability in the subsystem provides A3, yielding asymptotic convergence in $(q_1(t), p_1(t)) \in \mathcal{D}_{\tilde{q}_1}$ toward T-periodic solution $(q_1^*(t), p_1^*(t))$ by Lemma 4. This is equivalent to asymptotic convergence toward a T-periodic solution $(q_1^*(t), \dot{q}_1^*(t))$ in Lagrangian coordinates by Proposition 2. Hence, the first pair is asymptotically stable, providing asymptotic stability in the overall system on $T\mathcal{Q}$ conditionally to $\mathcal{Z}_{\tilde{q}_1}$. Moreover, if the subsystem has exponentially fast convergence, the overall system will be exponentially stable conditionally to $\mathcal{Z}_{\tilde{q}_1}$. □

We have shown that passive feedback in the presence of symmetry provides full-order stability (conditionally to $\mathcal{Z}_{\tilde{q}_1}$) from a minimum phase property [8]. We will later show that the invariant set $\mathcal{Z}_{\tilde{q}_1}$ can be made attractive using output linearization, allowing these stability results to hold globally. However, we first design a controlled reduction based on this control framework to provide A1 and A3 for generating limit cycles.

3.2 Almost-Cyclic Lagrangians

In order to invoke Theorem 5, we construct a control law for system (2.4) such that the following claims hold:

Claim 1. $\mathcal{Z}_{\tilde{q}_1}$ is an invariant surface of closed-loop system (2.4).

Claim 2. The restriction of closed-loop dynamics (2.3) to $\mathcal{Z}_{\tilde{q}_1}$ can be given by

$$M_2(q_2)\ddot{q}_2 + C_2(q_2, \dot{q}_2)\dot{q}_2 + N(q_2) \quad = \quad v_2, \tag{3.17}$$

where C_2 is the Coriolis matrix derived from inertia submatrix M_2, and v_2 is some auxiliary input.

These claims, particularly the decoupling of reduced system (3.17), satisfy A1 and enable the stability results of Section 3.1. Therefore, we wish to break Lagrangian invariance in a manner that establishes constraint (3.11) for Claim 1, so as to allow geometric reduction with respect to this conservation law. This reduction will define a projection map from phase space $T\mathcal{Q} = T\mathbb{T}^n$ onto reduced space $T\mathbb{T}^{n-1} \cong T\mathbb{T}^n \bmod T\mathbb{S}^1$, on which the decoupled subsystem (3.17) is defined and can be stabilized by designing an appropriate controller $v_2(q_2, \dot{q}_2)$. We will see that the overall *reduction-based* control law is fundamentally related to passive control (3.6).

In particular, we want to control the mechanical system so that its closed-loop dynamics correspond to a special type of controlled Lagrangian that depends on the cyclic variable through conserved momentum function $\lambda(q_1)$. We adopt the shaping terms presented in [49], which we will show provide Claims 1-2.

Definition 8. Given Lagrangian $\mathcal{L}$ that is cyclic in q_1, the corresponding *almost-cyclic* Lagrangian $\mathcal{L}_\lambda : T\mathbb{S}^1 \times T\mathbb{T}^{n-1} \to \mathbb{R}$ is defined, in coordinates, as

$$\begin{aligned}
\mathcal{L}_\lambda(q, \dot{q}) \quad &:= \quad \mathcal{K}(q_2, \dot{q}) - \mathcal{V}(q_2) + \mathcal{L}_\lambda^{\text{aug}}(q, \dot{q}) \\
&= \quad \mathcal{K}_\lambda(q, \dot{q}) + Q_\lambda^T(q)\dot{q} - \mathcal{V}_\lambda(q) \\
&= \quad \frac{1}{2}\dot{q}^T M_\lambda(q_2)\dot{q} + Q_\lambda^T(q)\dot{q} - \mathcal{V}_\lambda(q),
\end{aligned}$$

where the shaped energy terms are defined as

$$M_\lambda(q_2) = M(q_2) + \begin{pmatrix} 0 & 0 \\ 0 & \frac{M_{12}^T(q_2)M_{12}(q_2)}{m_1(q_2)} \end{pmatrix} \tag{3.18}$$

$$Q_\lambda(q) = \begin{pmatrix} 0 & -\frac{\lambda(q_1)}{m_1(q_2)}M_{12}(q_2) \end{pmatrix}^T \tag{3.19}$$

$$\mathcal{V}_\lambda(q) = \mathcal{V}(q_2) - \frac{1}{2}\frac{\lambda(q_1)^2}{m_1(q_2)}. \tag{3.20}$$

Remark 1. The almost-cyclic Lagrangian (ACL) is not invariant under the rotating action of the cyclic variable's symmetry group, due to the energy augmenting terms in $\mathcal{L}_\lambda^{\text{aug}}$ that depend on $\lambda(q_1)$. This contains *gyroscopic* terms $Q_\lambda^T\dot{q}$ that model external forces imposed by our controller in the E-L system (cf. [59]). Although these terms store no energy (much like a damper), it is convenient to include them in the ACL for our analysis (allowing the auxiliary input to be defined independent of the shaping control). In the case without inertial cross-coupling, we see $Q_\lambda = 0$, $M_\lambda = M \;\Leftrightarrow\; \mathcal{K}_\lambda = \mathcal{K}$, implying that $\mathcal{L}_\lambda$ is obtained through potential energy shaping.

Remark 2. The choice of M_λ is based on the *Schur complement* of block m_1 in matrix M, which is defined as $\text{schur}(M, m_1) = M_2 - M_{12}^T m_1^{-1} M_{12}$ [85]. Therefore, the inertia shaping is chosen such that $\text{schur}(M_\lambda, m_1) = M_2$.

Proposition 4. $\mathcal{K}_\lambda(q_2, \dot{q}_1, \dot{q}_2)$ is lower-bounded by reduced $\mathcal{K}_2(q_2, \dot{q}_2) = \frac{1}{2}\dot{q}_2^T M_2(q_2)\dot{q}_2$.

Proof. Given that $\mathcal{K}_\lambda$ is quadratic in $\dot{q}$, it is shown in [85] that

$$\inf_{\dot{q}_1} \mathcal{K}_\lambda(q_2, \dot{q}_1, \dot{q}_2) = \frac{1}{2}\dot{q}_2^T \text{schur}(M_\lambda, m_1)\dot{q}_2 = \frac{1}{2}\dot{q}_2^T M_2(q_2)\dot{q}_2.$$

Since $\mathcal{K}_\lambda$ is cyclic in q_1, we also have $\inf_{(q_1,\dot{q}_1)} \mathcal{K}_\lambda = \mathcal{K}_2$, implying $\mathcal{K}_\lambda \geq \mathcal{K}_2$ for all $(q, \dot{q})$. □

This offers a meaningful physical interpretation of the controlled reduction, where the underlying subsystem kinetic energy $\mathcal{K}_2$ is fundamental to the shaped dynamics. We will show in Section 3.4 that the decoupling provided on surface $\mathcal{Z}_{\tilde{q}_1}$ results in equality between related energy quantities.

Given full actuation, the (symmetry-breaking) feedback transformation of $\mathcal{L}$ into $\mathcal{L}_\lambda$ is achieved with *reduction-based* control law

$$u^\lambda(q, \dot{q}) := C(q, \dot{q})\dot{q} + N(q) + M(q)M_\lambda(q)^{-1}\left(-C_\lambda(q, \dot{q})\dot{q} - N_\lambda(q) + v\right), \tag{3.21}$$

where $N_\lambda = \nabla_q \mathcal{V}_\lambda$ is the vector of almost-cyclic potential torques and vector v is the auxiliary control input. We find it convenient to combine the shaped Coriolis and gyroscopic matrices in $C_\lambda = C_{M_\lambda} + C_{Q_\lambda}$, where Coriolis matrix C_{M_λ} is derived from M_λ as usual and the gyroscopic forces are given by $C_{Q_\lambda}(q)\dot{q} = \frac{d}{dt}\nabla_{\dot{q}}[Q_\lambda^T(q)\dot{q}] - \nabla_q[Q_\lambda^T(q)\dot{q}]$. This latter term is linear in $\dot{q}$ and skew-symmetric [49], so the important properties of a typical Coriolis matrix still hold for C_λ (e.g., we will later exploit the skew-symmetry of $\dot{M}_\lambda - 2C_\lambda$).

Remark 3. The Schur complement can also be used for blockwise inversion of M_λ, resulting in the expression

$$M_\lambda^{-1}(q_2) = \begin{pmatrix} m_1^{-1}(q_2) + m_1^{-2}(q_2)M_{12}(q_2)M_2^{-1}(q_2)M_{12}^T(q_2) & -m_1^{-1}(q_2)M_{12}(q_2)M_2^{-1}(q_2) \\ -m_1^{-1}(q_2)M_2^{-1}(q_2)M_{12}^T(q_2) & M_2^{-1}(q_2) \end{pmatrix}.$$

It follows that $\begin{pmatrix} 1 & 0_{n-1} \end{pmatrix} M(q) M_\lambda(q)^{-1} = \begin{pmatrix} 1 & 0_{n-1} \end{pmatrix}$, and further calculation shows the first element of control law (3.21) constrained to (3.11) reduces to passive-feedback control (3.6) from Section 3.1:

$$\begin{aligned} \begin{pmatrix} 1 & 0_{n-1} \end{pmatrix} u^\lambda(q,\dot{q})\Big|_{\mathcal{Z}_{\tilde{q}_1}} &= \begin{pmatrix} 1 & 0_{n-1} \end{pmatrix} [C(q,\dot{q})\dot{q} + N(q) - C_\lambda(q,\dot{q})\dot{q} - N_\lambda(q) + v]\Big|_{\mathcal{Z}_{\tilde{q}_1}} \\ &= -c\dot{q}_1 + v_1. \end{aligned}$$

This renders surface $\mathcal{Z}_{\tilde{q}_1}$ invariant (when $v_1 = 0$) by the same argument providing (3.11), thus satisfying Claim 1. Moreover, this passive feedback law can be implemented mechanically, so the desired feedback transformation can be achieved on mechanical systems with one degree of underactuation.

Remark 4. Although (3.21) appears to invert the dynamics, we reinsert the original dynamics *in addition* to shaping terms in (3.18)-(3.20). We will show that these closed-loop dynamics restricted to surface $\mathcal{Z}_{\tilde{q}_1}$ cancel the nonlinearities needed to decouple subsystem (3.17). Since most of the natural nonlinearities are preserved, we can use orthogonal nullspace projection to express this controller in terms of lower-dimensional matrix inverses [80]. In some cases, the feedback transformation may be achievable for underactuated systems without mechanical dampers, based on energy *matching conditions* from [58, 59].

Now, plugging (3.21) into the control input of (2.3), we have the shaped closed-loop dynamics

$$M_\lambda(q)\ddot{q} + C_\lambda(q,\dot{q})\dot{q} + N_\lambda(q) \quad = \quad v \tag{3.22}$$

from the E-L equations[1] of $\mathcal{L}_\lambda$. We also have the associated control system (f_λ, g_λ) on $T\mathcal{Q}$ with input v, derived as in (2.4). The auxiliary control can be decomposed into the first input v_1 and subsystem input v_2. Assuming v_2 is defined by a time-invariant feedback control law on $T\mathbb{T}^{n-1}$, we incorporate this into the full-order ACL system by defining the new control system $(\hat{f}_\lambda, \hat{g}_\lambda)$ with input v_1:

$$\begin{aligned} \hat{f}_\lambda(q,\dot{q}) &:= f_\lambda(q,\dot{q}) + g_\lambda(q)\begin{pmatrix} 0 \\ v_2(q_2,\dot{q}_2) \end{pmatrix} \\ \hat{g}_\lambda(q) &:= g_\lambda(q)\begin{pmatrix} 1 \\ 0_{n-1\times 1} \end{pmatrix}. \end{aligned} \tag{3.23}$$

Here, vector field $\hat{f}_\lambda$ corresponds to the v_2-controlled E-L equations, which will be relevant later.

3.3 Reduced Subsystem

We achieve subsystem decoupling by geometric reduction with respect to functional conservation law (3.11). The reduction is obtained through a change of coordinates yielding a Lagrangian function associated with the reduced-order subsystem.

Definition 9. Let Lagrangian $\mathcal{L}$ be shaped into corresponding ACL $\mathcal{L}_\lambda$. Then, the *functional Routhian* $\mathcal{R}_\lambda : T\mathbb{T}^{n-1} \to \mathbb{R}$ is defined from $\mathcal{L}_\lambda$ by a partial Legendre transformation in coordinate q_1, constrained to (3.11):

$$\begin{aligned} \mathcal{R}_\lambda(q_2,\dot{q}_2) &:= [\mathcal{L}_\lambda(q,\dot{q}) - \lambda(q_1)\dot{q}_1]|_{\mathcal{J}_1(q,\dot{q})=\lambda(q_1)} \\ &= \frac{1}{2}\dot{q}_2^T M_2(q_2)\dot{q}_2 - \mathcal{V}(q_2). \end{aligned} \tag{3.24}$$

This transformation eliminates coordinates $(q_1, \dot{q}_1)$ from the Lagrangian formulation, where the bottom expression is exactly the Lagrangian of the n-DOF system with the first DOF fixed. We

[1]Given the gyroscopic terms, ACL $\mathcal{L}_\lambda$ has the general form of Lagrangian defined in [59] and thus preserves closed-loop E-L structure.

call this the $(n-1)$-DOF *subrobot* corresponding to the original system. After this reduction, the divided coordinates are expressed in terms of the conjugate momentum through integrable constraint equation (3.11), allowing reconstruction of full-order curves on $T\mathcal{Q}$ from reduced-order curves on $T\mathbb{T}^{n-1}$ by integrating (3.13) from the initial conditions. We can now prove Claim 2.

Proposition 5. The closed-loop E-L equations of $\mathcal{L}_\lambda$ restricted to $\mathcal{Z}_{\tilde{q}_1}$ are given by subsystem dynamics (3.17), i.e.,

$$\mathscr{EL}_{q_2}\left\{\mathcal{L}_\lambda(q,\dot{q})\right\}|_{\mathcal{Z}_{\tilde{q}_1}} \quad = \quad \mathscr{EL}_{q_2}\left\{\mathcal{R}_\lambda(q_2,\dot{q}_2)\right\}. \tag{3.25}$$

Proof. No natural terms in $\mathcal{L}$ are explicitly canceled by $\mathcal{L}_\lambda^{\text{aug}}$, so ACL $\mathcal{L}_\lambda$ can be expressed in terms of $\mathcal{R}_\lambda$ and remainder terms grouped in function Rem:

$$\mathcal{L}_\lambda(q_1,q_2,\dot{q}_1,\dot{q}_2) \quad = \quad \mathcal{R}_\lambda(q_2,\dot{q}_2) + \text{Rem}(q_1,q_2,\dot{q}_1,\dot{q}_2).$$

The shaping terms of $\mathcal{L}_\lambda$ are designed such that the E-L equations of Rem are zeroed on $\mathcal{Z}_{\tilde{q}_1}$:

$$\mathscr{EL}_{q}\left\{\text{Rem}(q,\dot{q})\right\}|_{\mathcal{Z}_{\tilde{q}_1}} \quad = \quad 0,$$

implying the restricted E-L equations (3.25), which are equivalent to (3.17) of the $(n-1)$-DOF subrobot. □

Therefore, Routhian $\mathcal{R}_\lambda$ yields the subrobot's control system $(f_{\mathcal{R}_\lambda}, g_{\mathcal{R}_\lambda})$ on reduced phase space $T\mathbb{T}^{n-1}$ with input v_2. We can then define v_2 with feedback from $(q_2,\dot{q}_2)$ to stabilize this subsystem about set-points or periodic orbits, thus satisfying A3. Given such a control law, we characterize the closed-loop reduced dynamics with vector field

$$\hat{f}_{\mathcal{R}_\lambda}(q_2,\dot{q}_2) \quad := \quad f_{\mathcal{R}_\lambda}(q_2,\dot{q}_2) + g_{\mathcal{R}_\lambda}(q_2)v_2(q_2,\dot{q}_2). \tag{3.26}$$

Given $v_1 = 0$ and conservation law (3.11), Proposition 5 implies that there exists a map between solutions of $\hat{f}_\lambda$ and solutions of $\hat{f}_{\mathcal{R}_\lambda}$ (the full proof is given for the more general multistage case in Appendix B).

Theorem 6. Let $\mathcal{L}_\lambda$ be an ACL with functional Routhian $\mathcal{R}_\lambda$. Then, $(q_1(t),q_2(t),\dot{q}_1(t),\dot{q}_2(t))$ is an integral curve to closed-loop vector field $\hat{f}_\lambda$ on $[t_0,t_f]$ satisfying initial boundary condition

$\mathcal{J}_1(q(t_0), \dot{q}(t_0)) = \lambda(q_1(t_0))$, if and only if $(q_2(t), \dot{q}_2(t))$ is an integral curve to closed-loop vector field $\hat{f}_{\mathcal{R}_\lambda}$ on $[t_0, t_f]$ and $(q_1(t), q_2(t), \dot{q}_1(t), \dot{q}_2(t))$ satisfies $\mathcal{J}_1(q(t), \dot{q}(t)) = \lambda(q_1(t))$ on $[t_0, t_f]$.

Remark 5. In other words, robot system (2.4) is said to be *feedback-reducible* to the corresponding $(n-1)$-DOF subrobot. Reduced integral curves $(q_2(t), \dot{q}_2(t))$ can be solved independently as stated in A1. Assumptions A2-A3 simply depend on the behavior of the reduced subsystem (3.17), enabling the application of Lemma 4 to show stability of divided coordinates $(q_1, \dot{q}_1)$ and Theorem 5 to consequently show stability of the overall system.

Remark 6. Auxiliary control v_1 can be used to accommodate initial conditions outside the desired invariant surface $\mathcal{Z}_{\tilde{q}_1}$, e.g., correcting for constraint violations when changing the set-point $\tilde{q}_1$ to track a piecewise constant trajectory. Noting that $\mathcal{Z}_{\tilde{q}_1}$ is the zero level-set of scalar output function $h(q, \dot{q}) := \mathcal{J}_1(q, \dot{q}) - \lambda(q_1)$, we can use output linearization to render this surface globally attractive. For $(q(t_0), \dot{q}(t_0)) \in \mathcal{Z}_{\tilde{q}_1}$, i.e., $h(q, \dot{q}) \equiv 0$, we necessarily have $v_1 \equiv 0$ to invoke Theorem 6 associated with these zero dynamics. We derive such a controller in Section 4.4 for the general case of controlled reduction by stages.

3.4 Almost-Cyclic Hamiltonians

Based on the Lagrangian shaping that defines ACL $\mathcal{L}_\lambda$, we can prove many beneficial properties by studying the analogous almost-cyclic Hamiltonian (ACH). We first redefine the generalized momenta for the shaped system:

$$\begin{aligned} \widehat{p} \;=\; \widehat{\mathcal{J}}(q, \dot{q}) \;&:=\; \nabla_{\dot{q}} \mathcal{L}_\lambda(q, \dot{q}) \\ &=\; M_\lambda(q)\dot{q} + Q_\lambda(q). \end{aligned} \tag{3.27}$$

Note that $\nabla_{\dot{q}_1} \mathcal{L} = \nabla_{\dot{q}_1} \mathcal{L}_\lambda \implies p_1 = \widehat{p}_1$, so we consider the same functional conservation law (3.11) and invariant surface (3.12), i.e., $\mathcal{J}_1(q, \dot{q}) = \widehat{\mathcal{J}}_1(q, \dot{q}) = \lambda(q_1)$. Now, the ACH can easily be expressed in the form given in [59].

Definition 10. Given Hamiltonian $\mathcal{H}$ cyclic in q_1, the corresponding *almost-cyclic* Hamiltonian $\mathcal{H}_\lambda : T^*\mathbb{S}^1 \times T^*\mathbb{T}^{n-1} \to \mathbb{R}$ is defined, in canonical coordinates $(q, \widehat{p})$, as

$$\mathcal{H}_\lambda(q, \widehat{p}) \;=\; \frac{1}{2}\widehat{p}^T M_\lambda^{-1}(q)\widehat{p} - Q_\lambda^T(q) M_\lambda^{-1}(q)\widehat{p} + Q_\lambda^T(q) M_\lambda^{-1}(q) Q_\lambda(q) + \mathcal{V}_\lambda(q). \tag{3.28}$$

As we saw with the ACL, $\mathcal{H}_\lambda$ is not invariant under the cyclic coordinate's group action due to dependence on $\lambda(q_1)$. Therefore, symmetry is broken in the associated PDEs

$$\begin{pmatrix} \dot{q} \\ \dot{\widehat{p}} \end{pmatrix} = \begin{pmatrix} 0_{n\times n} & I_{n\times n} \\ -I_{n\times n} & 0_{n\times n} \end{pmatrix} \begin{pmatrix} \nabla_q \mathcal{H}_\lambda \\ \nabla_{\widehat{p}} \mathcal{H}_\lambda \end{pmatrix} + \begin{pmatrix} 0_{n\times 1} \\ v \end{pmatrix} \tag{3.29}$$

which are equivalent to ACL system (3.22). We also have the following dual relationship between the ACL and ACH by the Legendre transformation:

$$\mathcal{H}_\lambda(q,\widehat{p}) = \left[\widehat{p}^T\dot{q} - \mathcal{L}_\lambda(q,\dot{q})\right]\big|_{\widehat{p}=\widehat{\mathcal{J}}(q,\dot{q})} \tag{3.30}$$

$$\mathcal{L}_\lambda(q,\dot{q}) = \left[\widehat{p}^T\dot{q} - \mathcal{H}_\lambda(q,\widehat{p})\right]\big|_{\widehat{p}=\widehat{\mathcal{J}}(q,\dot{q})}. \tag{3.31}$$

3.4.1 Reduced Hamiltonian

Returning now to functional conservation law (3.11), definition (3.27) of the conjugate coordinates allows a simplified expression for the reduced subsystem's momentum map:

$$\begin{aligned} \widehat{\mathcal{J}}_2(q,\dot{q})\Big|_{\mathcal{Z}_{\tilde{q}_1}} &= \nabla_{\dot{q}_2}\mathcal{L}_\lambda(q,\dot{q})|_{\mathcal{Z}_{\tilde{q}_1}} \\ &= M_2(q_2)\dot{q}_2. \end{aligned} \tag{3.32}$$

Therefore, the full momentum map constrained to $\mathcal{Z}_{\tilde{q}_1}$ is given by

$$\widehat{\mathcal{J}}(q,\dot{q})\Big|_{\mathcal{Z}_{\tilde{q}_1}} = M_{\mathcal{Z}}(q_2)\dot{q}, \tag{3.33}$$

with simplified inertia matrix

$$M_{\mathcal{Z}}(q_2) = \begin{pmatrix} m_1(q_2) & M_{12}(q_2) \\ 0 & M_2(q_2) \end{pmatrix}. \tag{3.34}$$

This constrained momentum map will be helpful for studying the reduced subsystem. The reduced Hamiltonian $\mathcal{H}_{\mathcal{R}_\lambda}$ corresponding to functional Routhian $\mathcal{R}_\lambda$ is obtained in reduced-order

canonical coordinates of $T^*\mathbb{T}^{n-1}$ by

$$\begin{aligned}\mathcal{H}_{\mathcal{R}_\lambda}(q_2,\widehat{p}_2) &= \left[\widehat{p}_2^T\dot{q}_2 - \mathcal{R}_\lambda(q_2,\dot{q}_2)\right]\big|_{\widehat{p}_2=M_2(q_2)\dot{q}_2} \\ &= \frac{1}{2}\widehat{p}_2^T M_2^{-1}(q_2)\widehat{p}_2 + \mathcal{V}(q_2). \end{aligned} \tag{3.35}$$

This is exactly the Hamiltonian function of the corresponding $(n-1)$-DOF subrobot. We can now use (3.24), (3.30), and (3.33) to show that the restriction of $\mathcal{H}_\lambda$ to $\mathcal{Z}_{\tilde{q}_1}$ equals $\mathcal{H}_{\mathcal{R}_\lambda}$:

$$\begin{aligned}\mathcal{H}_\lambda(q,\widehat{p})|_{\mathcal{Z}_{\tilde{q}_1}} &= \left[\widehat{p}^T\dot{q} - \mathcal{L}_\lambda(q,\dot{q})\right]\big|_{\{\widehat{p}=\widehat{\mathcal{J}}(q,\dot{q}),\ \widehat{\mathcal{J}}_1(q,\dot{q})=\lambda(q_1)\}} \\ &= \left[\widehat{p}_1^T\dot{q}_1 + \widehat{p}_2^T\dot{q}_2 - \mathcal{L}_\lambda(q,\dot{q})\right]\big|_{\{\widehat{p}=\widehat{\mathcal{J}}(q,\dot{q}),\ \mathcal{J}_1(q,\dot{q})=\lambda(q_1)\}} \\ &= \left[\widehat{p}_2^T\dot{q}_2 - \mathcal{R}_\lambda(q_2,\dot{q}_2)\right]\big|_{\widehat{p}_2=M_2(q_2)\dot{q}_2} \\ &= \mathcal{H}_{\mathcal{R}_\lambda}(q_2,\widehat{p}_2). \end{aligned} \tag{3.36}$$

This offers an energetic interpretation to the controlled reduction: the shaped Hamiltonian is exactly the subsystem Hamiltonian on the surface $\mathcal{Z}_{\tilde{q}_1}$. In other words, the shaped system behaves and can be controlled as the lower-dimensional subrobot. The above equality also allows a simplified expression for the shaped Hamilton equations.

The diagonal blocks in upper-triangular matrix $M_{\mathcal{Z}}$ are positive definite, so invertibility gives a bijective mapping between coordinate momenta and velocities: $\widehat{p} = M_{\mathcal{Z}}(q_2)\dot{q} \iff \dot{q} = M_{\mathcal{Z}}^{-1}(q_2)\widehat{p}$, where blockwise inversion gives

$$M_{\mathcal{Z}}^{-1}(q_2) = \begin{pmatrix} m_1^{-1}(q_2) & -m_1^{-1}(q_2)M_{12}(q_2)M_2^{-1}(q_2) \\ 0 & M_2^{-1}(q_2) \end{pmatrix}. \tag{3.37}$$

In order to express the second PDE, note that (3.36) provides the subsystem expression

$$[\nabla_{q_2}\mathcal{H}_\lambda]|_{\mathcal{Z}_{\tilde{q}_1}} = \nabla_{q_2}\left[\mathcal{H}_\lambda|_{\mathcal{Z}_{\tilde{q}_1}}\right] = \nabla_{q_2}\mathcal{H}_{\mathcal{R}_\lambda}.$$

The shaped Hamilton equations constrained to $\mathcal{Z}_{\tilde{q}_1}$ are then given by

$$\dot{q} = \nabla_{\widehat{p}}\mathcal{H}_\lambda\big|_{\mathcal{Z}_{\tilde{q}_1}} = M_{\mathcal{Z}}^{-1}(q_2)\widehat{p} \tag{3.38}$$

$$\dot{\widehat{p}} = -\nabla_q\mathcal{H}_\lambda|_{\mathcal{Z}_{\tilde{q}_1}} + v = \begin{pmatrix} -\frac{c}{m_1(q_2)}(\widehat{p}_1 - M_{12}(q_2)M_2^{-1}\widehat{p}_2) \\ -\nabla_{q_2}\mathcal{H}_{\mathcal{R}_\lambda}(q_2,\widehat{p}_2) \end{pmatrix} + \begin{pmatrix} v_1 \\ v_2 \end{pmatrix}. \tag{3.39}$$

Therefore, the restriction dynamics can be given by the Hamiltonian system of the $(n-1)$-DOF subrobot:

$$\begin{pmatrix} \dot{q}_2 \\ \dot{\widehat{p}}_2 \end{pmatrix} = \begin{pmatrix} 0_{n-1\times n-1} & I_{n-1\times n-1} \\ -I_{n-1\times n-1} & 0_{n-1\times n-1} \end{pmatrix} \begin{pmatrix} \nabla_{q_2}\mathcal{H}_{\mathcal{R}_\lambda} \\ \nabla_{\widehat{p}_2}\mathcal{H}_{\mathcal{R}_\lambda} \end{pmatrix} + \begin{pmatrix} 0_{n-1\times 1} \\ v_2 \end{pmatrix}. \tag{3.40}$$

Remark 7. The reduced covector field is a map in coordinates $(q_2, \widehat{p}_2) \mapsto (\dot{q}_2, \dot{\widehat{p}}_2)$. This provides A1 needed for the limit cycle stability results of Section 3.1. In other words, given a controller $v_2(q_2, \widehat{p}_2)$ that stabilizes the reduced subsystem, a reduction-based controller (3.21) can be designed to construct full-order stability. The upper-triangular structure in PDEs (3.38)-(3.39), known as *feedforward form*, suggests an analogy to forwarding control (the dual to backstepping for systems with lower-triangular structure [8, 47]).

3.4.2 Connections to passivity

We also know from [54, 61] that the shaped system has a new passive output

$$y \;=\; \nabla_{\widehat{p}}\mathcal{H}_\lambda \;=\; M_\lambda^{-1}(\widehat{p} - Q_\lambda) \;=\; \dot{q}.$$

In order to show this new passivity property and the associated storage function, we will invoke the positive-definite and skew-symmetry properties of ACL systems proven in Appendix A.

Theorem 7. ACL system (3.22) is passive with respect to input v and output $\dot{q}$.

Proof. Recalling that $Q_\lambda^T\dot{q}$ is an artificial energy term, we choose *stored* ACH $\widehat{\mathcal{H}_\lambda}(q,\dot{q}) = \mathcal{K}_\lambda(q,\dot{q}) + \mathcal{V}_\lambda(q)$ as the storage function. We can assume without loss of generality that $\widehat{\mathcal{H}_\lambda}$ is nonnegative, since positive-definite M_λ (Lemma 14) implies that $\mathcal{K}_\lambda$ is nonnegative and $\mathcal{V}_\lambda$ is bounded below given bounded q_1 (provided by passive control (3.6)). Then,

$$\begin{aligned} \dot{\widehat{\mathcal{H}_\lambda}} &= \dot{q}^T M_\lambda(q)\ddot{q} + \frac{1}{2}\dot{q}^T\dot{M}_\lambda(q)\dot{q} + \dot{q}^T\nabla_q\mathcal{V}_\lambda(q) \\ &= \dot{q}^T\left\{-C_\lambda(q,\dot{q})\dot{q} - N_\lambda(q) + v\right\} + \frac{1}{2}\dot{q}^T\dot{M}_\lambda(q)\dot{q} + \dot{q}^T N_\lambda(q) \\ &= \frac{1}{2}\dot{q}^T\left\{\dot{M}_\lambda(q) - 2C_\lambda(q,\dot{q})\right\}\dot{q} + \dot{q}^T v \\ &= \dot{q}^T v, \end{aligned}$$

where the last equality follows from skew-symmetry by Lemma 15. This satisfies Definition 3. □

We can also show an analogous passivity property for ACL system (3.22) restricted to $\mathcal{Z}_{\tilde{q}_1}$.

Proposition 6. Restricted system (3.17) is passive with respect to input v_2 and output $\dot{q}_2$.

Proof. Note that constraint (3.11) implies $u_1 \equiv 0$. Choosing storage function $\mathcal{H}_{\mathcal{R}_\lambda}(q_2, \dot{q}_2) \geq 0$, which corresponds to the energy of a subrobot with input v_2 and output $\dot{q}_2$, the result follows from the robot passivity property. □

Remark 8. Hence, reduction-based control (3.21) performs feedback passivation with respect to storage function $\widehat{\mathcal{H}_\lambda}$ for input v and output $\dot{q}$. This property reduces to passivity with respect to input v_2 and output $\dot{q}_2$ on the surface $\mathcal{Z}_{\tilde{q}_1}$. We have shown the passivity-based nature of controlled reduction, where we can use this new passivity property for damping assignment as in [58]. Generally speaking, the feedback transformation for controlled reduction corresponds to an *intrinsic* gyroscopic case[2] of controlled Lagrangians/Hamiltonians [76] or, equivalently,[3] IDA passivity-based control [58]. The intrinsic property means that no canonical transformation exists such that the Hamiltonian becomes quadratic in the new coordinates – the Hamiltonian cannot be strictly expressed as kinetic plus potential energy. This is because our target dynamics are associated with the special structure of an ACL, or equivalently an ACH, to enable the controlled reduction.

In order to apply this method to general robots, we need to show that any robot can attain the special almost-cyclic form through the passivity-based feedback transformation of (3.21). Moreover, one stage of reduction may not suffice for solving a particular control problem given complex robot dynamics – the reduced control system $(f_{\mathcal{R}_\lambda}, g_{\mathcal{R}_\lambda})$ may be similarly difficult to stabilize as the full-order system. This leads to our discussion of controlled reduction by stages for mechanical systems.

[2]The gyroscopic terms $Q_\lambda^T \dot{q}$ are intrinsic to the ACH system because $[\nabla_q Q_\lambda]^T \neq \nabla_q Q_\lambda$ (cf. [59]).

[3]The general case of controlled Lagrangians is shown equivalent to IDA passivity-based control (modulo a coordinate change) in [58, 59].

CHAPTER 4

REDUCTION-BASED CONTROL OF MECHANICAL SYSTEMS

A mechanical system must have extensive symmetries in order to apply reduction-based control for significant dimensionality reduction. In the literature, systems with cyclic variables are commonly assumed to be a special class of mechanical systems, but we can prove this property and a stronger form of symmetry for the large class of open kinematic chains.

In this section, we redefine the configuration vector as $q = (q_1, \ldots, q_n) = ({q_1^i}^T, {q_{i+1}^n}^T)^T \in \mathcal{Q}$, where each scalar q_i is the i^{th} coordinate and each vector q_i^j contains coordinates $q_i, \ldots, q_j$, for $1 \leq i \leq j \leq n$. We now present a symmetry property of inertia matrices introduced in [48, 49], known as recursive cyclicity:

Definition 11. An $n \times n$-matrix M is *recursively cyclic* in the first k coordinates if each lower-right $(n-i+1) \times (n-i+1)$ submatrix is cyclic in $q_1, \ldots, q_i$, for $1 \leq i \leq k \leq n$. In other words, it has the form

$$
\begin{aligned}
M(q_2^n) &= \begin{pmatrix} m_{q_1}(q_2^n) & M_{q_1,q_2^n}(q_2^n) \\ M^T_{q_1,q_2^n}(q_2^n) & M_{q_2^n}(q_3^n) \end{pmatrix} \\
&= \begin{pmatrix} m_{q_1}(q_2^n) & \multicolumn{1}{c}{\text{———}} & M_{q_1,q_2^n}(q_2^n) & \multicolumn{1}{c}{\text{————————}} \\ | & \ddots & & \vdots \\ M^T_{q_1,q_2^n}(q_2^n) & & m_{q_{i-1}}(q_i^n) & M_{q_{i-1},q_i^n}(q_i^n) \\ | & \cdots & M^T_{q_{i-1},q_i^n}(q_i^n) & M_{q_i^n}(q_{i+1}^n) \end{pmatrix}
\end{aligned}
$$

with base case $i = k$. The matrix is simply said to be recursively cyclic if this property holds for all n coordinates, i.e., the base case is $i = n$ where submatrix $M_{q_n^n}(q_{n+1}^n) = m_{q_n}$ is a scalar constant $(q_{n+1}^n = \emptyset)$.

We can prove that inertia matrices of open kinematic chains, a large class of mechanical systems, have this symmetry property. This will provide an applicable class of mechanical systems for controlled reduction and several previously reported methods that assume cyclic variables (e.g.,

[40, 58, 74, 76, 78]).

4.1 Symmetries in Serial Kinematic Chains

We begin by considering the class of serial kinematic chains, later extending these observations to branched kinematic chains.

Lemma 5. The kinetic energy $\mathcal{K}(q, \dot{q}) = \frac{1}{2}\dot{q}^T M(q)\dot{q}$ of any n-DOF serial kinematic chain is cyclic in coordinate q_1 corresponding to the first DOF, i.e., $\frac{\partial}{\partial q_1}\mathcal{K}(q, \dot{q}) = 0$. Equivalently, inertia matrix $M(q)$ is cyclic in q_1.

Proof. It is shown in [86] that the kinetic energy of an n-DOF robot is invariant under rotations of the world coordinate frame. This property follows from the fact that the mass/inertia of a single link is constant, and all other links are relative to the first link. Therefore, the kinetic energy, being the sum of link kinetic energies as detailed in [55], is invariant under the orientation of the first link (relative to the world frame). Since the first degree-of-freedom is always referenced to the world frame, it follows that $\frac{\partial}{\partial q_1}\mathcal{K}(q, \dot{q}) = 0$ and thus q_1 is a cyclic coordinate with respect to kinetic energy. □

Lemma 6. The $n \times n$ inertia matrix M of any n-DOF serial kinematic chain contains a lower-right $(n-1) \times (n-1)$ submatrix $M_{q_2^n}$, which is the inertia matrix of the $(n-1)$-DOF subrobot with coordinates q_2^n corresponding to the original robot with its first DOF fixed.

Proof. Fix $q_1 = c$, $\dot{q}_1 = 0$, where c is constant. The top-most row and left-most column of M are zeroed in the constrained kinetic energy

$$\mathcal{K}(q, \dot{q})|_{q_1=c, \dot{q_1}=0} \quad = \quad \frac{1}{2}\dot{q}^T M(q)\dot{q}\Big|_{q_1=c, \dot{q_1}=0}.$$

Since M is cyclic by Lemma 5, the lower-right $(n-1) \times (n-1)$ submatrix $M_{q_2^n}$ is invariant under this constraint. Then, this constrained kinetic energy is equal to the $(n-1)$-DOF subrobot's kinetic energy:

$$\mathcal{K}(q, \dot{q})|_{q_1=c, \dot{q_1}=0} \quad = \quad \frac{1}{2}\dot{q}_2^{n^T} M_{q_2^n}(q_2^n)\dot{q}_2^n \quad = \quad \mathcal{K}_2(q_2^n, \dot{q}_2^n).$$

Equivalently, submatrix $M_{q_2^n}$ is the inertia matrix of this subrobot. □

Theorem 8. The inertia matrix of any serial kinematic chain is recursively cyclic.

Proof. We begin this proof by induction by examining the cyclicity of the base case. The 1-DOF subrobot corresponding to the lower-rightmost (scalar) submatrix of an n-DOF inertia matrix is trivially cyclic within the 1-DOF subconfiguration, since the mass/inertia of a single link is constant (as argued in the proof of Lemma 5).

As for the general case, consider the m-DOF subrobot of an n-DOF serial chain, where $1 < m \leq n$. As described earlier, this m-DOF subrobot is simply the n-DOF robot with the first $n - m$ coordinates fixed (note that these fixed coordinates do not affect the m-DOF submatrix as argued in the proof of Lemma 6). This subrobot's inertia matrix $M_{q^n_{n-m+1}}$, which is cyclic in q_{n-m+1} by Lemma 5 (within the m-DOF subconfiguration), contains an $(m-1)$-DOF subrobot's inertia matrix $M_{q^n_{n-m+2}}$ by Lemma 6. Fixing cyclic coordinate q_{n-m+1}, submatrix $M_{q^n_{n-m+2}}$ is then cyclic with respect to the next coordinate q_{n-m+2} by Lemma 5 (now within the $(m-1)$-DOF subconfiguration) and contains an $(m-2)$-DOF subrobot's inertia matrix by Lemma 6. Hence, it follows by induction that serial-chain inertia matrices are recursively cyclic. □

Note that this proof, originally introduced in [48, 49], depends on a relative coordinate system, so Theorem 8 always holds modulo a coordinate transformation.

4.2 Symmetries in Branched Kinematic Chains

This property is partially extended to branched kinematic chains by showing that any branched chain can be mapped to a higher-order serial chain that is constrained to be equivalent [50]. We can then invoke Theorem 8 down part of the chain:

Theorem 9. The inertia matrix of an n-DOF branched kinematic chain is recursively cyclic in the first $k = n - m$ coordinates, where the remaining m coordinates are part of the chain's *irreducible tree structure*, $1 \leq m \leq n$.

In other words, the submatrix corresponding to the remaining part of the redundant serial chain is irreducible. We now derive conditions for this tree structure, which is trivially the last DOF for serial chains.

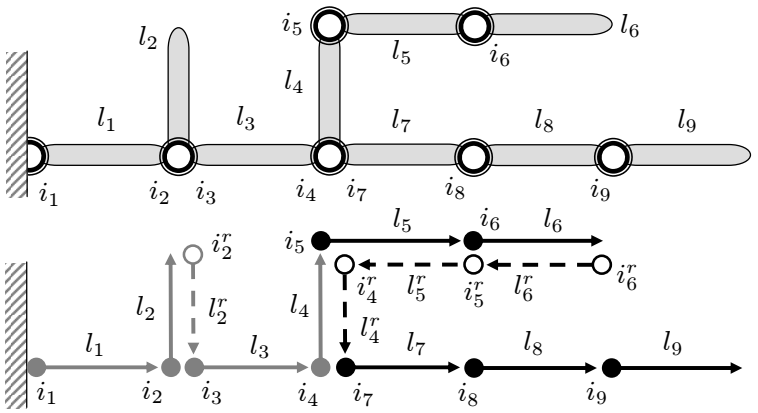

Figure 4.1: A branched kinematic chain (top) modeled as a redundant serial chain in a directed graph (bottom). The feedback-reducible part is shown in gray and the irreducible tree structure is shown in black.

4.2.1 Mapping branched chains to serial chains

A popular theory for modeling multibody systems with tree structure is presented in [87]. Such systems have a uniquely defined path between any two bodies (and are composed of nested tree substructures). In this framework, a branched chain is characterized by a directed graph of vertices and arcs originating from a carrier/base body. Dynamics of each body are derived based on the path from the base vertex to the vertex of the concerned body. This is employed in [88] for simulating multilegged robots (and the authors even suggest the use of geometric reduction for possible control methods). We deviate slightly from this approach in order to identify the desired symmetries in the kinematic structure.

We model a branched chain as a single higher-order *redundant serial chain* that essentially wraps around each branch (i.e., each radiating serial chain). Here, it is intuitive to describe each DOF as a vertex to be reduced from the directed graph, so we represent each interconnection as a vertex and each link/body as an arc, labeled in increasing order from the base vertex. An interconnection can be either a joint (one- to three-DOF) or a fixed-angle connection between links.

A branch is characterized by a directed path to the branch tip, along with a *redundant path* returning to the base of that branch (except for the last branch, which concludes the redundant serial chain, see Fig. 4.1). A redundant path is composed of zero-mass/inertia *redundant links* and *redundant interconnections*, always constrained as a fixed-angle connection (at the end of a branch) or a joint constrained to mirror a previous joint along the branch. In the example of Fig. 4.1, the first branch is a *simple branch*, since it only has a fixed-angle redundancy $i_2^r = \pi$, whereas

the second branch has variable constraints $i_4^r = i_5$, $i_5^r = i_6$ along with fixed $i_6^r = \pi$. Due to these trivial constraints, the higher-order redundant chain is described by a differential-algebraic system of equations, which can be trivially projected onto n-DOF constrained dynamics [69], by grouping like terms. The redundant dynamics evolve on this invariant constrained manifold, so solutions exist uniquely and are equivalent to branched-chain solutions by construction.

4.2.2 Irreducible tree structures

Recursive cyclicity does not always hold for the inertia matrix of a branched chain, because redundant joints of a non-simple branch are constrained equal to previous angles along the branch. For example, in Fig. 4.1 we see that $i_4^r = i_5$, and this constraint's right-hand-side is a coordinate from earlier in the chain. This introduces an inherently non-cyclic dependence on i_5 in the inertia submatrix associated with the coordinates from i_5 to the end of the chain. The necessary symmetries do not exist to reduce this part of the branched chain, the irreducible tree structure, using the framework of Theorem 6. However, we should not give up yet – there are symmetries in the chain prior to this troubling branch that can be exploited.

Proposition 7. The irreducible tree structure of an n-DOF branched chain is the minimal m-DOF tree substructure, $1 \leq m \leq n$, starting at the second joint of the first non-simple branch.

This is proven by applying Theorem 8 to the redundant serial chain until we reach the second joint of a non-simple branch, which has a variable constraint at the corresponding redundant interconnection (the base joint of such a branch does not affect the configuration of other branches from that base). For example, the irreducible tree structure of the branched chain in Fig. 4.1 is shown in black.

This result has two trivial cases. Case $m = 1$ occurs when the entire chain is feedback-reducible, such as with any serial chain (ignoring potential energy). We will not consider the opposite case $m = n$, when two or more non-simple chains branch directly from the carrier body, since these are best modeled as separate, decoupled serial chains. In general, any branched chain with only simple branches is entirely feedback-reducible, since all redundant joints are fixed angles and introduce no dependencies on previous angles to violate recursive cyclicity.

4.3 Controlled Reduction by Stages

Full-order matrix M generally depends explicitly on q_2 through q_k, so kinetic energy $\mathcal{K}$ does not have a typical symmetry property with respect to the rotating action of these variables. We consequently cannot divide out all k variables in one stage of controlled reduction, but the recursively cyclic matrix does provide a new cyclic variable in the reduced-order kinetic energy $\mathcal{K}_2(q_3^n, \dot{q}_2^n) = \dot{q}_2^{n^T} M_{q_2^n}(q_3^n)\dot{q}_2^n$ after dividing out cyclic q_1. In fact, every reduced subsystem has a new cyclic variable. Therefore, every subsystem on phase space $T\mathbb{T}^{n-i}$ is invariant under the rotating action of a new cyclic coordinate group $\mathbb{S}^1$, from which we can impose a controlled reduction to phase space $T\mathbb{T}^{n-i-1} \cong T\mathbb{T}^{n-i} \bmod T\mathbb{S}^1$, for $0 \leq i < n-1$. This method of controlled reduction *by stages* is applied to the encompassing class of open kinematic chains in [49–51].

4.3.1 k-Almost-cyclic Lagrangians

In order to impose k stages of controlled reduction, reduction-based control shapes robot dynamics into the special structure associated with a generalized ACL:

Definition 12. Let Lagrangian $\mathcal{L}$ have inertia matrix M that is recursively cyclic in the first k coordinates and potential energy $\mathcal{V}$ that is cyclic in the first k coordinates. Then, the corresponding *k-almost-cyclic* Lagrangian $\mathcal{L}_{\lambda_1^k} : T\mathbb{T}^k \times T\mathbb{T}^{n-k} \to \mathbb{R}$ is defined, in coordinates, as

$$\begin{aligned} \mathcal{L}_{\lambda_1^k}(q, \dot{q}) &:= \mathcal{K}(q_2^n, \dot{q}) - \mathcal{V}(q_{k+1}^n) + \mathcal{L}^{\text{aug}}_{\lambda_1^k}(q, \dot{q}) \\ &= \mathcal{K}_{\lambda_1^k}(q, \dot{q}) + Q^T_{\lambda_1^k}(q)\dot{q} - \mathcal{V}_{\lambda_1^k}(q) \\ &= \frac{1}{2}\dot{q}^T M_{\lambda_1^k}(q_2^n)\dot{q} + Q^T_{\lambda_1^k}(q)\dot{q} - \mathcal{V}_{\lambda_1^k}(q), \end{aligned} \tag{4.1}$$

where $M_{\lambda_1^k} \in \mathbb{R}^{n\times n}$, $Q_{\lambda_1^k} \in \mathbb{R}^n$, and $\mathcal{V}_{\lambda_1^k} \in \mathbb{R}$ will shortly be defined in terms of linear functions $\lambda_i : \mathbb{S}^1 \to \mathbb{R}$ of variables q_i, for $i \in \{1, k\}$.

Based on the recursively cyclic property, this generalized ACL shapes the cyclic variable found at each reduction stage into an almost-cyclic variable (i.e., recursively breaking symmetry). Therefore, each stage is characterized by a reduced-order ACL $\mathcal{L}_{\lambda_{i+1}^k}(q_{i+1}^n, \dot{q}_{i+1}^n)$ and a functional conservation

law describing the momentum conjugate to the new divided coordinate q_i:

$$\begin{aligned}\widetilde{J}_i(q_i^n, \dot{q}_i^n) &= \frac{\partial}{\partial \dot{q}_i}\mathcal{L}_{\lambda_i^k}(q_i^n, \dot{q}_i^n) \\ &= m_{q_i}(q_{i+1}^n)\dot{q}_i + M_{q_i, q_{i+1}^n}(q_{i+1}^n)\dot{q}_{i+1}^n \\ &= \lambda_i(q_i), \end{aligned} \tag{4.2}$$

for $i = 1, \ldots, k$. These momentum constraints again define an invariant submanifold $\mathcal{Z}_{\tilde{q}_1^k}$ parameterized by constant set-point vector $\tilde{q}_1^k \in \mathbb{R}^k$. This allows further stages of controlled reduction until the base functional Routhian of stage-k is reached, which has the form of Definition 9.

4.3.2 Reduced subsystems

To be precise, we now offer some definitions for the reduced subsystems.

Definition 13. Given k-ACL $\mathcal{L}_{\lambda_1^k}$, the *stage-*$(j-1)$ *functional Routhian* $\mathcal{L}_{\lambda_j^k} : T\mathbb{T}^{n-j+1} \to \mathbb{R}$ is obtained through a partial Legendre transformation in variable q_{j-1}:

$$\begin{aligned}\mathcal{L}_{\lambda_j^k}(q_j^n, \dot{q}_j^n) &:= \left[\mathcal{L}_{\lambda_{j-1}^k}(q_{j-1}^n, \dot{q}_{j-1}^n) - \lambda_{j-1}(q_{j-1})\dot{q}_{j-1}\right]\Big|_{\widetilde{J}_{j-1}(q_{j-1}^n, \dot{q}_{j-1}^n) = \lambda_{j-1}(q_{j-1})} \\ &= \mathcal{K}_{\lambda_j^k}(q_j^n, \dot{q}_j^n) + Q_{\lambda_j^k}^T(q_j^n)\dot{q}_j^n - \mathcal{V}_{\lambda_j^k}(q_j^n) \\ &= \frac{1}{2}\dot{q}_j^{n^T} M_{\lambda_j^k}(q_{j+1}^n)\dot{q}_j^n + Q_{\lambda_j^k}^T(q_j^n)\dot{q}_j^n - \mathcal{V}_{\lambda_j^k}(q_j^n), \end{aligned} \tag{4.3}$$

where $M_{\lambda_j^k} \in \mathbb{R}^{(n-j+1)\times(n-j+1)}$, $Q_{\lambda_j^k} \in \mathbb{R}^{n-j+1}$, and $\mathcal{V}_{\lambda_j^k} \in \mathbb{R}$ are defined as

$$M_{\lambda_j^k}(q_{j+1}^n) = M_{q_j^n}(q_{j+1}^n) + \sum_{i=j}^{k} \begin{pmatrix} 0 & 0 \\ 0 & \frac{M_{q_i, q_{i+1}^n}^T(q_{i+1}^n) M_{q_i, q_{i+1}^n}(q_{i+1}^n)}{m_{q_i}(q_{i+1}^n)} \end{pmatrix} \tag{4.4}$$

$$Q_{\lambda_j^k}(q_j^n) = \sum_{i=j}^{k} \begin{pmatrix} 0 & -\lambda_i(q_i) m_{q_i}^{-1}(q_{i+1}^n) M_{q_i, q_{i+1}^n}(q_{i+1}^n) \end{pmatrix}^T \tag{4.5}$$

$$\mathcal{V}_{\lambda_j^k}(q_j^n) = \mathcal{V}(q_{k+1}^n) - \frac{1}{2}\sum_{i=j}^{k} \frac{\lambda_i(q_i)^2}{m_{q_i}(q_{i+1}^n)}, \quad \text{for } j \in \{2, k\}. \tag{4.6}$$

Note that the above shaping terms define the k-ACL for $j = 1$. Given $j > 1$, the closed-form expression (4.3) explicitly shows all the shaping terms necessary for the remaining stages of

controlled reduction. Based on the definition of these terms, we also have the recursive expression

$$\begin{aligned}\mathcal{L}_{\lambda_j^k}(q_j^n, \dot{q}_j^n) &= \mathcal{L}_{\lambda_{j+1}^k}(q_{j+1}^n, \dot{q}_{j+1}^n) + \frac{1}{2} m_{q_j}(q_{j+1}^n)(\dot{q}_j)^2 + \dot{q}_j M_{q_j, q_{j+1}^n}(q_{j+1}^n)\dot{q}_{j+1}^n \\ &\quad + \frac{1}{2}\dot{q}_{j+1}^{n\,T} \frac{M_{q_j,q_{j+1}^n}^T(q_{j+1}^n) M_{q_j,q_{j+1}^n}(q_{j+1}^n)}{m_{q_j}(q_{j+1}^n)} \dot{q}_{j+1}^n - \frac{\lambda_j(q_j)}{m_{q_j}(q_{j+1}^n)} M_{q_j,q_{j+1}^n}(q_{j+1}^n)\dot{q}_{j+1}^n \\ &\quad + \frac{1}{2}\frac{\lambda_j(q_j)^2}{m_{q_j}(q_{j+1}^n)}.\end{aligned}$$

This shows the implicit generalized ACL $\mathcal{L}_{\lambda_{j+1}^k}$ of the next reduction stage, which is imposed by the last three terms. As for the base case, we have a standard functional Routhian.

Definition 14. Given k-ACL $\mathcal{L}_{\lambda_1^k}$, the *stage-$k$ functional Routhian* $\mathcal{R}_\lambda = \mathcal{L}_{\lambda_{k+1}^k} : T\mathbb{T}^{n-k} \to \mathbb{R}$ is obtained through a partial Legendre transformation in variable q_k:

$$\begin{aligned}\mathcal{R}_\lambda(q_{k+1}^n, \dot{q}_{k+1}^n) &:= \left[\mathcal{L}_{\lambda_k^k}(q_k^n, \dot{q}_k^n) - \lambda_k(q_k)\dot{q}_k\right]\Big|_{\widetilde{J}_k(q_k^n, \dot{q}_k^n) = \lambda_k(q_k)} \\ &= \frac{1}{2}\dot{q}_{k+1}^{n\,T} M_{q_{k+1}^n}(q_{k+1}^n)\dot{q}_{k+1}^n - \mathcal{V}(q_{k+1}^n).\end{aligned}$$

Full-order k-ACL $\mathcal{L}_{\lambda_1^k}$ and each reduction stage's functional Routhian have an associated control system as defined in Section 3.2. In particular, we have full-order control system $(f_{\lambda_1^k}, g_{\lambda_1^k})$ on $T\mathbb{T}^n$ with input v, and k-reduced control system $(f_{\mathcal{R}_\lambda}, g_{\mathcal{R}_\lambda})$ on $T\mathbb{T}^{n-k}$ with subsystem input v_{k+1}^n. Applying this subsystem control based on feedback from $(q_{k+1}^n, \dot{q}_{k+1}^n)$, we have full-order control system $(\hat{f}_{\lambda_1^k}, \hat{g}_{\lambda_1^k})$ on $T\mathbb{T}^n$ with input v_1^k and k-reduced vector field $\hat{f}_{\mathcal{R}_\lambda}$ on $T\mathbb{T}^{n-k}$. For $v_1^k = 0$, we have the following mapping between integral curves of these two closed-loop systems.

Theorem 10. Let $\mathcal{L}_{\lambda_1^k}$ be a k-ACL with corresponding stage-k functional Routhian $\mathcal{R}_\lambda$. Then, $\left(q_1^k(t), \dot{q}_1^k(t), q_{k+1}^n(t), \dot{q}_{k+1}^n(t)\right)$ is an integral curve to closed-loop vector field $\hat{f}_{\lambda_1^k}$ on $[t_0, t_f]$ satisfying initial boundary conditions

$$\widetilde{J}_j(q_j^n(t_0), \dot{q}_j^n(t_0)) \;=\; \lambda_j(q_j(t_0))$$

for all $j \in \{1, k\}$, if and only if $(q_{k+1}^n(t), \dot{q}_{k+1}^n(t))$ is an integral curve to closed-loop vector field $\hat{f}_{\mathcal{R}_\lambda}$ on $[t_0, t_f]$ and $\left(q_1^k(t), \dot{q}_1^k(t), q_{k+1}^n(t), \dot{q}_{k+1}^n(t)\right)$ satisfies

$$\widetilde{J}_j(q_j^n(t), \dot{q}_j^n(t)) \;=\; \lambda_j(q_j(t))$$

on $[t_0, t_f]$ for all $j \in \{1, k\}$.

This generalization of Theorem 6 is proven in Appendix B. The recursive decoupling of subsystems is apparent by examining the Hamilton PDEs defined in conjugate coordinates $\widetilde{p} = \widetilde{J}(q, \dot{q})$, which again have feedforward form when constrained to submanifold $\mathcal{Z}_{\tilde{q}_1^k}$. In particular, we see the block upper-triangular structure

$$\dot{q} \;=\; \begin{pmatrix} m_{q_1}(q_2^n) & \multicolumn{2}{c}{\text{————}} & M_{q_1,q_2^n}(q_2^n) \\ 0 & m_{q_2}(q_3^n) & & M_{q_2,q_3^n}(q_3^n) \\ 0 & & \ddots & M_{q_{k+1}^n}(q_{k+1}^n) \end{pmatrix}^{-1} \widetilde{p}. \tag{4.7}$$

4.3.3 Application to open kinematic chains

Based on the previously identified symmetries, control can transform an open kinematic chain's Lagrangian into a k-ACL without explicitly canceling natural terms.

Theorem 11. For any fully-actuated n-DOF open-chain robot with an m-DOF irreducible tree structure, $1 \leq m < n$, and a potential energy that is cyclic in the first k coordinates, $1 \leq k \leq (n - m)$, there exists a feedback control law transforming the system Lagrangian into the corresponding k-ACL through addition of shaping terms.

Proof. Theorem 9 shows that inertia matrix M is recursively cyclic in the first $n - m$ coordinates. The following feedback control law then transforms the system Lagrangian into the k-ACL of Definition 12 to enable k stages of controlled reduction:

$$u^{\lambda_1^k}(q, \dot{q}) \;:=\; C(q, \dot{q})\dot{q} + N(q) + M(q)M_{\lambda_1^k}(q)^{-1}\left(-C_{\lambda_1^k}(q, \dot{q})\dot{q} - N_{\lambda_1^k}(q) + v\right), \tag{4.8}$$

where $C_{\lambda_1^k}$ and $N_{\lambda_1^k}$ are defined as in Section 3.2 from the closed-loop E-L equations of $\mathcal{L}_{\lambda_1^k}$. □

Such a robot is thus feedback-reducible down to its corresponding $(n - k)$-DOF subrobot. This result is referred to as the *Subrobot Theorem* in [48–50]. The reduction-based control law is a direct generalization of (3.21) and recursively breaks the symmetry of each cyclic coordinate group $\mathbb{S}^1$ in the special almost-cyclic manner.

Remark 9. Given the necessary symmetries in a robot's potential energy, we can impose a controlled reduction down to the m-DOF irreducible tree structure by adding shaping terms. Initial

conditions satisfying (4.2) allow the shaped dynamics of an n-DOF robot to project onto the dynamics of the corresponding $(n-k)$-DOF subrobot. This subsystem is entirely decoupled from the first k coordinates and thus behaves and can be controlled as a typical $(n-k)$-DOF robot. Moreover, the first k DOF evolve in a controlled manner according to functional momentum constraints (4.2) given $\lambda_j(q_j) = -c_j(q_j - \tilde{q}_j)$, $1 \leq j \leq k$. Applying Theorems 2-4 one stage at a time, the divided coordinates are controlled to set-points or periodic orbits. Therefore, stability in $T\mathbb{T}^{n-k}$ implies stability in $T\mathbb{T}^n$ conditioned on these functional conservation laws. In the next section, we will show how to make attractive the invariant set defined by these constraints, by which we can establish a global form of stability.

Remark 10. The first element of overall control (4.8) is equivalent to passive-feedback control $\frac{\partial \lambda_1}{\partial q_1}\dot{q}_1$ under functional conservation law (4.2) for $i = 1$. If we were to define subcontrollers that provide energy shaping one stage of reduction at a time, we would similarly find that the first term of each subcontroller is equivalent to $\frac{\partial \lambda_i}{\partial q_i}\dot{q}_i$ under conservation law (4.2), for all $1 < i \leq k$.

It is important to note that the inertia matrix, skew-symmetry, and passivity properties from Section 3.4 and Appendix A are easily generalized to k-ACL systems (cf. [49]). Moreover, we can revisit the assumption that the potential energy is cyclic in the first k coordinates. In the case of rigid zero-gravity systems, this is easily satisfied, but most robots will not have k-cyclic potential energies to apply Theorem 11. We can use potential energy shaping to impose a "controlled symmetry" from [23, 24] (e.g., eliminate any potential energy dependence on the variables we wish to reduce), thus satisfying the assumptions of Theorem 11 in closed loop. We will do exactly this in Section 5.2, defining a control law that replaces the original potential energy with that of the target planar subsystem (which is found by fixing the biped's lean coordinate to vertical).

We have shown that controlled reduction eludes the lower bound of dynamic model reduction for serial kinematic chains shown in [65]. In the case of serial kinematic chains, we can impose a feedback transformation to k-ACL dynamics enabling controlled reduction by stages to an arbitrarily lower-dimensional subsystem. We now derive an auxiliary controller to render globally attractive the invariant surface $\mathcal{Z}_{\tilde{q}_1^k}$ defined by (4.2).

4.4 Attractivity of the Zero Dynamics

The implications of Theorems 2-6 and Theorem 10 only hold from the set of states satisfying the desired functional conservation law(s). We must use an additional controller outside of this set to exploit these results in a global sense. Therefore, we employ the output linearization approach of [45, 49, 89], first defining output functions quantifying the error from these desired constraints:

$$y_i \;=\; h_i(q_i^n, \dot{q}_i^n) \;:=\; \dot{q}_i - \frac{1}{m_{q_i}(q_{i+1}^n)} \left(\lambda_i(q_i) - M_{q_i, q_{i+1}^n}(q_{i+1}^n) \dot{q}_{i+1}^n \right), \tag{4.9}$$

for $i \in \{1, k\}$. Alternatively, we could use $\bar{h}_i(q_i^n, \dot{q}_i^n) = \widetilde{J}_i(q_i^n, \dot{q}_i^n) - \lambda_i(q_i)$ to avoid inverting terms.

We design control law v_1^k to zero the output vector y by linearizing the output dynamics into a GES system. Given a system of relative degree one (to be defined shortly), we want the first-order output dynamics

$$\begin{aligned} \dot{y} &= L_{\hat{f}_{\lambda_1^k}} h + (L_{\hat{g}_{\lambda_1^k}} h) v_1^k \\ &= -\xi y, \end{aligned} \tag{4.10}$$

for some positive-definite gain matrix ξ. These closed-loop dynamics render invariant surface $\mathcal{Z}_{\tilde{q}_1^k}$ – the zero dynamics – globally exponentially attractive.

In order to invert the original output dynamics, we must compute the Lie derivative of output vector function h with respect to $\hat{g}_{\lambda_1^k}$. We denote $L_{\hat{g}_{\lambda_1^k}} h$ as $k \times k$ matrix A:

$$A(q) \;:=\; \begin{pmatrix} \nabla_q h_1 & \dots & \nabla_q h_k \end{pmatrix}^T \hat{g}_{\lambda_1^k}(q).$$

Each matrix element $A_{i,j}$ is the Lie derivative $L_{\hat{g}_{\lambda_1^k} e_j} h_i$, where e_j is the j^{th} standard basis vector of $\mathbb{R}^k$. Matrix $A(q)$ is positive-definite (thus invertible), since it is lower-triangular and

$$L_{\hat{g}_{\lambda_1^k} e_i} h_i \;=\; \frac{1}{m_{q_i}(q_{i+1}^n)},$$

where $m_{q_i}(q_{i+1}^n) > 0$ by the positive-definite property of $M(q)$. This implies that $L_{\hat{g}_{\lambda_1^k}} h$ is strictly bounded away from zero, so the system is said to have relative degree one – the first-order output dynamics are linearizable.

The control law that achieves the desired linearization is

$$v_1^k(q,\dot{q}) \;:=\; -A(q)^{-1}\left(\begin{pmatrix} L_{\hat{f}_{\lambda_1^k}} h_1(q,\dot{q}) \\ \vdots \\ L_{\hat{f}_{\lambda_1^k}} h_k(q_k^n,\dot{q}_k^n) \end{pmatrix} + \begin{pmatrix} \xi_1 & 0 & 0 \\ 0 & \ddots & 0 \\ 0 & 0 & \xi_k \end{pmatrix} \begin{pmatrix} h_1(q,\dot{q}) \\ \vdots \\ h_k(q_k^n,\dot{q}_k^n) \end{pmatrix}\right), \quad (4.11)$$

where $L_{\hat{f}_{\lambda_1^k}} h_i$ is the Lie derivative of h_i with respect to $\hat{f}_{\lambda_1^k}$, and control gains $\xi_i > 0$ for $i \in \{1, k\}$. It is clear that v_1^k is well-defined by the positive-definiteness of $A(q)$ and the control gain matrix. Moreover, $v_1^k\big|_{\mathcal{Z}_{\tilde{q}_1^k}} = 0$, so the restricted controller does not interfere with Theorem 10.

If the first control term u_1 must be implemented mechanically for an underactuated system, we could instead define an output linearizing controller for auxiliary inputs v_2^n. This may involve output dynamics with higher relative degree, where matrix $A(q) \equiv 0$, requiring higher-order Lie derivatives [89].

CHAPTER 5

THREE-DIMENSIONAL BIPEDAL WALKING

In this thesis, the primary application of reduction-based control is bipedal walking robots in 3-D space. Work towards 3-D dynamic walking began with models of the sagittal and frontal planes-of-motion (without heading, see Fig. 1.1), resulting in spatially 3-D dynamic gaits (e.g., [30, 33, 34, 46, 90]). However, results on fully 3-D (i.e., directional) dynamic walking are limited, with some of the earliest theoretical results presented in [48–50].

We now revisit these results, employing reduction-based control to build 3-D gaits about arbitrary headings, based on subsystem limit cycles in the sagittal plane-of-motion (where bilateral symmetry yields periodic motion from step to step). Since bipeds have both continuous and discrete dynamics, we begin the chapter by introducing hybrid systems, followed by our models of interest. We will then turn our attention to building a reduction-based control law to generate asymptotically stable walking gaits.

5.1 Bipedal Walking Robots

A simple bipedal walking robot has two phases, a single-support/swing phase and a double-support/impact phase, and thus is modeled as a hybrid system. In three dimensions, non-trivial feet introduce one to three degrees of underactuation at the point of contact between the foot and ground, so we assume that the biped has flat feet[1] with full actuation at the stance ankle (we will later discuss relaxing actuation in the yaw DOF). We assume, and will later verify, that the stance foot remains in contact with ground and does not slip during the continuous swing phase. We model foot-ground impacts to be instantaneous and perfectly plastic. Since knee-lock impacts introduce another level of complexity to the hybrid model, we assume foot-ground impacts are the only discrete events. This does not necessarily preclude knees without impacts [91]. The knee-lock

[1]Note that this assumption is justified for an approximation of small feet that lie flat on the ground with sufficient friction during the entirety of each swing phase.

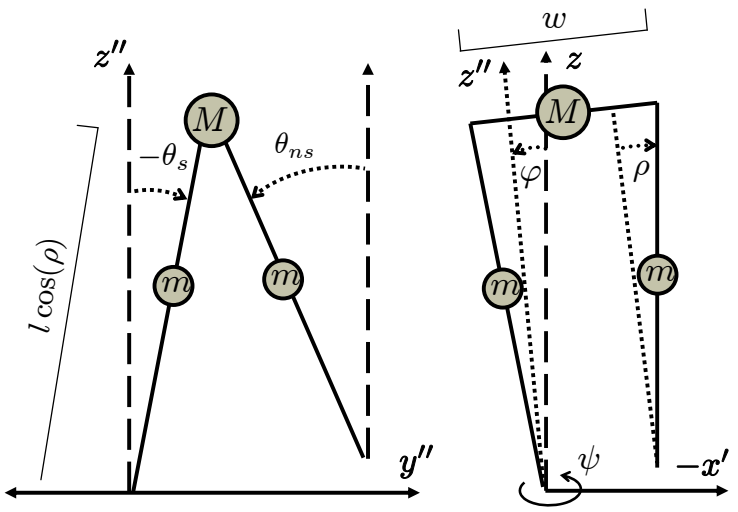

Figure 5.1: The sagittal (left) and frontal (right) planes of a hipped 3-D bipedal robot. Note that leg splay angle ρ is a constant modeling parameter.

and flat foot assumptions can be relaxed in the controlled reduction framework as recently shown in [90].

5.1.1 Four-DOF biped model

We now construct the model of a 4-DOF bipedal robot with a hip and splayed legs (Fig. 5.1). Although this is a 3-D extension of the 2-D compass-gait biped seen in the sagittal plane of Fig. 5.1, it is important to note that the 3-D model does not have stable passive walking gaits down slopes. We therefore will use reduction-based control on this serial-chain robot, which is feedback-reducible by Theorem 8 and Theorem 11, to construct pseudo-passive 3-D walking gaits from the sagittal plane.

The configuration space for the 4-DOF biped can be represented by $\mathcal{Q}_{4\mathrm{D}} = \mathrm{SO}(3) \times \mathbb{S}^1$ [24]. In particular, 3×3-matrix $R_{\mathrm{s}} \in \mathrm{SO}(3)$ is the orientation of the stance leg and $\theta_{\mathrm{ns}} \in \mathbb{S}^1$ is the relative shape the nonstance/swing leg. However, before we obtain the equations of motion, we must parameterize the configuration space $\mathcal{Q}_{4\mathrm{D}}$. An element of SO(3) can be minimally represented by an ordered set of three ZYX Euler angles[2] $(\psi, \varphi, \theta_{\mathrm{s}}) \in \mathbb{T}^3$, which correspond to the yaw, roll, and pitch angles of the stance leg (and are the robot's first three DOF). For the sake of distinguishing the sagittal-plane configuration, we take $\mathcal{Q}_{4\mathrm{D}} = \mathbb{T}^2 \times \mathbb{T}^2$, with coordinates $q = (\psi, \varphi, \theta^T)^T$, where

[2]Note that this local parameterization's singularity is at $\varphi = -\pi/2$, which corresponds to an irrelevant fall configuration.

ψ is the yaw (or heading), φ is the roll (or lean) from vertical, and $\theta = (\theta_{\rm s}, \theta_{\rm ns})^T$ is the vector of sagittal-plane (pitch) variables as in the 2-D compass-gait model. All other parameters, including leg splay angle ρ, are held constant.

Given state $x = (q^T, \dot{q}^T)^T$, this model's hybrid control system is

$$\mathscr{HC}_{\rm 4D} : \begin{cases} \dot{x} = f_{\rm 4D}(x) + g_{\rm 4D}(x)u & x \in D_{\rm 4D} \backslash G_{\rm 4D} \\ x^+ = \Delta_{\rm 4D}(x^-) & x^- \in G_{\rm 4D} \end{cases}.$$

We derive the continuous dynamics for $\mathscr{HC}_{\rm 4D}$ using Lagrangian mechanics from Section 2.1. We start with Lagrangian function

$$\mathcal{L}_{\rm 4D}(q, \dot{q}) = \frac{1}{2}\dot{q}^T M_{\rm 4D}(q)\dot{q} - \mathcal{V}_{\rm 4D}(q),$$

where recursively-cyclic 4×4 inertia matrix is given by (see Appendix C for term expressions)

$$M_{\rm 4D}(\varphi, \theta) = \begin{pmatrix} m_\psi(\varphi,\theta) & \text{---} & M_{\psi\varphi\theta}(\varphi,\theta) \\ | & m_\varphi(\theta) & M_{\varphi\theta}(\theta) \\ M^T_{\psi\varphi\theta}(\varphi,\theta) & M^T_{\varphi\theta}(\theta) & M_\theta(\theta) \end{pmatrix}.$$

The potential energy

$$\mathcal{V}_{\rm 4D}(\varphi, \theta) = \mathcal{V}_\theta(\theta)\cos(\varphi) - \frac{g}{2}(2m + M)(w - 2l\sin(\rho))\sin(\varphi) \tag{5.1}$$

contains the planar subsystem potential energy

$$\mathcal{V}_\theta(\theta) = \frac{gl}{2}\cos(\rho)((3m + 2M)\cos(\theta_{\rm s}) - m\cos(\theta_{\rm ns})). \tag{5.2}$$

The dynamical equations of motion for the fully actuated walker are then

$$M_{\rm 4D}(q)\ddot{q} + C_{\rm 4D}(q, \dot{q})\dot{q} + N_{\rm 4D}(q) = B_{\rm 4D}u, \tag{5.3}$$

where $C_{\rm 4D}$ and $N_{\rm 4D}$ are defined as usual and invertible 4×4-matrix

$$B_{\rm 4D} = \begin{pmatrix} I_{2\times2} & 0_{2\times2} \\ 0_{2\times2} & B_\theta \end{pmatrix} \text{ with } B_\theta = \begin{pmatrix} 1 & 1 \\ 0 & -1 \end{pmatrix}.$$

These dynamics are associated with the control system $(f_{4\mathrm{D}}, g_{4\mathrm{D}})$ with input u. We model actuator saturation at torque constant $U_{\max}$, so the control space is

$$U_{4\mathrm{D}} = \{u \in \mathbb{R}^4 : |u_i| \leq U_{\max}, \forall i \in \{1, 4\}\}.$$

In order to appropriately model walking on a flat surface, we introduce a unilateral constraint function representing the height of the swing foot[3]:

$$H_{4\mathrm{D}}(q) = l\cos(\rho)(\cos(\theta_{\mathrm{s}}) - \cos(\theta_{\mathrm{ns}}))\cos(\varphi) - (w - 2l\sin(\rho))\sin(\varphi).$$

States corresponding to feasible walking are in domain $D_{4\mathrm{D}}$, the subset of $T\mathcal{Q}_{4\mathrm{D}}$ where this height is nonnegative. Impact events are triggered by intersections with the guard, $G_{4\mathrm{D}} \subset D_{4\mathrm{D}}$, where the height of the swing foot is zero and strictly decreasing (to exclude events associated with scuffing):

$$G_{4\mathrm{D}} = \left\{ \begin{pmatrix} q \\ \dot{q} \end{pmatrix} \in D_{4\mathrm{D}} : H_{4\mathrm{D}}(q) = 0 \text{ and } \dot{H}_{4\mathrm{D}} = \left(\frac{\partial H_{4\mathrm{D}}(q)}{\partial q}\right)^T \dot{q} < 0 \right\}. \tag{5.4}$$

Following the method of [5,91], we derive the reset map associated with perfectly plastic impacts:

$$\Delta_{4\mathrm{D}}(q, \dot{q}) = \begin{pmatrix} \Gamma_{4\mathrm{D}} q \\ \Omega_{4\mathrm{D}}(q)\dot{q} \end{pmatrix}, \tag{5.5}$$

where angular velocity map[4] $\Omega_{4\mathrm{D}}(q) \in \mathbb{R}^{4\times 4}$ and angular position map

$$\Gamma_{4\mathrm{D}} = \begin{pmatrix} I_{2\times 2} & 0_{2\times 2} \\ 0_{2\times 2} & \Gamma_\theta \end{pmatrix} \text{ with } \Gamma_\theta = \begin{pmatrix} 0 & 1 \\ 1 & 0 \end{pmatrix}.$$

The signs of w and ρ are flipped at impact to model the change in stance leg. Technically the hybrid model then has two sets of continuous/discrete phases, but we forgo this caveat for simplicity and note that hybrid flows corresponding to walking gaits will be 2-periodic.

[3]The yaw-DOF (coordinate ψ) is about the vertical axis, and thus the height of the foot $H_{4\mathrm{D}}(q)$, measured across this vertical axis, is invariant under such rotations.

[4]This map's complexity prevents a closed-form symbolic derivation in Mathematica, so this is computed numerically at each impact event.

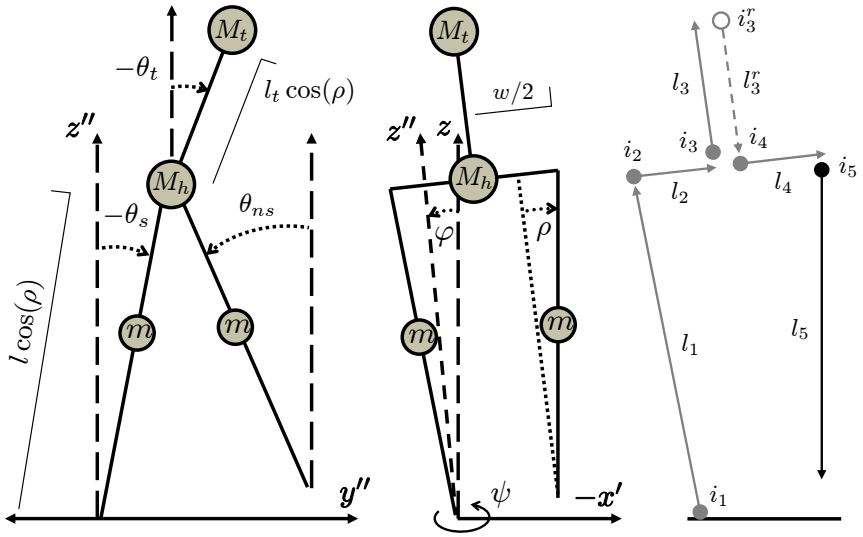

Figure 5.2: The sagittal and frontal planes of a 3-D bipedal torso robot, along with its serial-chain mapping. Note that i_2 is a fixed angle interconnection.

5.1.2 Five-DOF torso biped model

We now construct the model of a 5-DOF bipedal robot with a hip, splayed legs, and a torso (Fig. 5.2). Although this is a 3-D extension of the 2-D compass-gait-with-torso biped, the 3-D biped does not have stable passive walking gaits down slopes. This model is also entirely feedback-reducible, i.e., the irreducible tree structure is the last DOF.

For the sake of distinguishing the sagittal plane, we represent the configuration space of the 5-DOF biped by $\mathcal{Q}_{5\mathrm{D}} = \mathbb{T}^2 \times \mathbb{T}^3$ with coordinates $q = (\psi, \varphi, \theta^T)^T$, where ψ is the yaw (or heading), φ is the roll (or lean) from vertical, and $\theta = (\theta_\mathrm{s}, \theta_\mathrm{t}, \theta_\mathrm{ns})^T$ is the vector of sagittal-plane (pitch) variables as in the 2-D model.

This model's hybrid control system is

$$\mathscr{HC}_{5\mathrm{D}} : \begin{cases} \dot{x} = f_{5\mathrm{D}}(x) + g_{5\mathrm{D}}(x)u & x \in D_{5\mathrm{D}} \backslash G_{5\mathrm{D}} \\ x^+ = \Delta_{5\mathrm{D}}(x^-) & x^- \in G_{5\mathrm{D}} \end{cases}.$$

We derive the continuous dynamics for $\mathscr{HC}_{5\mathrm{D}}$ starting with Lagrangian function

$$\mathcal{L}_{5\mathrm{D}}(q, \dot{q}) = \frac{1}{2}\dot{q}^T M_{5\mathrm{D}}(q)\dot{q} - \mathcal{V}_{5\mathrm{D}}(q),$$

where recursively-cyclic 5×5 inertia matrix is given by (see Appendix C for term expressions)

$$M_{5\mathrm{D}}(\varphi,\theta) = \begin{pmatrix} m_\psi(\varphi,\theta) & \text{---} & M_{\psi\varphi\theta}(\varphi,\theta) \\ | & m_\varphi(\theta) & M_{\varphi\theta}(\theta) \\ M^T_{\psi\varphi\theta}(\varphi,\theta) & M^T_{\varphi\theta}(\theta) & M_\theta(\theta) \end{pmatrix}$$

and potential energy

$$\mathcal{V}_{5\mathrm{D}}(\varphi,\theta) \;=\; -\frac{g}{2}(2m + M_\mathrm{h} + M_\mathrm{t})(w - 2l\sin(\rho))\sin(\varphi) + \mathcal{V}_\theta(\theta)\cos(\varphi) \tag{5.6}$$

contains the planar subsystem potential energy

$$\mathcal{V}_\theta(\theta) \;=\; \frac{g}{2}(l\cos(\rho)((3m + 2(M_\mathrm{h} + M_\mathrm{t}))\cos(\theta_\mathrm{s}) - m\cos(\theta_\mathrm{ns})) + 2l_\mathrm{t}M_\mathrm{t}\cos(\theta_\mathrm{t})). \tag{5.7}$$

The equations of motion for the fully actuated biped are then

$$M_{5\mathrm{D}}(q)\ddot{q} + C_{5\mathrm{D}}(q,\dot{q})\dot{q} + N_{5\mathrm{D}}(q) = B_{5\mathrm{D}}u, \tag{5.8}$$

where $C_{5\mathrm{D}}$ and $N_{5\mathrm{D}}$ are defined as usual with invertible

$$B_{5\mathrm{D}} = \begin{pmatrix} I_{2\times 2} & 0_{2\times 3} \\ 0_{3\times 2} & B_\theta \end{pmatrix} \text{ with } B_\theta = \begin{pmatrix} 1 & 1 & 0 \\ 0 & -1 & 1 \\ 0 & 0 & -1 \end{pmatrix}.$$

These equations are associated with the control system $(f_{5\mathrm{D}}, g_{5\mathrm{D}})$ with input u. We model actuator saturation at torque constant U_max, so the control space is

$$U_{5\mathrm{D}} = \{u \in \mathbb{R}^5 : |u_i| \leq U_\mathrm{max}, \forall i \in \{1,5\}\}.$$

Since the torso does not affect the height of the swing foot, we use the same unilateral constraint function as before, $H_{5\mathrm{D}}((\psi,\varphi,\theta_\mathrm{s},\theta_\mathrm{t},\theta_\mathrm{ns})^T) = H_{4\mathrm{D}}((\psi,\varphi,\theta_\mathrm{s},\theta_\mathrm{ns})^T)$. States corresponding to feasible walking are in domain $D_{5\mathrm{D}}$, the subset of $T\mathcal{Q}_{5\mathrm{D}}$ where this height is nonnegative. Impact events are triggered by intersections with guard $G_{5\mathrm{D}} \subset D_{5\mathrm{D}}$, where the height of the swing foot is zero

and strictly decreasing:

$$G_{5\mathrm{D}} \;=\; \left\{ \begin{pmatrix} q \\ \dot{q} \end{pmatrix} \in D_{5\mathrm{D}} : H_{5\mathrm{D}}(q) = 0 \;\text{ and }\; \dot{H}_{5\mathrm{D}} = \left(\frac{\partial H_{5\mathrm{D}}(q)}{\partial q} \right)^T \dot{q} < 0 \right\}. \tag{5.9}$$

Again deferring the details to [5, 91], we can compute the reset map

$$\Delta_{5\mathrm{D}}(q, \dot{q}) \;=\; \begin{pmatrix} \Gamma_{5\mathrm{D}} q \\ \Omega_{5\mathrm{D}}(q)\dot{q} \end{pmatrix}, \tag{5.10}$$

where angular velocity map $\Omega_{5\mathrm{D}}(q) \in \mathbb{R}^{5\times 5}$ and angular position map

$$\Gamma_{5\mathrm{D}} = \begin{pmatrix} I_{2\times 2} & 0_{2\times 3} \\ 0_{3\times 2} & \Gamma_\theta \end{pmatrix} \;\text{ and }\; \Gamma_\theta = \begin{pmatrix} 0 & 0 & 1 \\ 0 & 1 & 0 \\ 1 & 0 & 0 \end{pmatrix}.$$

The signs of w and ρ are flipped at impact to model the change in stance leg.

Now that we have described our biped models of interest, we construct a general reduction-based control law to generate walking gaits.

5.2 Reduction-Based Control Law

Given the multistage controlled reduction result of Theorem 11, the controller is designed to recursively break cyclic symmetries in the special almost-cyclic manner. For a general biped, the inner loop of the control law shapes the robot's energy into the 2-almost-cyclic form, and the nested outer loop plays two roles:

1. Implements passivity-based control on the reduced planar subsystem to construct robust gaits on flat ground.

2. Renders exponentially attractive surface $\mathcal{Z}$ defined by constraints (4.2) so that Theorem 10 holds.

We present this control law for a general n-DOF biped, building upon the construction of the single-stage control law from [46]. As mentioned earlier, we will model actuator saturation to demonstrate this method's practicality. We ignore saturation during the control law derivation,

but simulations will show that it is indeed robust to clipping effects. We begin by describing the Lagrangian-shaping inner loop.

5.2.1 Inner loop

We adopt the Lagrangian-shaping control law (4.8) to transform the system Lagrangian into a 2-ACL for controlled reduction to the planar subsystem. As seen in (5.1) and (5.6), the n-DOF potential energy $\mathcal{V}$ is not cyclic in the second variable φ, so we impose a "controlled symmetry" with respect to the second coordinate's rotation group $\mathbb{S}^1$ [24]. This is most naturally accomplished with potential shaping to replace $\mathcal{V}$ with the planar biped's cyclic potential energy, $\mathcal{V}_\theta$ (e.g., (5.2) or (5.7)), constructed from a scaled height due to leg splay. We will incorporate this shaping into the inner loop, and later revisit another form of controlled symmetry in the outer loop to achieve slope invariance.

We begin with the 2-ACL of (4.1) for $k = 2$:

$$\mathcal{L}_{\lambda_1^2}(q, \dot{q}) \;=\; \frac{1}{2}\dot{q}^T M_{\lambda_1^2}(q_2^n)\dot{q} + Q_{\lambda_1^2}^T(q)\dot{q} - \mathcal{V}_{\lambda_1^2}(q), \tag{5.11}$$

where $M_{\lambda_1^2}$, $Q_{\lambda_1^2}$, and $\mathcal{V}_{\lambda_1^2}$ are defined in (4.4)-(4.6), substituting $\mathcal{V}_\theta$ for $\mathcal{V}_{\mathcal{R}_\lambda}$. Direct calculation shows that the stage-2 functional Routhian associated with 2-ACL $\mathcal{L}_{\lambda_1^2}$ is the Lagrangian of the scaled planar walker:

$$\mathcal{L}_\theta(\theta, \dot{\theta}) \;=\; \frac{1}{2}\dot{\theta}^T M_\theta(\theta)\dot{\theta} + \mathcal{V}_\theta(\theta), \tag{5.12}$$

which yields the reduced control system (f_θ, g_θ) with subsystem input v_θ.

Given this target reduction, the feedback control law that shapes $\mathcal{L}$ into $\mathcal{L}_{\lambda_1^2}$ is

$$u \;:=\; B^{-1}\left(C(q,\dot{q})\dot{q} + N(q) + M(\varphi,\theta)M_{\lambda_1^2}(\varphi,\theta)^{-1}\left(-C_{\lambda_1^2}(q,\dot{q})\dot{q} - N_{\lambda_1^2}(q) + Bv\right)\right), \tag{5.13}$$

where $C_{\lambda_1^2}$ and $N_{\lambda_1^2} = \frac{\partial}{\partial q}\mathcal{V}_{\lambda_1^2}$ are the shaped terms as in (4.8), and the vector $v = (v_\psi, v_\varphi, v_\theta^T)^T$ contains the auxiliary control inputs of the outer loop, to be defined later. Finally, using conserved momentum functions $\lambda_1(\psi) = -\alpha_1(\psi - \tilde{\psi})$ and $\lambda_2(\varphi) = -\alpha_2\varphi$, for $\alpha_1, \alpha_2 > 0$, we establish steering control to constant angle $\tilde{\psi}$ in the yaw/heading DOF and lateral correction to vertical in the

roll/lean DOF. Inputting (5.13) into biped control system (f, g), we have the shaped dynamics

$$M_{\lambda_1^2}(\varphi, \theta)\ddot{q} + C_{\lambda_1^2}(q, \dot{q})\dot{q} + N_{\lambda_1^2}(q) \quad = \quad Bv, \tag{5.14}$$

which project onto the target dynamics of the scaled planar biped by Theorem 10. We associate the full-order shaped dynamics with the new control system $(f_{\lambda_1^2}, g_{\lambda_1^2})$ as in Section 3.2, with outer loop input v to be defined next.

5.2.2 Outer loop

In order to enforce constraint (4.2) for the decoupling of $\hat{f}_\theta$ provided by Theorem 10, we use control law (4.11) as input v_1^2 to render $\mathcal{Z}$ exponentially attractive. The robot's sagittal plane (the reduced subsystem) is decoupled along this surface, so we control it as a planar biped with well-known passivity-based techniques in v_θ. The first of these techniques is that of slope-changing "controlled symmetries," which will allow our biped to walk on flat ground given planar walking cycles down slopes [23, 24, 39].

In three dimensions, the orientation of the ground (the slope) can be represented by a rotation of the world frame, i.e., an element of SO(3). Thus, any change of slope is characterized by a group action of SO(3) on the biped's configuration space $\mathcal{Q}$. If we measured our 4-DOF biped's joint angles with respect to relative axes, the group action for any $A \in \mathrm{SO}(3)$ would be

$$\Phi_A(R_\mathrm{s}, \theta_\mathrm{ns}) \quad = \quad (A \cdot R_\mathrm{s}, \theta_\mathrm{ns}),$$

or, for the 5-DOF biped,

$$\Phi_A\left(R_\mathrm{s}, (\theta_\mathrm{t}, \theta_\mathrm{ns})\right) \quad = \quad \left(A \cdot R_\mathrm{s}, (\theta_\mathrm{t}, \theta_\mathrm{ns})\right).$$

The behavior of a passive biped strongly depends on the ground slope. Although both the kinetic energy and impact equations are invariant under the slope changing action Φ, this is not the case for the potential energy [24]. We can, however, control the robot's potential to the desired world orientation and thus impose symmetry on the system, i.e., a *controlled symmetry*. Any stable limit cycle down a slope can then be mapped to a stable limit cycle on an arbitrary slope.

For the planar two-link compass-gait biped, stable passive limit cycles exist down shallow slopes

between about 3° and 5°, as shown in [3, 4, 9]. The compass-gait-with-torso biped also has passive walking gaits after applying a PD control law (e.g., a spring-damper) to stabilize the torso upright [38]. Since we measure our sagittal-plane joint angles with respect to fixed axes as shown in Figs. 5.1-5.2, the group action for either planar robot simplifies to $\Phi_A(\theta) = \theta + \beta$, where $\beta = \sigma - \gamma$ is the angle of rotation parameterizing $A \in \mathrm{SO}(2)$, σ is the slope angle yielding the desired passive limit cycle (such as $\pi/50$), and γ is the actual ground slope angle for controlled "pseudo-passive" walking. Therefore, we implement controlled symmetries on this sagittal-plane subsystem to generate limit cycles on flat ground ($\gamma = 0$) using control law

$$v_\theta^\beta(\theta) \;:=\; B_\theta^{-1} \frac{\partial}{\partial \theta} \left(\mathcal{V}_\theta(\theta) - \mathcal{V}_\theta(\theta + \beta) \right). \tag{5.15}$$

We can then invoke the main result of [24] in the following:

Theorem 12. Let $\eta : [0, T] \to T\mathcal{Q}_\theta$ be a periodic hybrid flow of planar hybrid control system $\mathscr{HC}_\theta$ with continuous dynamics $\mathscr{EL}_\theta(\mathcal{L}_\theta) = v_\theta$ for $v_\theta = 0$ (i.e., a passive hybrid limit cycle). Then, letting $v_\theta = v_\theta^\beta(\theta)$ from (5.15), $\Phi_A \circ \eta : [0, T] \to T\mathcal{Q}_\theta$ is a periodic hybrid flow of the closed-loop system (i.e., a pseudo-passive hybrid limit cycle).

Similarly, the overall subsystem control law for the 5-DOF biped is

$$\begin{aligned} v_\theta &= v_\theta^\beta(\theta) + v_{\mathrm{pd}}(\theta, \dot{\theta}) \\ &= v_\theta^\beta(\theta) + B_\theta^{-1} \begin{pmatrix} 0 & -k_{\mathrm{p}}(\theta_{\mathrm{t}} + \beta) - k_{\mathrm{d}} \dot{\theta}_{\mathrm{t}} & 0 \end{pmatrix}^T, \end{aligned} \tag{5.16}$$

with proportional-derivative gains $k_{\mathrm{p}}, k_{\mathrm{d}} > 0$, respectively, to upright the torso. Note, however, that Theorem 12 does not necessarily hold in the planar subsystems of our 3-D bipeds due to out-of-plane coupling in the impact equations. This subsystem mapping is instead approximate, which we will find sufficient for building full-order gaits on flat ground.

These coupled impact equations also amplify state perturbations in several dimensions, having implications for the robustness of the desired subsystem limit cycle. This is critically important for steering motions, which inherently deviate from straight-ahead limit cycles. In order to increase overall robustness, we implement passivity-based reference energy tracking from [36] on the 4-DOF biped's planar subsystem, which has nearly constant energy in the hipped 4-DOF case. Note that the torso's PD-controller for the 5-DOF model results in non-trivial energy variation, preventing the application of this form of passivity-based control. We omit the time-varying case of passivity-based

energy tracking from [92, 93], which has not proven significantly beneficial [93].

To begin, we define the Lyapunov-like storage function

$$S(\theta, \dot{\theta}) \;=\; \frac{1}{2}(\mathcal{H}_\theta(\theta, \dot{\theta}) - \mathcal{H}_\theta^{ref})^2 \;\geq\; 0,$$

where $\mathcal{H}_\theta^{ref}$ is constant and $\mathcal{H}_\theta$ is the planar subsystem energy after imposing controlled symmetry:

$$\begin{aligned} \mathcal{H}_\theta &= \mathcal{K}_\theta + \mathcal{V}_\theta^\beta \\ &= \mathcal{K}_\theta + \mathcal{V}_\theta + (-\mathcal{V}_\theta + \mathcal{V}_\theta^\beta), \end{aligned} \tag{5.17}$$

with $\mathcal{K}_\theta = \frac{1}{2}\dot{\theta}^T M_\theta(\theta)\dot{\theta}$ and $\mathcal{V}_\theta^\beta = \mathcal{V}_\theta(\theta + \beta)$.

Due to the passivity property of robots, we have

$$\dot{\mathcal{H}}_\theta \;=\; \dot{\theta}^T \left(B_\theta v_\theta - \frac{\partial \mathcal{V}_\theta}{\partial \theta} + \frac{\partial \mathcal{V}_\theta^\beta}{\partial \theta} \right)$$

along trajectories of the shaped system. And, applying passivity-based control

$$\begin{aligned} v_\theta &= v_\theta^\beta + \bar{v}_\theta \\ &= B_\theta^{-1} \left(\frac{\partial \mathcal{V}_\theta}{\partial \theta} - \frac{\partial \mathcal{V}_\theta^\beta}{\partial \theta} \right) + \bar{v}_\theta, \end{aligned} \tag{5.18}$$

on the 2-D subsystem, it follows that $\dot{\mathcal{H}}_\theta = \dot{\theta}^T \bar{v}_\theta$. Then, taking the derivative of the storage function yields $\dot{S} = (\mathcal{H}_\theta - \mathcal{H}_\theta^{ref})\dot{\theta}^T \bar{v}_\theta$.

If we wisely choose the auxiliary input $\bar{v}_\theta$ for energy tracking, such as feedback law

$$\bar{v}_\theta(\theta, \dot{\theta}) \;:=\; -B_\theta^{-1} p(\mathcal{H}_\theta - \mathcal{H}_\theta^{ref})\dot{\theta} \tag{5.19}$$

with $p > 0$, then we have the negative semidefinite storage rate

$$\dot{S} \;=\; -2p||\dot{\theta}||^2 S \;\leq\; 0.$$

It is proven in [36] that under reasonable conditions (including control input saturation), this implies exponential convergence of a planar biped's total energy to the reference energy between step impacts. If the reference is chosen to be the constant energy corresponding to a stable limit

Table 5.1: 4-DOF Biped Model Parameters

Physical	Hip Mass	Leg Mass	Hip Width	Leg Length	Leg Splay	Saturation
Variable	M	m	w	l	ρ	$U_{\max}$
Value	10 kg	5 kg	0.1 m	1 m	0.0188 rad	20 Nm

Control	λ_1-gain	λ_1-angle	λ_2-gain	h_1-gain	h_2-gain	v_θ^β-angle	$\bar{v}_\theta$-gain	$\bar{v}_\theta$-energy
Variable	α_1	$\tilde{\psi}$	α_2	ξ_1	ξ_2	β	p	$\mathcal{H}_\theta^{ref}$
Value	15	0 rad	10	30	15	$\pi/50$ rad	20	154.8742 J

cycle (assuming that the limit cycle has nearly constant energy), then this passivity-based controller expands the limit cycle's basin of attraction.

The subsystem control law (5.16) or (5.18) for the 4-DOF or 5-DOF biped, respectively, is incorporated into the full-order shaped system $(f_{\lambda_1^2}, g_{\lambda_1^2})$ by defining the new control system $(\hat{f}_{\lambda_1^2}, \hat{g}_{\lambda_1^2})$ with input $v_1^2 = (v_\psi, v_\varphi)^T$ as in (3.23). The controlled 2-reduced vector field $\hat{f}_\theta$ is defined by (3.26).

5.3 Four-DOF Biped Simulations

We now examine our 4-DOF biped, introduced in Section 5.1, with physical parameters shown in Table 5.1. In order to walk straight-ahead using reduction-based control law (5.13), we choose momentum function λ_1 with gain constant $\alpha_1 = 15$ and desired heading $\tilde{\psi} = 0$ to counteract the yaw motion induced by the hip. The other control parameters are given in Table 5.1. Applying (5.13) under saturation constant $U_{\max} = 20$ Nm, the hybrid control system $\mathscr{HC}_{4\mathrm{D}}$ yields the closed-loop hybrid system $\mathscr{H}_{4\mathrm{D}}^{\mathrm{cl}}$ for the controlled reduction depicted in Fig. 5.3.

Generally speaking, we cannot analyze the stability of $\mathscr{H}_{4\mathrm{D}}^{\mathrm{cl}}$ using the restricted Poincaré map associated with the planar subsystem. We cannot invoke Theorem 4 to show stability of the divided coordinates *a priori*, because joint velocities encounter a discontinuous jump off the conserved quantity surface $\mathcal{Z}_{4\mathrm{D}}$ at every impact event (except for the special case of hipless bipeds studied in [45] and [51]). Away from this surface, solutions of $\hat{f}_{\lambda_1^2}$ and $\hat{f}_\theta$ cannot be analytically related by Theorem 10, so the beneficial decoupling effect for the planar limit cycle does not hold.

We tune the output linearizing control law v_1^2 with sufficiently large gains ξ_1, ξ_2 to quickly correct this error during each step cycle, so that any perturbed trajectory does not leave the basin of attraction of the subsystem limit cycle (which is expanded by passivity-based law $\bar{v}_\theta$). We can then numerically verify stability of the full-order biped walking straight-ahead on flat ground.

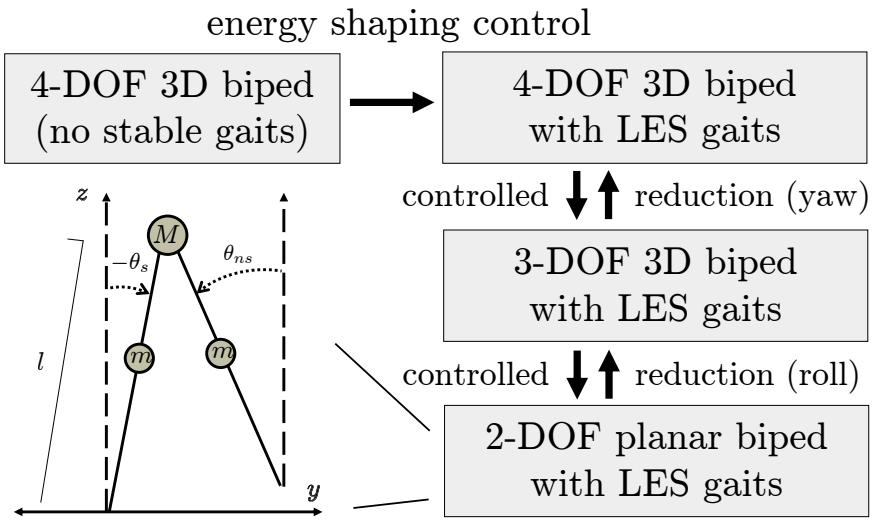

Figure 5.3: Controlled reduction overview of 4-DOF biped: the first reduction stage divides out the yaw DOF of the transverse plane, and the second stage divides out the lean DOF of the frontal plane, yielding the dynamics of the planar 2-DOF compass-gait biped.

5.3.1 Straight-ahead walking

Simulations in Matlab show that $\mathscr{H}_{4\mathrm{D}}^{\mathrm{cl}}$ produces a 2-periodic hybrid orbit, $\mathcal{O}_{4\mathrm{D}}$ of Fig. 5.4, which is constructed from its planar subsystem's hybrid orbit. The intersection between $\mathcal{O}_{4\mathrm{D}}$ and Poincaré section $G_{4\mathrm{D}}$ over two steps is the 2-fixed point

$$x^* \approx (0.0699, 0.0135, -0.3074, 0.3102, 0.0774, -0.0508, -1.6907, -2.0610)^T.$$

We numerically calculate the eigenvalue magnitudes of the linearized Poincaré map $\delta P_{4\mathrm{D}}^2$ about this 2-fixed point to be within the unit circle:

$$|\mathrm{eig}\{x^*\}| \approx \{0.2047, 0.2047, 0.1286, 0.0383, 0.0037, 0.0000, 0.0000, 0.0000\},$$

thus confirming that $\mathcal{O}_{4\mathrm{D}}$ is LES. We see in Fig. 5.4 that the yaw dynamics of the transverse plane and the lean dynamics of the frontal plane follow 2-periodic hybrid orbits. These motions are naturally induced by the robot's hip during each step cycle (and we verify that these motions disappear when $w = 0, \rho = 0$), but evolve in a controlled periodic manner due to our choice of conserved momentum functions.

At the perfectly plastic impact events, the swing foot's velocity component normal to ground is instantaneously dissipated, resulting in a discontinuous loss of total stored (unshaped) energy.

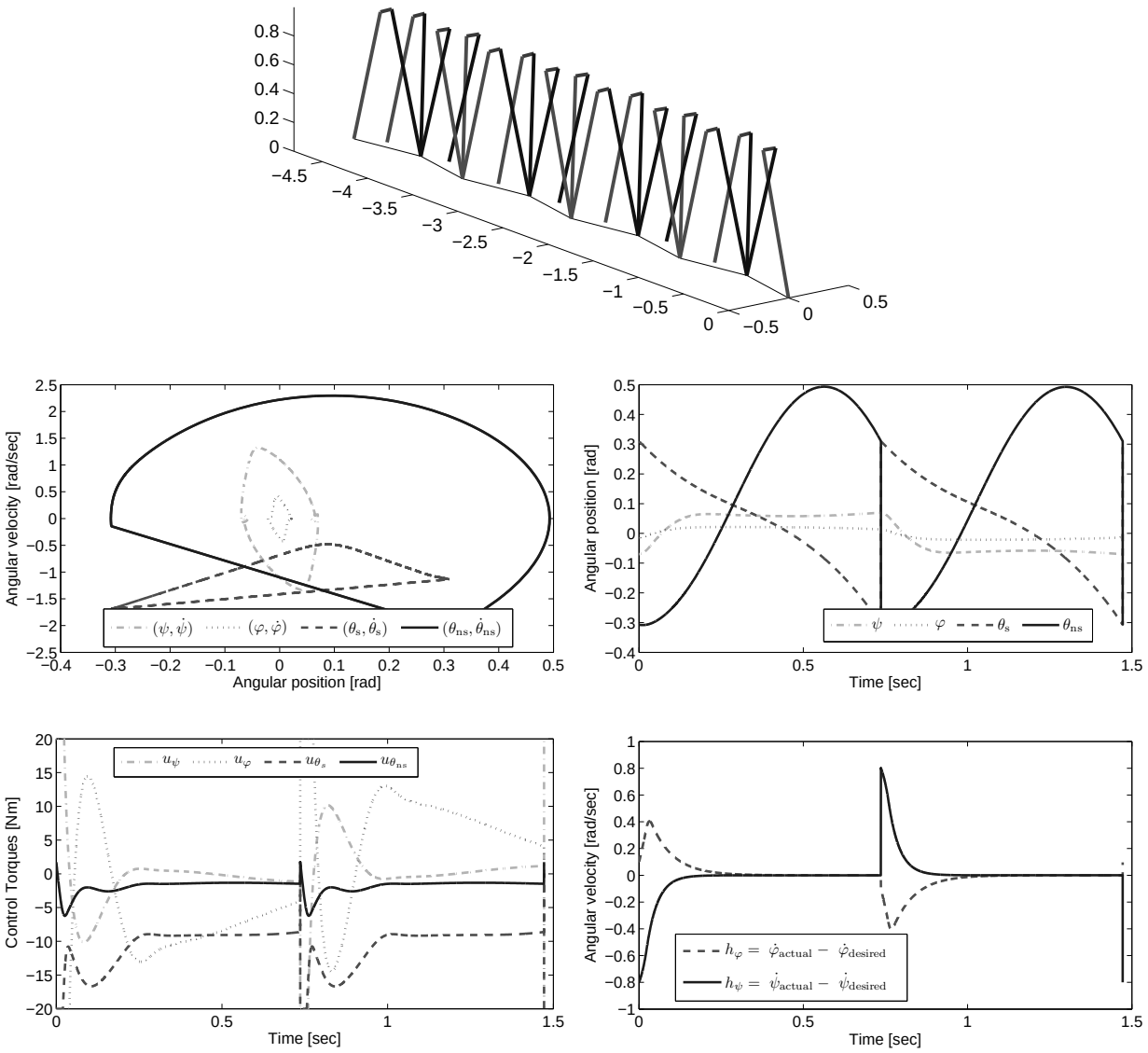

Figure 5.4: 4-DOF biped's 2-periodic straight-ahead gait animation (top), phase portrait (middle left), joint trajectory (middle right), saturated control (bottom left), and conserved quantity errors (bottom right). The phase portrait shows planar slices of $\mathcal{O}_{\rm 4D}$ by plotting angular positions against angular velocities, illustrating 2-step periodicity in the phase space.

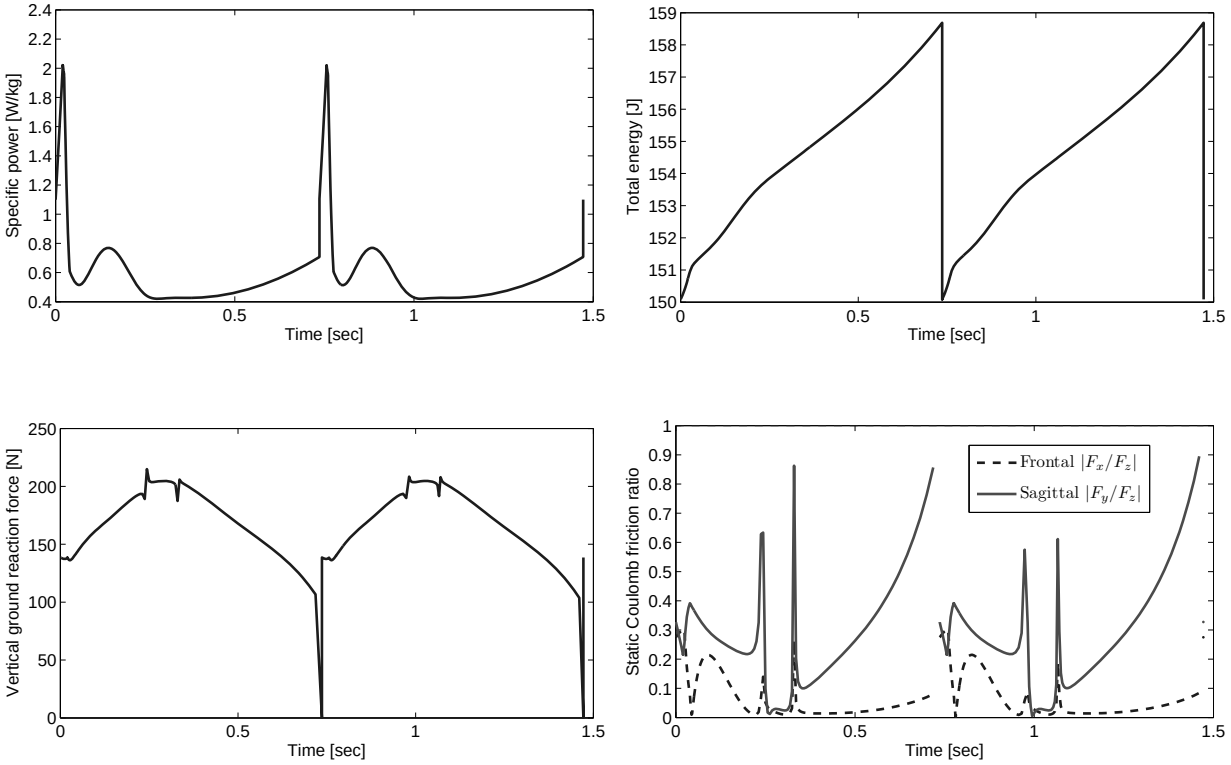

Figure 5.5: Characteristics of 4-DOF biped's 2-periodic straight-ahead gait: instantaneous specific power (top left), total stored energy (top right), vertical ground reaction force (bottom left), and Coulomb friction ratios (bottom right).

We see in Fig. 5.5 that this loss is gradually replenished by controlled symmetries law (5.15) as the virtual gravity vector accelerates the biped between impact events. However, the clipped input spikes (Fig. 5.4) and corresponding impulses in instantaneous power $\dot{q}^T\tau$ (Fig. 5.5) are artifacts of subcontrollers (5.18) and (4.11) acting to proportionally correct the error in conserved quantities and planar-subsystem energy, respectively, introduced by each impact discontinuity. These spikes might raise concern about violating contact constraints at the stance foot, but we can show that our choice of input saturation enforces these constraints.

5.3.2 Contact constraints

This simulation uses a model of a kinematic chain with its base fixed at the contact point between stance foot and ground. However, bipedal locomotion is unilaterally constrained in the vertical contact force: the robot's foot can only exert a negative force against ground, resulting in an equal and opposite (positive) reaction force. When this vertical ground reaction force (GRF) becomes zero, the robot loses contact with ground and begins a flight phase, which would violate our fixed-

base assumption. We must satisfy another contact constraint to prevent slipping: the ratio of each horizontal GRF component to the vertical GRF component remains smaller than the static Coulomb friction coefficient [94], i.e., the GRF vector remains inside the friction cone.

We therefore calculate the GRF vector $F_{\text{ext}} = (F_x, F_y, F_z)^T$ needed to keep the stance foot fixed at this ground contact point throughout the 4-DOF walking gait, and verify the two conditions needed for the validity of the above simulation:

1. The vertical GRF component remains strictly positive, i.e., $F_z(t) > 0$ for all t.
2. The GRF vector remains within the friction cone, i.e., $|F_x(t)/F_z(t)|, |F_y(t)/F_z(t)| < \mu$ for all t with static Coulomb friction coefficient $\mu = 1$ (provided by rubber feet).

This requires us to model an extended $(n+3)$-DOF system with generalized configuration vector $q_{\text{e}} = (q_{\text{pos}}^T, q^T)^T$, where $q_{\text{pos}} = (x_{\text{pos}}, y_{\text{pos}}, z_{\text{pos}})^T \in \mathbb{R}^3$ is the Cartesian coordinate vector for the stance ankle. Therefore, system (5.3) with a floating base at the stance ankle becomes

$$M_{\text{4D}}^{\text{e}}(q_{\text{e}})\ddot{q}_{\text{e}} + C_{\text{4D}}^{\text{e}}(q_{\text{e}}, \dot{q}_{\text{e}})\dot{q}_{\text{e}} + N_{\text{4D}}^{\text{e}}(q_{\text{e}}) \;=\; B_{\text{4D}}^{\text{e}} u + \begin{pmatrix} F_{\text{ext}} \\ 0_{n\times 1} \end{pmatrix}, \tag{5.20}$$

Applying saturated control law (5.13), we have the closed-loop system with extended state $x_{\text{e}} = \binom{q_{\text{e}}}{\dot{q}_{\text{e}}}$:

$$\dot{x}_{\text{e}} \;=\; f_{\text{e}}(x_{\text{e}}) + g_{\text{e}}(x_{\text{e}})F_{\text{ext}}. \tag{5.21}$$

Following the derivation from [5], we define output vector $y_{\text{e}} = h_{\text{e}}(x_{\text{e}}) := q_{\text{pos}}$, which must be identically zero to satisfy the contact constraints:

$$\dot{h}_{\text{e}} \;=\; L_{f_{\text{e}}} h_{\text{e}} + (L_{g_{\text{e}}} h_{\text{e}})F_{\text{ext}} \;\equiv\; 0, \tag{5.22}$$

where Lie derivative $L_{g_{\text{e}}} h_{\text{e}} = \nabla_{x_{\text{e}}} h_{\text{e}} g_{\text{e}} = 0$. Taking the next time-derivative,

$$\ddot{h}_{\text{e}} \;=\; L_{f_{\text{e}}}^2 h_{\text{e}} + L_{g_{\text{e}}} L_{f_{\text{e}}} h_{\text{e}} F_{\text{ext}} \;\equiv\; 0 \tag{5.23}$$

$$\implies F_{\text{ext}} \;=\; -(L_{g_{\text{e}}} L_{f_{\text{e}}} h_{\text{e}})^{-1} L_{f_{\text{e}}}^2 h_{\text{e}}, \tag{5.24}$$

where $L_{g_{\text{e}}} L_{f_{\text{e}}} h_{\text{e}}$ is the (invertible) top-left 3×3 submatrix of $M_{\text{4D}}^{\text{e}^{-1}}$ and $L_{f_{\text{e}}}^2 h_{\text{e}} = [I_{3\times 3} \quad 0_{3\times n}]\, f_{\text{e}}$.

The vertical GRF component F_z is plotted through the 4-DOF walking gait in Fig. 5.5, verifying strict positivity. The Coulomb friction ratios $|F_x(t)/F_z(t)|$ and $|F_y(t)/F_z(t)|$ are also shown to

be within the friction cone limits for rubber feet. We have confirmed the validity of the above simulations, and we similarly verify these conditions for the remaining simulations in this thesis.

5.3.3 Robustness to perturbations

We examine gait robustness by perturbing the 2-fixed point corresponding to the biped with passivity-based energy tracking (gain $p = 20$) and the biped without passivity-based energy tracking (gain $p = 0$). Using perturbations $\delta q = 0.01$, $\delta \dot{q} = 0.05$, we simulate six steps and observe the response for each system. We see in the state trajectories of Fig. 5.6 that the walker begins to fall without energy tracking but recovers nicely with the passivity-based control. Moreover, the energy plots show that the former system is unable to contain the subsystem energy after the perturbation (leading to instability), but the passivity-controlled system sufficiently insulates the subsystem energy and allows convergence to the limit cycle. In general, we observe that limit cycle convergence takes far fewer steps when using the passivity-based energy-tracking subcontroller.

5.3.4 Steering

This inherent robustness is also useful for attenuating perturbations from steering, which enter the system as changes in heading set-point $\tilde{\psi}$ of control law (5.13). In particular, we instruct the 4-DOF biped to perform a 90° turn over several steps as in the human steering study of [95, 96]. Starting with $\tilde{\psi} = 0$, a simple event-based supervisory controller increments this desired heading every other step by steering angle $s = \delta\tilde{\psi} = \pi/10$ until $\tilde{\psi} = \pi/2$. The turning maneuver, phase portrait, joint trajectories, saturated torques, and conserved quantity errors are shown in Fig. 5.7. We see that the zero dynamics subcontroller corrects the conserved quantities between each step. The passivity-based control keeps the sagittal subsystem energy $\mathcal{H}_\theta$ at the desired level, despite the injected energy from yaw rotation. Once the biped meets desired heading $\tilde{\psi} = \pi/2$, its gait stably converges to the straight-ahead 2-periodic limit cycle of $\mathcal{O}_{4\mathrm{D}}$ with a horizontally-shifted yaw orbit. Since turning motions inherently deviate from straight-ahead limit cycles, we say for now that the biped is *robust* to this sequence of steering angles. We return to the notion of steering stability in Sections 5.4.2 and 6.3.

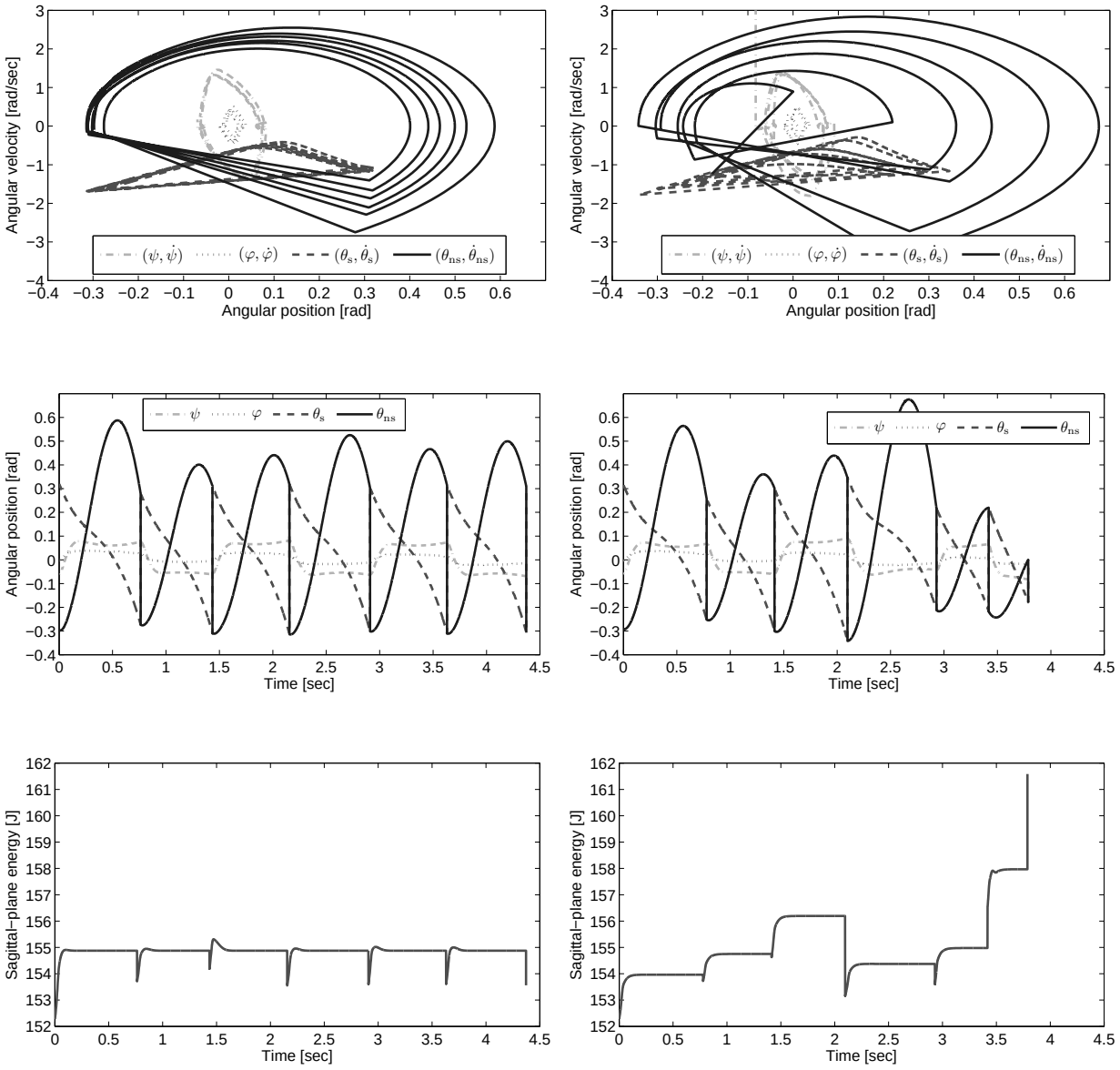

Figure 5.6: Perturbation responses of 4-DOF biped with passivity-based energy tracking (left) and without (right): phase portrait (top), joint trajectories (middle), and planar-subsystem energy trajectory (bottom).

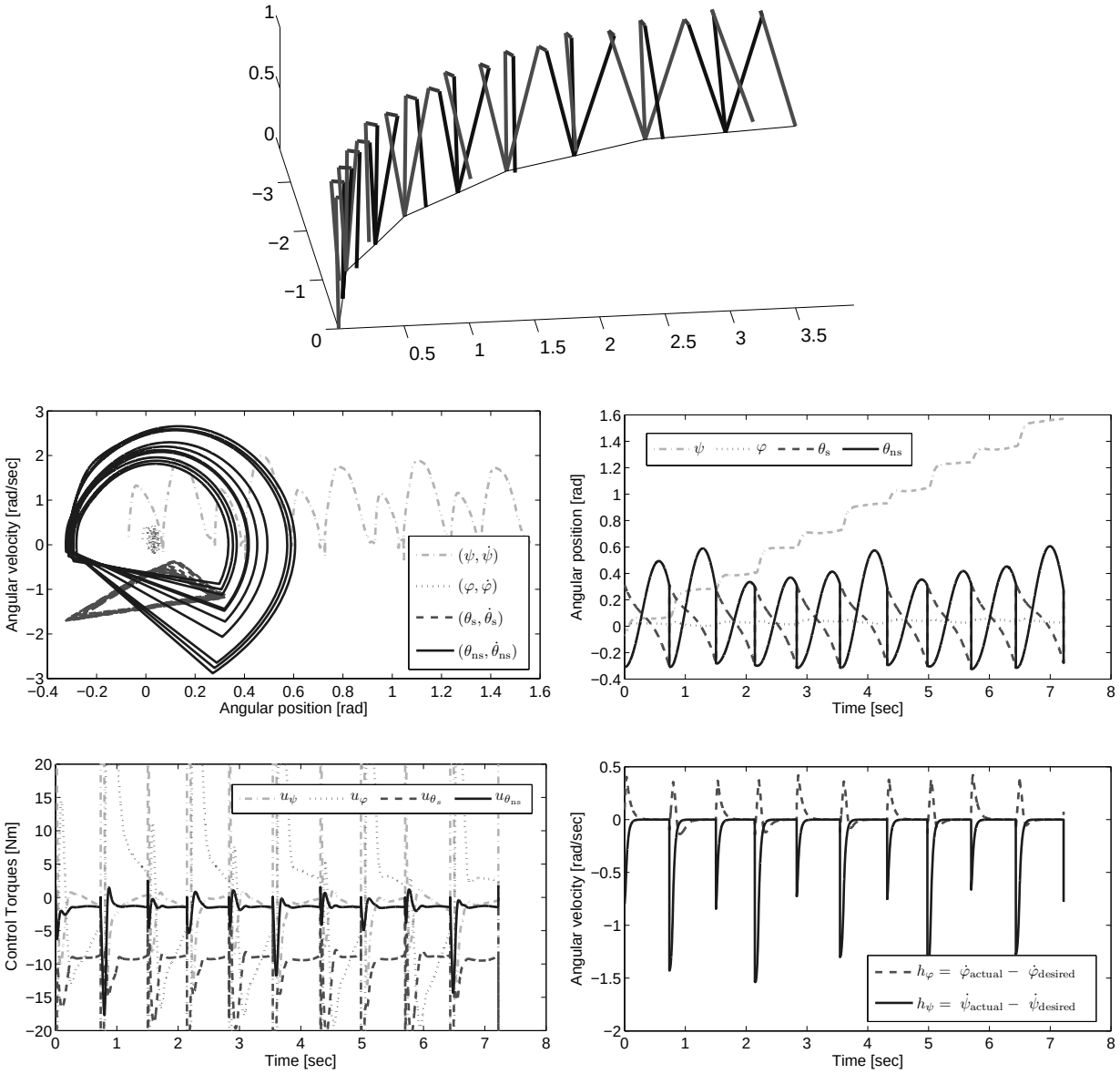

Figure 5.7: 4-DOF biped's 90°-turning maneuver's animation (top), phase portrait (middle left), joint trajectory (middle right), saturated control (bottom left), and conserved quantity errors (bottom right).

Table 5.2: 5-DOF Biped Model Parameters

Physical	Hip Mass	Leg Mass	Hip Width	Leg Length	Leg Splay
Variable	M_{h}	m	w	l	ρ
Value	10 kg	5 kg	0.1 m	1 m	0.0188 rad

Physical Cont'd	Torso Mass	Torso Length	Saturation
Variable	M_{t}	l_{t}	$U_{\max}$
Value	10 kg	0.5 m	30 Nm

Control	λ_1-gain	λ_1-angle	λ_2-gain	h_1-gain	h_2-gain	v_{pd}-gain	v_{pd}-gain	v_θ^β-angle
Variable	α_1	$\tilde{\psi}$	α_2	ξ_1	ξ_2	k_{p}	k_{d}	β
Value	20	0 rad	30	30	15	700	200	0.052 rad

5.4 Five-DOF Biped Simulations

After applying feedback control law (5.13) under actuator saturation, closed-loop hybrid system $\mathscr{H}_{5\mathrm{D}}^{\mathrm{cl}}$, with physical and control parameters in Table 5.2, provides the controlled reduction depicted in Fig. 5.8. As was the case with the 4-DOF biped, we cannot analyze the stability of $\mathscr{H}_{5\mathrm{D}}^{\mathrm{cl}}$ using the restricted Poincaré map associated with the reduced subsystem. We will show, however, that $\mathscr{H}_{5\mathrm{D}}^{\mathrm{cl}}$ is similarly robust to brief errors off $\mathcal{Z}_{5\mathrm{D}}$ by considering the biped's full-order behavior.

5.4.1 Straight-ahead walking

When walking straight-ahead on flat ground, $\mathscr{H}_{5\mathrm{D}}^{\mathrm{cl}}$ produces a 2-step periodic orbit, $\mathcal{O}_{5\mathrm{D}}^{\mathrm{st}}$ of Fig. 5.9, which is constructed from its planar subsystem's limit cycle. The intersection between $\mathcal{O}_{5\mathrm{D}}^{\mathrm{st}}$ and Poincaré section $G_{5\mathrm{D}}$ is the 2-fixed point

$$x^{*\mathrm{st}} \approx (0.0544, 0.0062, -0.2543, 0.0021, 0.2558, 0.0673, -0.0173, -1.2871, 0.0673, -1.7233)^T .$$

We numerically calculate the eigenvalues of the linearized Poincaré map $\delta P_{5\mathrm{D}}^2$ about this fixed-point over two steps:

$$|\mathrm{eig}\{x^{*\mathrm{st}}\}| \approx \{0.7629, 0.7629, 0.2745, 0.0736, 0.0344, 0.0134, 0.0034, 0.0003, 0.0003, 0.0000\} .$$

All magnitudes are within the unit circle, thus confirming LES. We also see that the yaw and lean dynamics follow 2-periodic orbits, a natural result of the controlled reduction.

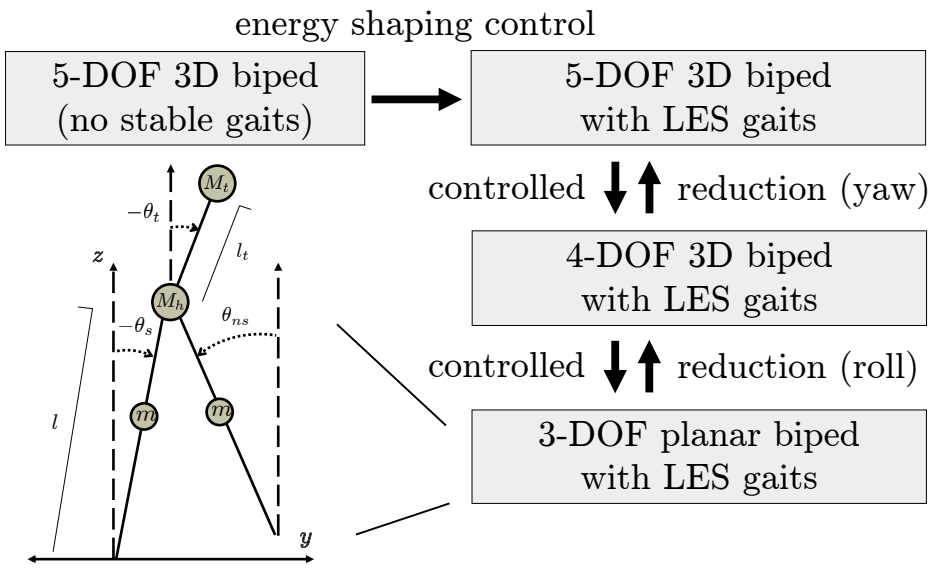

Figure 5.8: Controlled reduction overview of 5-DOF biped: the first reduction stage divides out the yaw DOF of the transverse plane, and the second stage divides out the lean DOF of the frontal plane, yielding the dynamics of the planar 3-DOF compass-gait-with-torso biped.

5.4.2 Steering

We demonstrate steering capabilities with the 90° turning maneuver seen in Fig. 5.10. Starting with $\tilde{\psi} = 0$, an event-based supervisory controller increments this desired yaw angle every other step by steering angle $s = \delta\tilde{\psi} = \pi/14$ until $\tilde{\psi} = \pi/2$. Once the biped meets this heading, its gait stably converges to the straight-ahead limit cycle of $\mathcal{O}^{\text{st}}_{\text{5D}}$ with a horizontally-shifted yaw orbit.

If we instead continue this constant-curvature steering, we observe convergence to a periodic turning gait *modulo yaw*:

$$x^{*\text{tu}(s)} + (s \quad 0_{1\times 9})^T \;=\; P^2_{\text{tu}(s)}\left(x^{*\text{tu}(s)}\right),$$

where the 2-fixed point of orbit $\mathcal{O}^{\text{tu}(s)}_{\text{5D}}$ is given by

$$x^{*\text{tu}(s)} \;\approx\; (0.2147, 0.0185, -0.2534, 0.0043, 0.2488, 0.0015, -0.0052, -1.2706, 0.0601, -1.7303)^T.$$

This orbit is confirmed LES (modulo s) with eigenvalues

$$|\text{eig}\{x^{*\text{tu}(s)}\}| \;\approx\; \{0.7835, 0.3594, 0.2111, 0.2111, 0.0386, 0.0047, 0.0047, 0.0003, 0.0001, 0.0000\}.$$

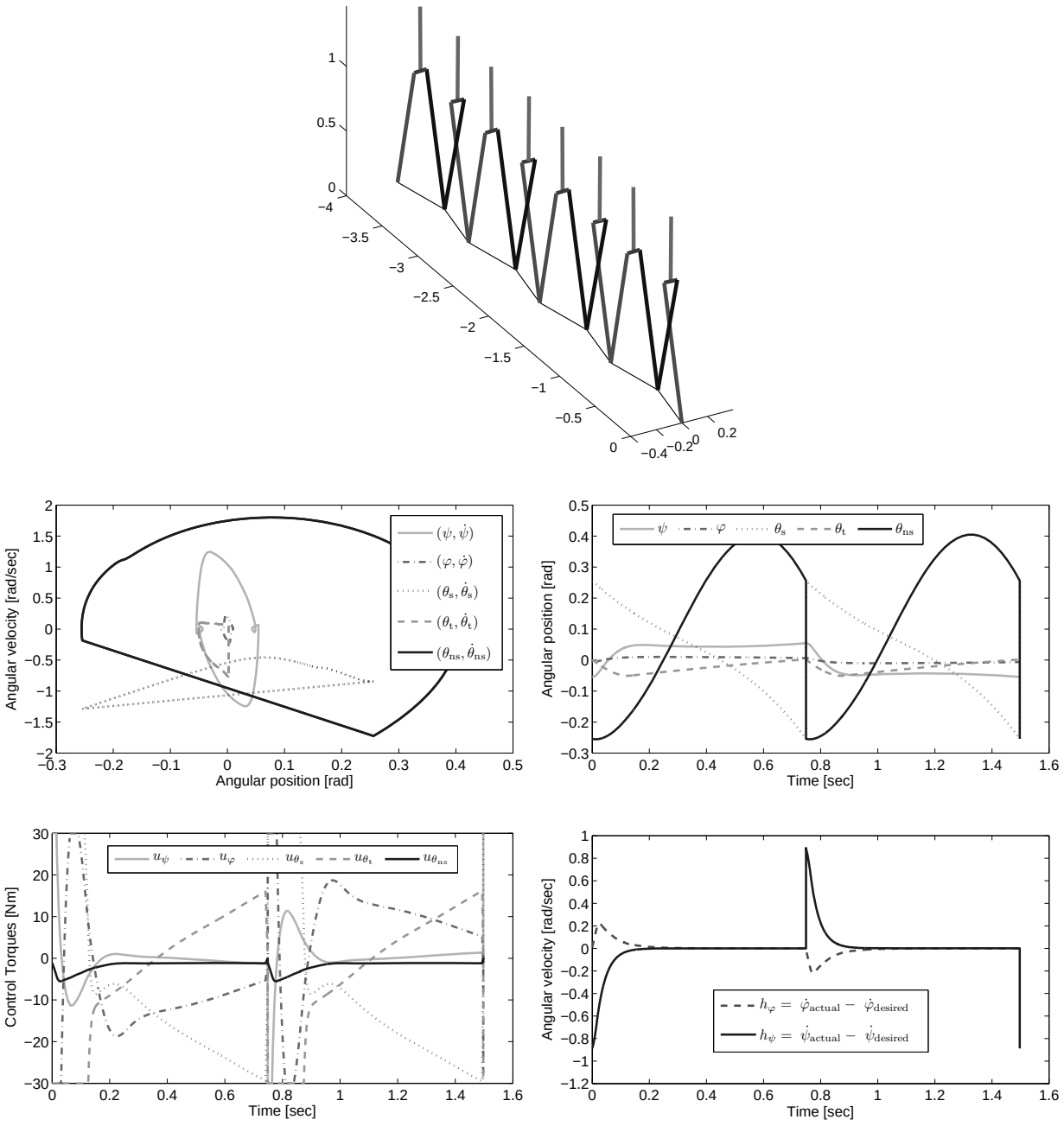

Figure 5.9: 5-DOF biped's 2-periodic straight-ahead gait animation (top), phase portrait (middle left), joint trajectory (middle right), saturated control (bottom left), and conserved quantity errors (bottom right).

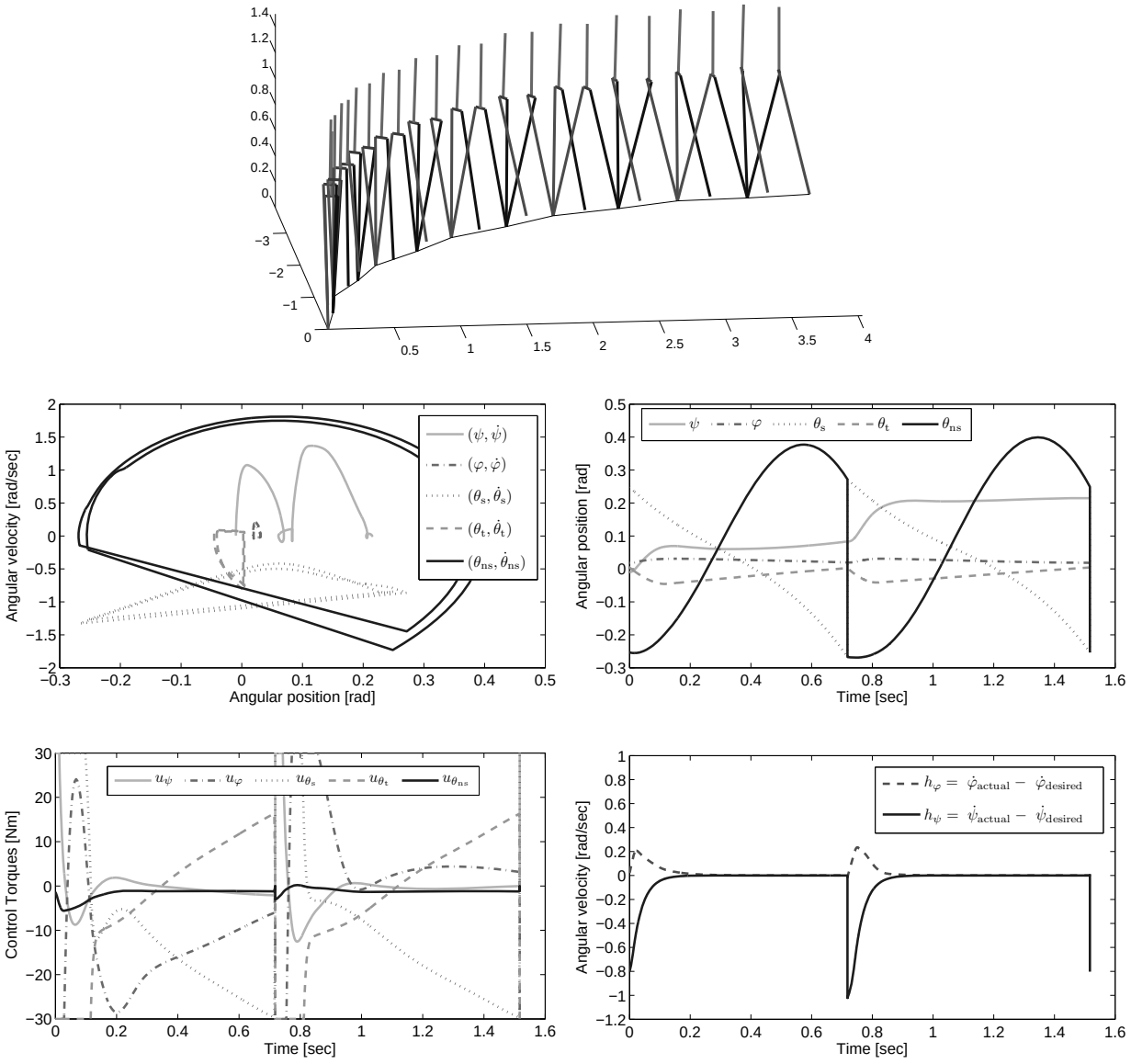

Figure 5.10: 5-DOF biped's 2-periodic turning gait animation (top), phase portrait (middle left), joint trajectory (middle right), saturated control (bottom left), and conserved quantity errors (bottom right).

We see in Fig. 5.10 that $\mathcal{O}_{5D}^{tu(s)}$ has a perturbed subsystem orbit compared to $\mathcal{O}_{5D}^{st}$, since the outer leg swings a longer distance in arclength[5] (1.081 m) than the inner leg (1.033 m) along this curved path. This behavior occurs naturally (without reference trajectories) and resembles the turning perturbations in the human studies of [95], which we discuss further in Chapter 7. In general, we find that stable turning gaits exist for a wide range of steering angles, as documented in [43,50,51]. We show how the 2-fixed-point and gait characteristics of linear step length and time period evolve over the range of steering angles $[0, 0.235]$ in Fig. 5.11. Beyond this range, we notice a period-doubling bifurcation leading to chaotic instability, shown in Fig. 5.12.

5.5 Energetic Efficiency

We can analyze the energetic cost of these gaits by integrating $\dot{q}^T\tau$ to obtain the net work per step. In particular, we use this to calculate the *specific mechanical cost of transport* c_{mt} (mechanical work done per unit weight per unit distance), which is a dimensionless metric commonly adopted to study the efficiency of a locomotor control strategy on a given mechanical system [15,97].

We find that the cost of the 4-DOF biped for straight-ahead walking is $c_{mt} = 0.073$ and for turning is $c_{mt} = 0.071$. The cost for the 5-DOF straight-ahead and turning gaits are lower at $c_{mt} = 0.036$ and $c_{mt} = 0.037$, respectively. These numbers are comparable with human walking (in terms of metabolic cost) at $c_{mt} = 0.5$ and the Cornell biped at $c_{mt} = 0.055$, and far surpass Honda ASIMO at $c_{mt} = 1.6$ as seen in Fig. 5.13 [15]. The improved efficiency of the 5-DOF gaits over the 4-DOF gaits is attributable to the torso link, which naturally leans into the direction of walking during substantial portions of the gait. In other words, the torso's center of mass contributes a gravitational force to the forward ballistic motion. This is exploited in the optimized gaits of [5,34] resulting in more exaggerated torso pitch.

We must note, however, that this metric does not account for power consumption of the on-board control system or the actuators – the *energetic* cost of transport c_{et} (energy consumed per unit weight per unit distance) must be computed for this purpose [15]. Since the models presented have only been studied in simulation, we can only speculate about energetic cost based on the efficiency (in terms of c_{mt}) of the underlying reduction-based control strategy. A conservative estimate that assumes fifty percent actuator efficiency with no regeneration during negative work still results in

[5] Although the outer leg swings a longer distance in arclength than the inner leg for sharp turns, the linear distance between step placements has an inverse relationship for large steering angles as seen in Fig. 5.11.

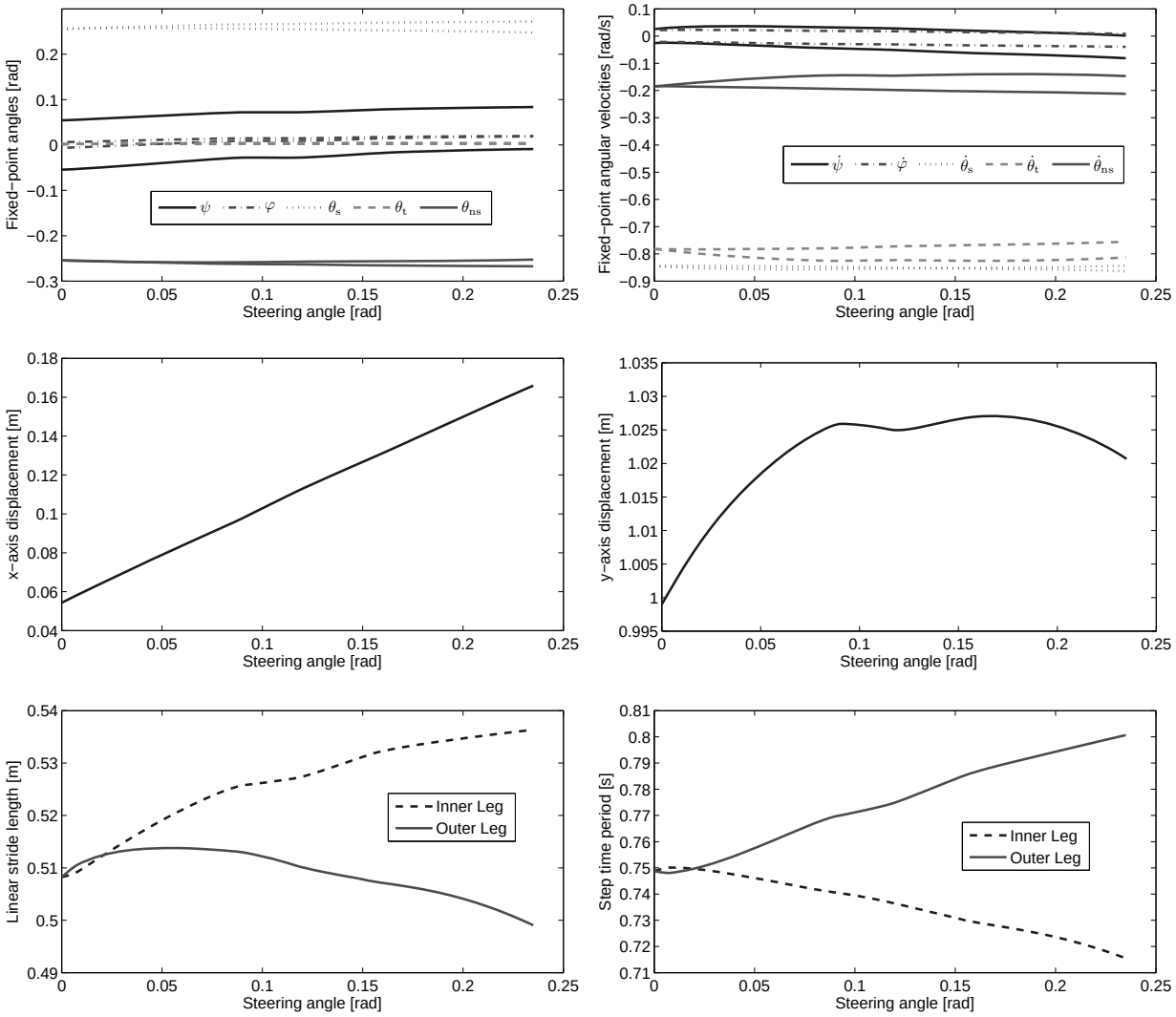

Figure 5.11: Evolution of 5-DOF biped's turning 2-fixed-point $x^{*\mathrm{tu}(s)}$ (top), x-axis displacement (middle left), y-axis displacement (middle right), linear step length (bottom left), and step time period (bottom right) over steering angle $s \in [0, 0.235]$.

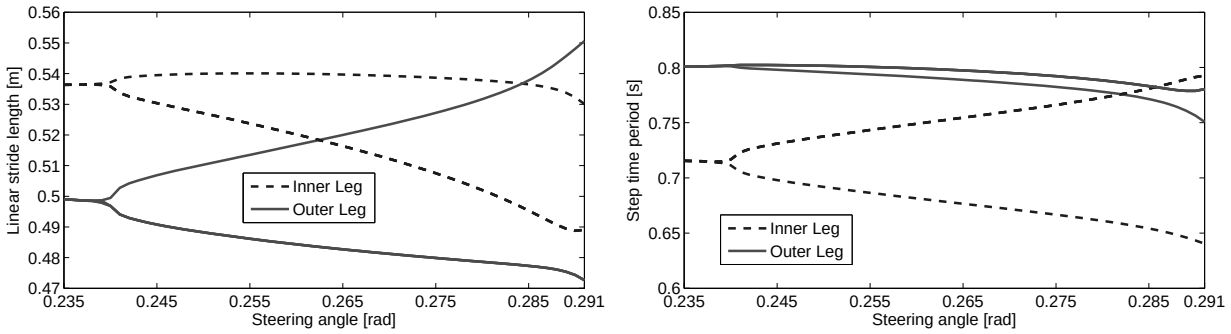

Figure 5.12: Bifurcation diagram of 5-DOF biped's linear step length (left) and time period (right) over steering angle $s \in [0.235, 0.2914]$.

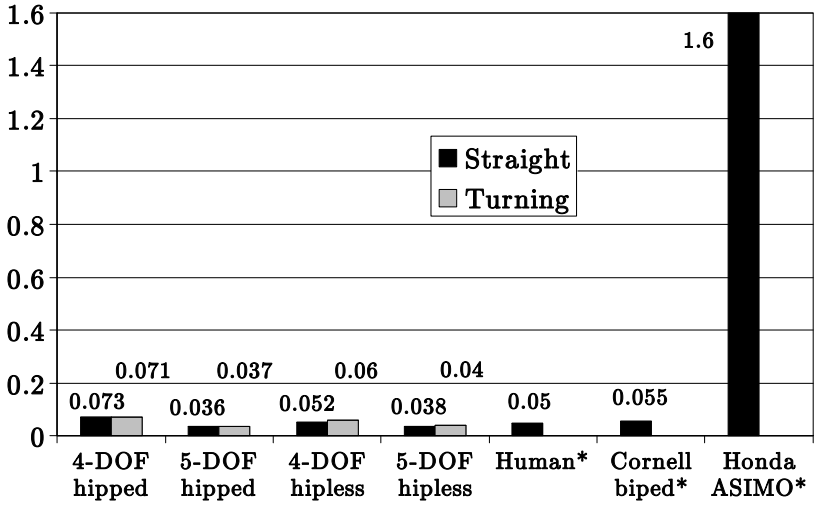

Figure 5.13: Specific mechanical cost of transport (mechanical work done per unit weight per unit distance) for various mechanisms. Hipless model results can be found in Section 6.5. *Data obtained from [15].

favorable comparisons with human data and the Collins biped. This demonstrates a strength of the energy-shaping control paradigm, and controlled reduction in particular, which aim to minimally cancel natural dynamics for energetic efficiency. Moreover, this suggests that robot walkers similar to the 4-DOF or 5-DOF models (perhaps even the humanoid studied in [80]) could be constructed to walk dynamically with limited energy consumption.

5.6 Remarks

Given our assumption of full actuation, one might instead consider inverting the plant to linearize the system and track some pre-designed gait trajectory. However, we cannot impose arbitrary dynamics or use large gains due to input torque saturation and contact constraints. Impact events also introduce velocity discontinuities that usually do not coincide with reference limit cycles. Limited control gains cannot necessarily attenuate this tracking error during the short time between impacts. On the other hand, we have observed that reduction-based energy shaping remains within saturation limits, so the planar subsystem remains decoupled for any state on the conserved quantity surface $\mathcal{Z}$. This results in walking gaits with sizeable basins of attraction, especially when utilizing passivity-based energy tracking.

Underactuated methods of partial feedback linearization that enforce virtual holonomic con-

straints rather than reference trajectories have been successful on 3-D bipeds with unactuated ankles [34,35]. Although controlled reduction requires actuation at the stance ankle, the yaw DOF input could be realized mechanically with a passive damper as shown in Section 3.2. This would allow a more feasible (and arguably anthropomorphic) implementation with a 2-DOF ankle actuator for lean and pitch – humans routinely actuate these DOFs during walking and certainly have passive yaw damping through ankle tendons and/or rotational friction when pivoting about the ground contact point. In fact, peak power output during a human walking gait occurs at the ankle pitch DOF during push-off [98], which we observe in our reduction-based results (with the caveat that double-support is instantaneous so push-off appears to occur immediately at impact).

We have shown that increasingly complex bipedal robots can achieve stable directional 3-D walking with reduction-based control. This method embraces the beneficial passive dynamics of the robot in order to produce time-invariant and asymptotically stable walking with human-like swaying motion. This provides robustness to small perturbations (e.g., steering), naturally resulting in multiple types of dynamic walking gaits. We next show that these straight-ahead and turning gaits form a set of motion primitives for planning stable walking paths through 3-D environments.

CHAPTER 6

GAIT PRIMITIVES FOR MOTION PLANNING

We saw in the previous chapter that reduction-based control yields directional control authority to produce asymptotically stable turning gaits. Related results for underactuated 3-D bipeds are presented in [35], where virtual constraints are enforced to restrict analysis to the periodic motion of a reduced-order subsystem. Both methods demonstrate steering capabilities, with the latter showing input-to-state stability for steering along paths with sufficiently mild curvature.

In order to build bipedal robots that can quickly and efficiently navigate through real-world environments, the stability of dynamic walking must be considered when *planning* walking paths with significant steering. Therefore, we present in this chapter the motion planning framework of [43, 99] for bipeds that exhibit asymptotically stable (i.e., dynamic) walking behavior. We show that straight-ahead and turning gaits form a set of *gait primitives* that can be sequentially composed under bounded curvature and switching conditions without causing the biped to fall. This employs a discrete-time analogy of the switching controller-composition method of [52], where (Lyapunov) funnels show stability for sequential paddle-and-ball batting maneuvers.

6.1 Quasi-Static Motion Planning

We begin by reviewing some motivating work in humanoid path planning based on primitives satisfying postural ZMP constraint (1.4). Note, however, the important distinction that satisfying this ZMP condition does not necessarily imply stable walking motion [6, Section 10.8].

Full-body posture planning is achieved in [19] by initially computing a large set of statically-stable configurations. A path between goal configurations is then found by growing a rapidly-exploring random tree, which connects samples only if a collision-free ZMP-constrained path exists. This is used in [20] for locomotion planning, restricting the problem to a discrete set of foot placements connected by valid stepping motions. A similar method in [21] pre-computes a small set of ZMP-constrained motion primitives, which bias the sampling of configurations between planned foot

placements. These primitives prescribe high-quality motions that can be shaped to match common tasks such as for walking and climbing. Instead of tracking pre-computed trajectories, our approach is based on autonomous LES limit cycles.

A two-stage global planner is proposed in [17] that first uses a sampling-based algorithm to find a collision-free path for the *functional decomposition* of the robot body. That is, the robot is modeled as a bounding box on a walking surface, reducing the initial planning problem to configuration space SE(2) – x, y position and orientation. Randomly generated samples are locally connected by *Dubins curves* (circular arcs with tangential line segments [100]), and these SE(2) paths are given to a walking pattern generator that produces whole-body motions for ZMP-constrained locomotion. We will show that the nature of our gait primitives allows a similar functional decomposition approach for generating stable dynamic walking paths composed of constant-curvature arc segments.

6.2 Asymptotically Stable Gait Primitives

We can now formalize the notion of asymptotically stable gait primitives corresponding to strategies for straight-ahead walking and turning[1] clockwise (CW) or counter-clockwise (CCW). These strategies will enable motion planning for dynamic walkers in 3-D space.

Definition 15. An *asymptotically stable gait primitive* is a pair $\mathcal{G} = (P^h_{\text{cl}}, x^*)$, where P_{cl} is a closed-loop Poincaré map for which x^* is an asymptotically stable h-fixed-point (modulo yaw).

Since asymptotically stable limit cycles are fundamental to dynamic walking, we often call these *dynamic* gait primitives for brevity. For the purpose of sequential composition, a gait can be arbitrarily oriented about the z-axis for walking along any heading:

Proposition 8. Given $\mathcal{G} = (P^h_{\tilde{\psi}_i}, x^*_{\psi_i})$ with steady-state heading ψ_i and desired heading $\tilde{\psi}_i$,

$$x^*_{\psi_j} \quad := \quad x^*_{\psi_i} + (s \quad 0_{2n-1})^T$$

is the LES h-fixed-point of $P^h_{\tilde{\psi}_j}$ with $\psi_j = \psi_i + s$ and $\tilde{\psi}_j = \tilde{\psi}_i + s$, for any $s \in \mathbb{S}^1$.

Moreover, each primitive is independent of world position (this does not appear in state x), and each closed-loop hybrid system is *autonomous* (no reference trajectories). In other words, gait primitives are invariant with respect to time and SE(2) (spatial-temporal symmetry). A general set

[1] Note that our steering strategies resemble human "spin" turns [101], which we discuss in Chapter 7.

of gait primitives $\mathcal{P}^s = \{\mathcal{G}^{\text{st}}, \mathcal{G}^{\text{tu}(s)}, \mathcal{G}^{\text{tu}(-s)}\}$, continuously parameterized by steering angle $s = \delta\tilde{\psi}$, can thus be sequentially composed from step to step. Each gait has a nominal walking arc on the ground plane, with which we can plan walking paths. Switching between the closed-loop hybrid systems associated with each gait primitive will result in transient variations, so we must first consider the stability of such transitions.

6.3 Sequential Composition of Gait Primitives

In order to sequentially compose gait primitives in a stable manner, we present a discrete switched system analogy to the funneling approach of [52]. We consider a set of dynamic gait primitives for a general biped, where we do not have an analytical/closed-form expression for the Poincaré map between steps.

A biped employs[2] gait primitive $\mathcal{G}^i = (P_i, x_i^*)$ during step cycle i by implementing the controller yielding Poincaré map P_i associated with closed-loop hybrid system $\mathscr{H}^i$. Gait primitives are selected at every impact event, so every step has an associated gait transition.

Definition 16. The *gait transition* of step i is defined by pair $\mathcal{T}_i = (x_i, \mathcal{G}^{i+1})$, where x_i is the state at the i^{th} impact event and $\mathcal{G}^{i+1}$ is the gait primitive during step cycle $i+1$. Moreover, $\mathcal{T}_i$ is said to be *switching* if $\mathcal{G}^{i+1} \neq \mathcal{G}^i$.

Hence, $\mathcal{T}_{i+1}$ is related to $\mathcal{T}_i$ by $x_{i+1} = P_{i+1}(x_i)$. And, in the case of 2-step periodic gaits, switching may only occur ever other step, implying $\mathcal{G}^{i+1} = \mathcal{G}^i$ for even i.

Definition 17. A gait transition $\mathcal{T}_i = (x_i, \mathcal{G}^{i+1})$ is *stable* if $x_i \in BoA(x_{i+1}^*)$, where x_{i+1}^* is the LES fixed-point of P_{i+1} from gait primitive $\mathcal{G}^{i+1}$ of step cycle $i+1$.

State x_i may be the result of any gait primitive. By invariance of the basin of attraction, if $\mathcal{G}^{i+1} = \mathcal{G}^i$ and $\mathcal{T}_{i-1}$ is stable, then $\mathcal{T}_i$ is also stable. In order to determine stability for switching transitions, we first require some properties of "nearby" gait primitives.

Assumption 4. For every $s \in [-S, S]$, there exists LES fixed-point $x^{*\text{tu}(s)}$ of $P_{\text{tu}(s)}$ with corresponding $BoA(x^{*\text{tu}(s)})$. Then, by definition there exists a non-empty open ball of radius $r_s > 0$ about $x^{*\text{tu}(s)}$ such that

$$\mathcal{B}(x^{*\text{tu}(s)}, r_s) \subset BoA(x^{*\text{tu}(s)}).$$

[2]Turning gaits are implicity understood to be modulo steering angle s, and we assume that each gait primitive is oriented coincident with the biped's heading at the preceding gait transition.

Moreover, assume $x^{*\mathrm{tu}(s)}$ and r_s are continuous functions of s.

Property 1. The turning fixed-point $x^{*\mathrm{tu}(s)}$ converges to straight-ahead fixed-point $x^{*\mathrm{st}} = x^{*\mathrm{tu}(0)}$ in metric space $(\mathbb{R}^{2n}, d)$ as $|s| \to 0$, where d is Euclidean distance. Formally speaking, $\lim_{|s|\to 0} r_s^* = 0$ for $r_s^* := d(x^{*\mathrm{tu}(s)}, x^{*\mathrm{st}})$.

In other words, turning motion more closely resembles straight-ahead motion for smaller steering angles. We know that turning curvature $\kappa = \pm 1/R$ converges to straight-line curvature $\kappa = 0$ as turning radius $R \to \infty \Leftrightarrow |s| \to 0$. Thus, Property 1 follows from Assumption 4 by continuity. Loosely speaking, Property 1 implies the basins of attraction also converge, which we exploit next.

Lemma 7. Given Property 1, there exists positive steering angle $\bar{S} \leq S$ such that for all $s \in [-\bar{S}, \bar{S}]$:

1. $x^{*\mathrm{st}} \in BoA(x^{*\mathrm{tu}(s)})$
2. $x^{*\mathrm{tu}(s)} \in BoA(x^{*\mathrm{st}})$
3. $x^{*\mathrm{tu}(-s)} \in BoA(x^{*\mathrm{tu}(s)})$

Proof. [1.1] We first define minimal ball radius $r := \min_{s\in[-S,S]}(r_s)$, positive by compactness of $[-S, S]$, so

$$\mathcal{B}(x^{*\mathrm{tu}(s)}, r) \subset \mathcal{B}(x^{*\mathrm{tu}(s)}, r_s) \subset BoA(x^{*\mathrm{tu}(s)}),$$

for all $s \in [-S, S]$. Now, since $r > 0$ and $\lim_{|s|\to 0} r_s^* = 0$, $\exists\ \bar{S} \leq S$ such that $r_s^* < r$ for all $s \in [-\bar{S}, \bar{S}]$. Then, $x^{*\mathrm{st}} \in \mathcal{B}(x^{*\mathrm{tu}(s)}, r)$ for all $s \in [-\bar{S}, \bar{S}]$, and the claim follows.

[1.2] First, by definition of LES, $\exists\ r_\infty > 0$ such that $\mathcal{B}(x^{*\mathrm{st}}, r_\infty) \subset BoA(x^{*\mathrm{st}})$. Then, again $\exists\ \bar{S}$ such that $r_s^* < r_\infty$ for all $s \in [-\bar{S}, \bar{S}]$. Hence, $x^{*\mathrm{tu}(s)} \in \mathcal{B}(x^{*\mathrm{st}}, r_\infty)$ for all $s \in [-\bar{S}, \bar{S}]$, and the claim follows.

[1.3] Recall $x^{*\mathrm{tu}(s)} \to x^{*\mathrm{st}}$ as $|s| \to 0$, which means that for each $\epsilon/2 > 0$, $\exists\ \delta > 0$ such that for all $s \in [-\delta, \delta]$, $d(x^{*\mathrm{tu}(s)}, x^{*\mathrm{st}}) < \epsilon/2$. Then, the triangle inequality shows

$$\begin{aligned} d(x^{*\mathrm{tu}(s)}, x^{*\mathrm{tu}(\text{-}s)}) &\leq d(x^{*\mathrm{tu}(s)}, x^{*\mathrm{st}}) + d(x^{*\mathrm{tu}(\text{-}s)}, x^{*\mathrm{st}}) \\ &< \epsilon. \end{aligned}$$

Hence, if $r_s^{*\mathrm{tu}} := d(x^{*\mathrm{tu}(s)}, x^{*\mathrm{tu}(-s)})$, then $\lim_{s\to 0} r_s^{*\mathrm{tu}} = 0$.

Now, denoting each turning ball as $\mathcal{B}(x^{*\text{tu}(s)}, r_s)$, we can define minimal ball radius

$$r \;:=\; \min_{s\in[-S,S]}(r_s) \;>\; 0.$$

As we saw in 1.1, $\exists\ \bar{S}$ such that $r_s^{*\text{tu}} < r$ for all $s \in [-\bar{S}, \bar{S}]$. Then, $x^{*\text{tu}(-s)} \in \mathcal{B}(x^{*\text{tu}(s)}, r)$ for all $s \in [-\bar{S}, \bar{S}]$, and the claim follows. Equivalently, $x^{*\text{tu}(s)} \in BoA(x^{*\text{tu}(-s)})$.

Finally, we can take the minimum of $\bar{S}$ from each proof to find $\bar{S}$ for the overall Lemma. □

Remark 11. Recall that asymptotic stability implies convergence to fixed-points in infinite time, but trajectories eventually converge "close enough" to stably switch gaits. Note that in Lemma 7.1, $\mathcal{B}(x^{*\text{tu}(s)}, r)$ is an open ball so $x^{*\text{st}}$ cannot be on the boundary of $BoA(x^{*\text{tu}(s)})$. Therefore, points sufficiently close to $x^{*\text{st}}$ are also contained in $BoA(x^{*\text{tu}(s)})$. The same holds for the other three claims in Lemma 7.

Fortunately, we also have exponentially fast convergence to neighborhoods around fixed-points. Given enough time along a given primitive, the biped's state will be "funneled" into the basin of attraction of the next primitive upon switching (e.g., Fig. 1.4). This is called the *dwell time*, since the biped can be interpreted as a *discrete-time switched system* $x(i+1) = P_{\sigma(i)}(x(i))$, where switching signal $\sigma : \mathbb{Z}_+ \to \{0, s, -s\}$ chooses the primitive (parameterized by steering angle) at every step. This signal must be constrained to ensure stable composition of primitives, for which we invoke the main result of this chapter (cf. [102, 103] for analogous results on global stability of continuous-time switched systems):

Theorem 13. For any $s \in [-\bar{S}, \bar{S}]$ from Lemma 7, there exists a minimum number of steps $N \geq 1$, i.e., a lower bound on dwell time, such that for all integers $k \geq N$:

1. If $x \in BoA(x^{*\text{st}})$, then $P_{\text{st}}^k(x) \in BoA(x^{*\text{tu}(s)})$.
2. If $x \in BoA(x^{*\text{tu}(s)})$, then $P_{\text{tu}(s)}^k(x) \in BoA(x^{*\text{st}})$.
3. If $x \in BoA(x^{*\text{tu}(s)})$, then $P_{\text{tu}(s)}^k(x) \in BoA(x^{*\text{tu}(-s)})$.

Corollary 1. Consider primitive set $\mathcal{P}^s$ as in Theorem 13. For any $s \in [-\bar{S}, \bar{S}]$, there exists a minimum dwell time $N \geq 1$ such that for any integer $k \geq N$ the following holds: any switching transition $\mathcal{T}_{i+k}$ that follows a stable transition $\mathcal{T}_i$ is also stable.

Hence, we can design a supervisory controller to produce a constrained $\sigma(\cdot)$ for stable path planning, piecing together straight and curved gait segments such that the turns are not too sharp or the primitive switches too fast. The steering sharpness must be bounded by steering angle $\bar{S}$, a condition that can be verified in simulation (checking convergence from all fixed-points). However, minimum dwell time N depends explicitly on each gait primitive's basin of attraction and rate of exponential convergence, both of which can only be characterized numerically. It is now possible to use sum-of-squares programming to find invariant subsets of the basins of attraction [104, 105], which will enable conservative estimates for lower bounds on dwell time as in [103]. For the purposes of this thesis, we examine our lower bound using exhaustive simulation in Section 6.5.3. We first turn our attention to building walking paths from gait primitives.

6.4 Path Planning Formulation

Given these switching rules, we can define stable walking over a path of sequentially composed gait primitives.

Definition 18. A w-step *walking path execution* from initial condition $x(0) = x_0$ is defined by the ordered set $\mathcal{E}(x_0) = (\mathcal{T}_0, \mathcal{T}_1, \ldots, \mathcal{T}_{w-1})$, where $\mathcal{T}_0 = (x_0, \mathcal{G}^1)$.

Definition 19. A walking path execution $\mathcal{E}(x_0)$ is *robust* if all gait transitions $\mathcal{T}_i$ are stable.

In other words, the biped is guaranteed not to fall over.

6.4.1 Planning in SE(2)

Recall that state x describes the robot's motion with respect to its joints. In the context of path planning, we need to consider the robot's coordinates with respect to a world frame, i.e., its Euclidean coordinates on the walking surface. Assuming a flat surface, we need only model the biped's (x, y)-position (e.g., measured at the stance foot with respect to some world frame) along with heading ψ as the global orientation. Hence, every step i has an associated world configuration $c_i = (x^i_{\text{pos}}, y^i_{\text{pos}}, \psi_i)^T \in \text{SE}(2)$. The extension of a biped's discrete state to $x^{\text{e}}_i = (x^i_{\text{pos}}, y^i_{\text{pos}}, x^T_i)^T$ is trivial, as the new coordinates are easily updated according to robot kinematics. Through a slight abuse of notation, we denote a boundary-constrained w-step walking path execution as $\mathcal{E}^{c_w}_{c_0}(x^{\text{e}}_0)$, where c_0 is given by $x^{\text{e}}_0 = (c^T_0, \varphi_0, \theta^T_0, \dot{q}^T_0)^T$ and c_w is given by $x^{\text{e}}_w = P_w\left(x^{\text{e}}_{w-1}\right) = (c^T_w, \varphi_w, \theta^T_w, \dot{q}^T_w)^T$.

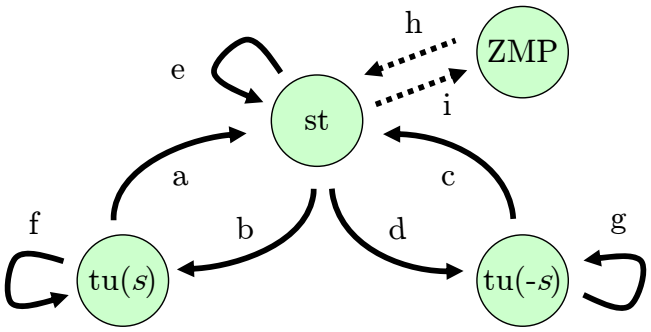

Figure 6.1: Directed graph of a discrete maneuver automaton for a biped that cannot stably switch directly between left and right turning gaits of large curvature, i.e., $x^{*\mathrm{tu}(-s)} \notin BoA_{\mathrm{tu}(s)}(x^{*\mathrm{tu}(s)})$ for some s such that $\bar{S} < |s| \leq S$. This graph also includes hypothetical edges for transitions to/from quasi-static states of locomotion.

We now have the framework to form paths that stably connect initial and final world configurations c_0, c_f. We can use Corollary 1 to define a class $\mathcal{C}_{c_0}^{c_f} = \left\{\mathcal{E}_{c_0}^{c_w} | c_w = c_f, w \geq 1\right\}$ of robust walking path executions between reachable configurations c_0 and c_f. Moreover, our finite set of gait primitives is continuously parameterized by s to allow a (large) continuous reachable set. After encoding the switching rules into a regular language [106], walking paths can be constructed by a finite-state machine (i.e., a discrete automaton [107]) that outputs a constrained switching signal $\sigma(\cdot)$ to the biped switched system. This so-called *maneuver automaton* can even accommodate primitive sets in which the CW and CCW turning primitives cannot be directly composed as in Fig. 6.1. Hence, the switching rules from Section 6.3 allow stability concerns to be abstracted away from the planning problem.

6.4.2 Walking arcs

As the biped switches between gaits, step cycle trajectories converge back and forth between attractive orbits, so we generally do not have a fixed mapping from gait transitions to path arcs. However, this mapping is very closely approximated with the nominal set of constant-curvature arcs associated with the gait primitives.

Definition 20. The *nominal walking arc* of primitive $\mathcal{G}$ is the tuple $\left(\delta x^*_{\mathrm{pos}}, \delta y^*_{\mathrm{pos}}, \delta\psi^*\right) \in \mathrm{SE}(2)$ of the gait's x-axis, y-axis, and heading displacements, respectively, from initial heading $\psi = 0$.

For the gait primitives we consider, the heading change equals the primitive's steering angle, i.e., $s = \delta\tilde{\psi} = \delta\psi^*$. In order to sequentially compose walking arcs with different orientations, we rotate

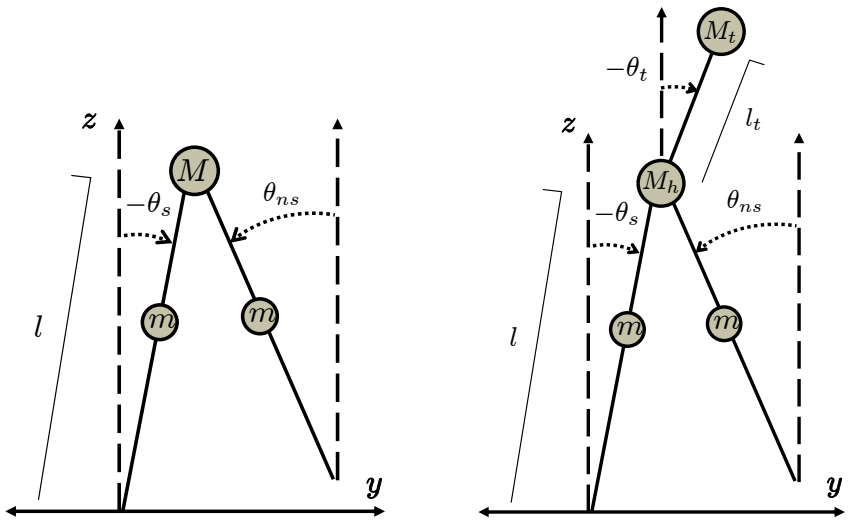

Figure 6.2: The sagittal planes of the standard (left) and torso (right) compass-gait bipeds.

the nominal arc's x-y coordinate frame with a group action of SO(2) to coincide with the initial heading ψ_i of the current gait transition $\mathcal{T}_i = (x_i, \mathcal{G}^{i+1})$:

$$\begin{pmatrix} \delta x_{\text{pos}}^{i+1} \\ \delta y_{\text{pos}}^{i+1} \end{pmatrix} = \begin{pmatrix} \cos(\psi_i) & -\sin(\psi_i) \\ \sin(\psi_i) & \cos(\psi_i) \end{pmatrix} \begin{pmatrix} \delta x_{\text{pos}}^{*i+1} \\ \delta y_{\text{pos}}^{*i+1} \end{pmatrix}. \tag{6.1}$$

This enables path planning in SE(2) with a discrete tree transversal of branching factor three, the cardinality of the primitive set (i.e., the action space). In other words, *stable dynamic locomotion planning reduces to a discrete graph search*, where the planning algorithm outputs a sequence $\mathcal{S}$ of steering angles parameterizing gait primitives. Although these walking paths (planned *a priori*) may have minor transient drift, periodic re-planning or kinodynamic planning methods (e.g., [108–110]) would enable reachability of specific goal configurations. We will discuss this in detail when presenting planned walking results in Section 6.6, but we first must define the primitive sets for our biped examples.

6.5 Primitives for 3-D Compass-Gait Bipeds

In order to demonstrate the fundamentals of dynamic gait primitives, we slightly deviate from the complex models presented in Chapter 5 by removing the hip link. In other words, we adopt the two hipless walkers from [51]: the 4-DOF compass-gait biped and 5-DOF compass-gait-with-torso biped. These are strict 3-D extensions of the commonly studied planar bipeds in Fig. 6.2. The

robots are given the respective control laws from Section 5.2 and are simulated with the respective parameters in Tables 5.1-5.2, except that hip width $w = 0$, leg splay angle $\rho = 0$, slope mapping angle $\beta = 0.052$ rad, and gain $p = 0$ (no passivity-based energy tracking).

We now derive a set of gait primitives for each model. These gaits will be 1-step periodic since each leg has identical dynamics without the hip link. We note, however, that this planning framework is applicable to any set of asymptotically stable h-periodic gaits (not necessarily from our reduction-based control method).

6.5.1 Straight-ahead gait primitives

The reduction-based control law (5.13) yields closed-loop hybrid systems $\mathscr{H}^{\mathrm{st}}_{4\mathrm{D}}$ and $\mathscr{H}^{\mathrm{st}}_{5\mathrm{D}}$ for straight-ahead walking on flat ground. For example, we set $\tilde{\psi} = 0$ (without loss of generality) and find the 1-fixed-points

$$\begin{aligned} x^{*\mathrm{st}}_{4\mathrm{D}} &\approx (0, 0, -0.2704, 0.2704, 0, 0, -1.4896, -1.7986)^T \\ x^{*\mathrm{st}}_{5\mathrm{D}} &\approx (0, 0, -0.2657, 0.0047, 0.2657, 0, 0, -1.3165, 0.0596, -1.5339)^T . \end{aligned}$$

We numerically verify LES of each periodic orbit by linearizing the associated Poincaré map, thus defining the *straight-ahead* gait primitives $\mathcal{G}^{\mathrm{st}}_{4\mathrm{D}} = (P^{\mathrm{st}}_{4\mathrm{D}}, x^{*\mathrm{st}}_{4\mathrm{D}})$ and $\mathcal{G}^{\mathrm{st}}_{5\mathrm{D}} = (P^{\mathrm{st}}_{5\mathrm{D}}, x^{*\mathrm{st}}_{5\mathrm{D}})$.

The associated hybrid periodic orbits $\mathcal{O}^{\mathrm{st}}_{4\mathrm{D}}$ and $\mathcal{O}^{\mathrm{st}}_{5\mathrm{D}}$ are illustrated in the plots of Fig. 6.3 and Fig. 6.4, respectively. We see that these upright gaits have no swaying in lean or yaw (which is to be expected for hipless bipeds). The 4-DOF sagittal plane has a periodic step length of 0.534 m and an approximate linear velocity of 0.727 m/s, whereas the 5-DOF sagittal plane has a periodic step length of 0.525 m and an approximate linear velocity of 0.692 m/s.

6.5.2 Turning gait primitives

We create turning gaits by introducing a periodic disturbance into each biped's straight-ahead system $\mathscr{H}^{\mathrm{st}}$ in the form of constant steering between steps. In particular, we augment the within-stride reduction-based controller with an event-based (or stride-to-stride) controller that increments yaw set-point $\tilde{\psi}$ at each step by steering angle s (positive for CW or negative for CCW steering). This yields closed-loop system $\mathscr{H}^{\mathrm{tu}(s)}$, for which trajectories converge to 1-step periodic turning gaits modulo heading change s, where CW and CCW gaits are symmetric with opposite yaw/lean.

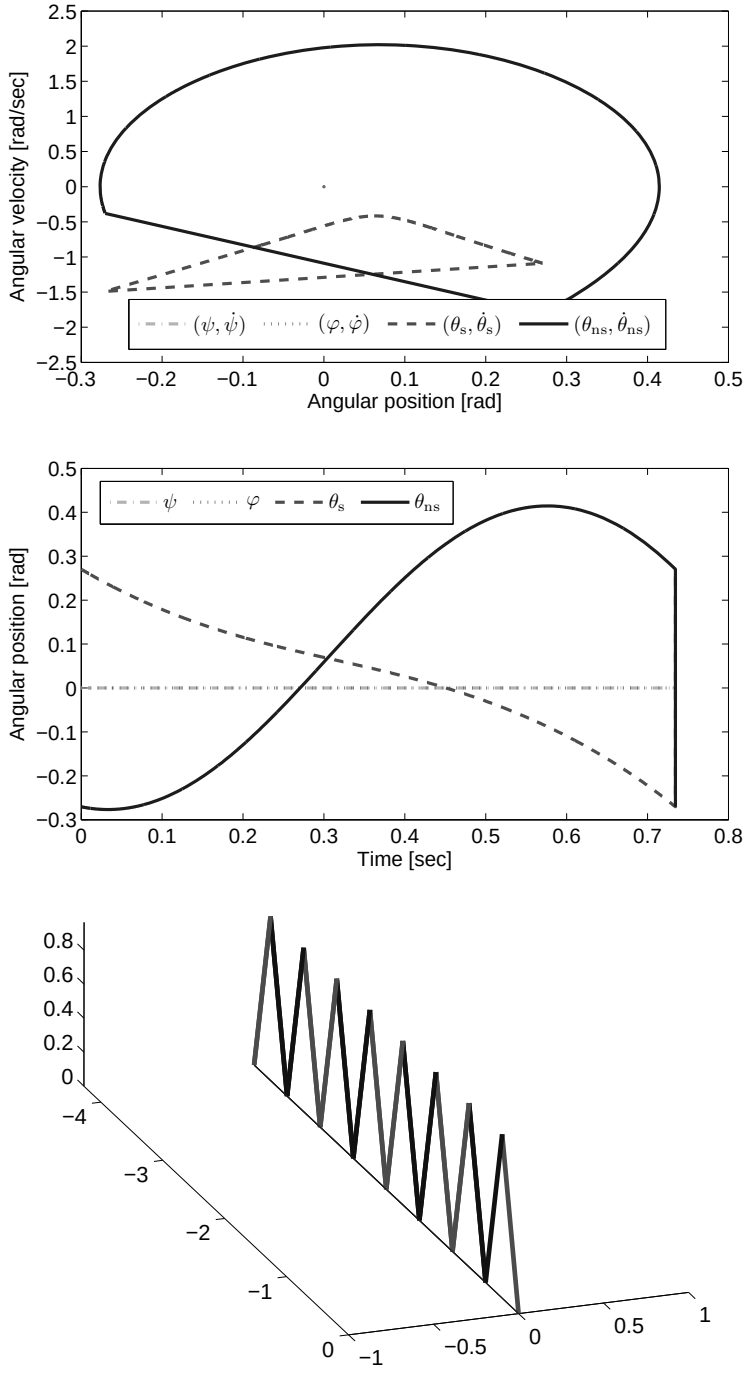

Figure 6.3: Hipless 4-DOF straight-ahead 1-step gait: phase portrait (top), coordinate trajectories (middle), and multi-step animation (bottom).

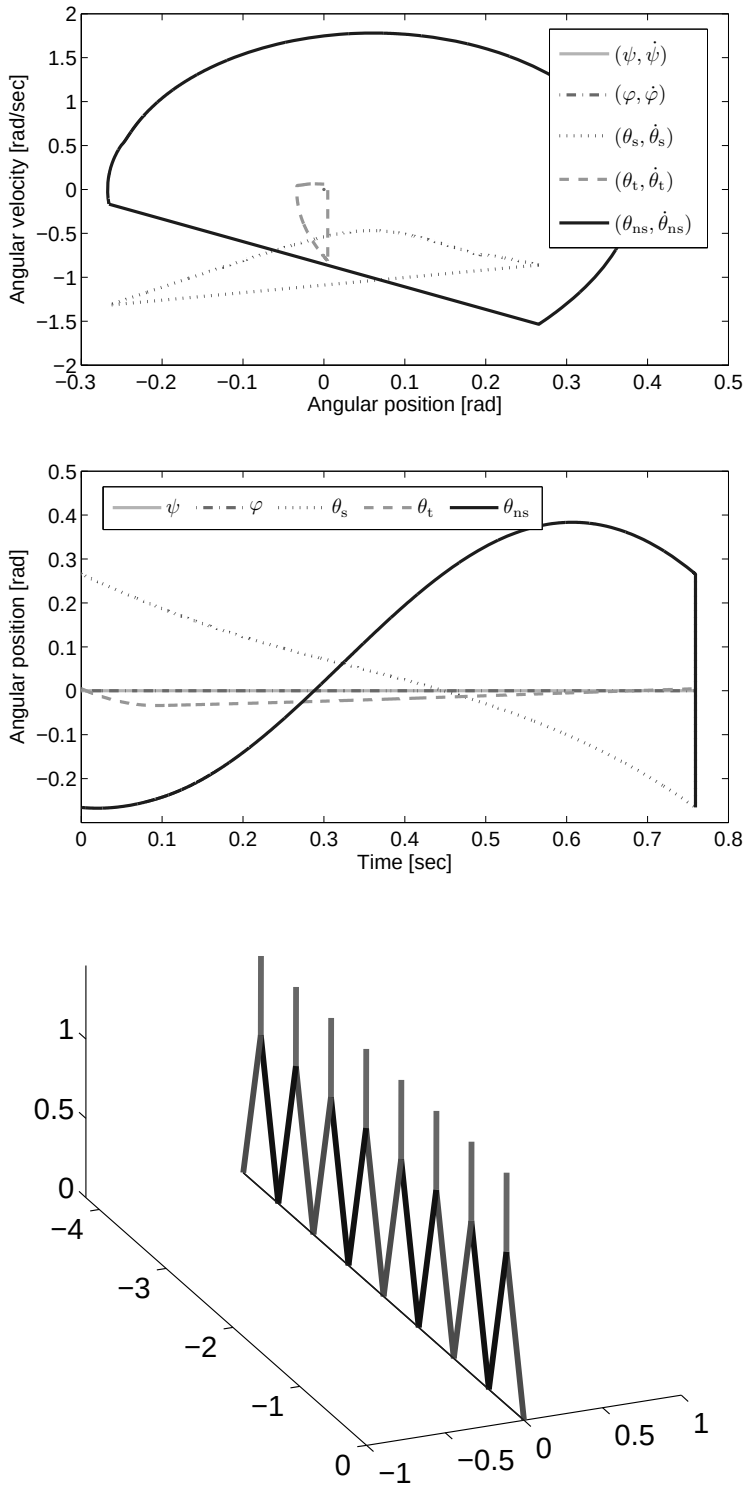

Figure 6.4: Hipless 5-DOF straight-ahead 1-step gait: phase portrait (top), coordinate trajectories (middle), and multi-step animation (bottom).

We want to show that for any sufficiently small $|s|$, constant-curvature steering induces an LES 1-fixed-point modulo yaw:

$$x^{*\mathrm{tu}(s)} + (s \quad 0_{2n-1})^T \quad = \quad P^{\mathrm{tu}(s)}\left(x^{*\mathrm{tu}(s)}\right)$$

with $BoA(x^{*\mathrm{tu}(s)})$. We can then define *CW-* and *CCW-turning* gait primitives $\mathcal{G}^{\mathrm{tu}(s)}$ and $\mathcal{G}^{\mathrm{tu}(-s)}$.

Starting the 4-DOF biped's augmented system from $x_{4\mathrm{D}}^{*\mathrm{st}}$, we observe that hybrid flows converge to some 1-fixed-point $x_{4\mathrm{D}}^{*\mathrm{tu}(s)}$ associated with $\mathcal{O}_{4\mathrm{D}}^{\mathrm{tu}(s)}$ for any choice of $s \in [-S_{4\mathrm{D}}, S_{4\mathrm{D}}]$, $S_{4\mathrm{D}} = 0.492$. We densely sample steering values in $[-S_{4\mathrm{D}}, S_{4\mathrm{D}}]$, finding the fixed-point for each sample and confirming LES. The continuous evolution of the fixed-point and gait characteristics of each primitive are plotted in Fig. 6.5. The x-axis and y-axis displacements for the nominal walking arc associated with each steering angle are given for the biped initialized at heading $\psi = 0$. We see that the steady-state step length and time duration change slowly as $|s|$ increases, which perturbs the sagittal-plane orbits compared to $\mathcal{O}_{4\mathrm{D}}^{\mathrm{st}}$. Increasing $|s|$ into the instability region outside $[-S_{4\mathrm{D}}, S_{4\mathrm{D}}]$, we observe period-doubling bifurcations yielding 2- and 4-step periodic LES orbits, ultimately leading to a chaotic strange attractor and falling. We observe similar behavior in Fig. 6.6 for the 5-DOF biped's orbit $\mathcal{O}_{5\mathrm{D}}^{\mathrm{tu}(s)}$ in stability region $[-S_{5\mathrm{D}}, S_{5\mathrm{D}}]$, $S_{5\mathrm{D}} = 0.45$, but with much richer bifurcations outside this region (see Fig. 6.7).

We demonstrate CW and CCW turning gaits by choosing $\hat{s} = 2\pi/13 = 0.4833$ for the 4-DOF biped, producing 1-step fixed-points

$$\begin{aligned} x_{4\mathrm{D}}^{*\mathrm{tu}(\hat{s})} &\approx (-0.0306, -0.0064, -0.2782, 0.2782, -0.0318, 0.0159, -1.5426, -2.1318)^T \\ x_{4\mathrm{D}}^{*\mathrm{tu}(-\hat{s})} &\approx (0.0306, 0.0064, -0.2782, 0.2782, 0.0318, -0.0159, -1.5426, -2.1318)^T, \end{aligned}$$

respectively. This also converges to a 13-periodic LES gait (modulo 2π in yaw) for a full circle maneuver [51]. The CW-turning gait is illustrated over one step in Fig. 6.8 (and CCW by symmetry), which shows the gait's natural leaning into the turn. We see in Fig. 6.5 that the nominal walking arc for this CW gait primitive is characterized by $\delta x_{\mathrm{pos}}^* = 0.2539$ m and $\delta y_{\mathrm{pos}}^* = 0.4878$ m. The signs of $\delta x_{\mathrm{pos}}^*$ and $\delta\psi^* = \hat{s}$ are flipped for the corresponding CCW gait.

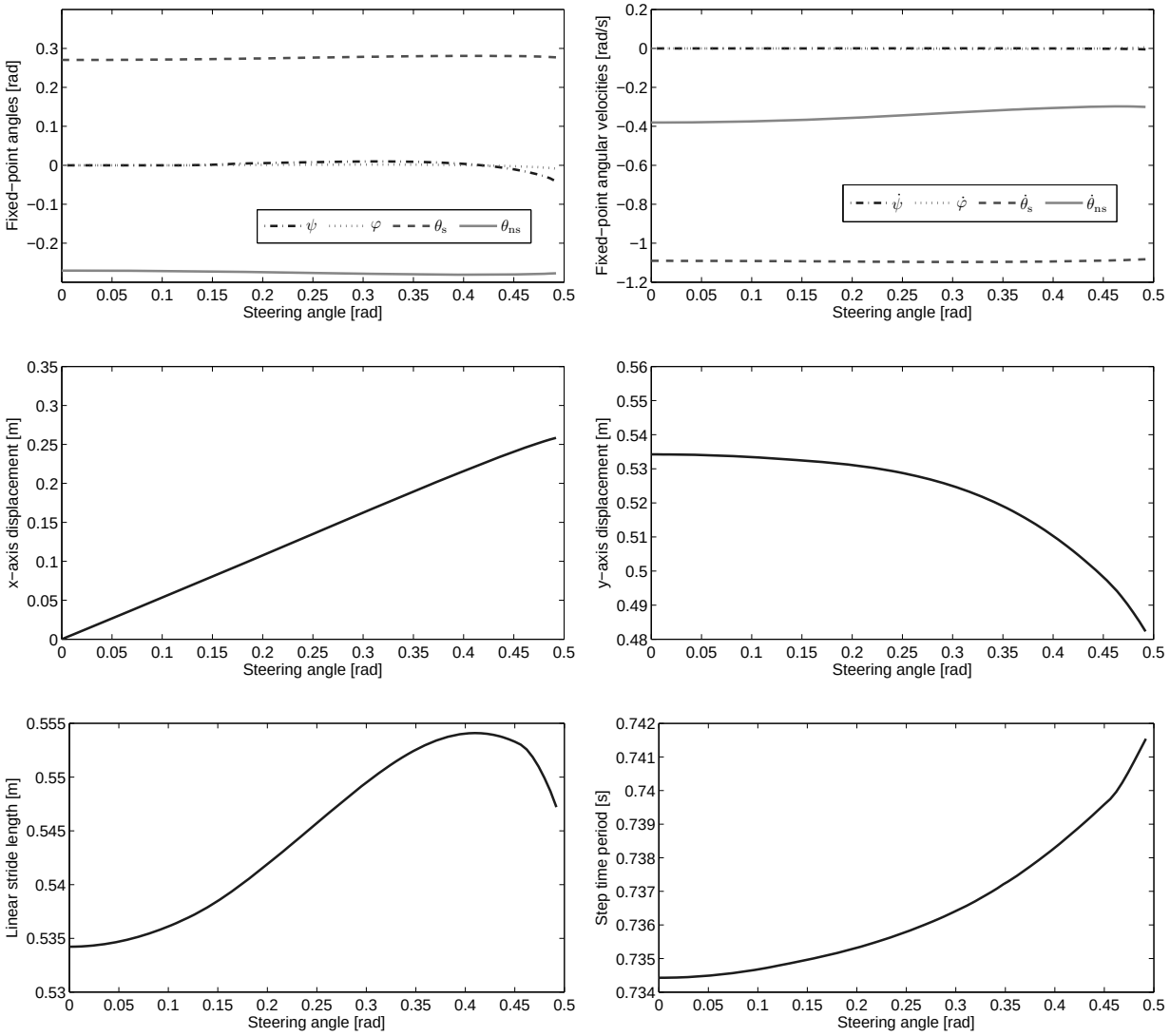

Figure 6.5: Evolution of hipless 4-DOF CW turning fixed-point $x_{4\mathrm{D}}^{*\mathrm{tu}(|s|)}$ (top), x-axis displacement (middle left), y-axis displacement (middle right), linear step length (bottom left), and step time period (bottom right) over steering angle $s \in [0, 0.492]$.

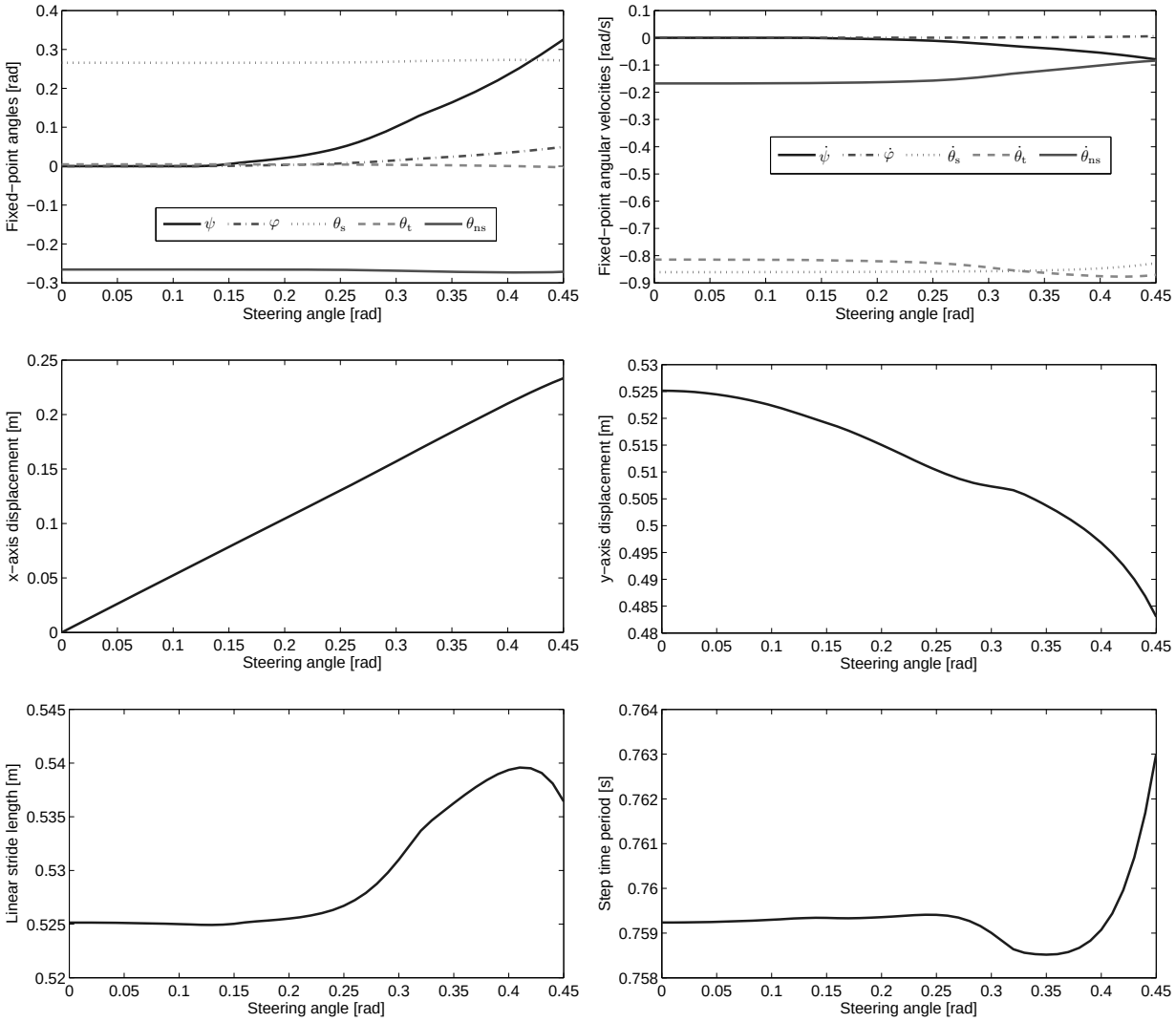

Figure 6.6: Evolution of hipless 5-DOF CW turning fixed-point $x_{5\mathrm{D}}^{*\mathrm{tu}(|s|)}$ (top), x-axis displacement (middle left), y-axis displacement (middle right), linear step length (bottom left), and step time period (bottom right) over steering angle $s \in [0, 0.45]$.

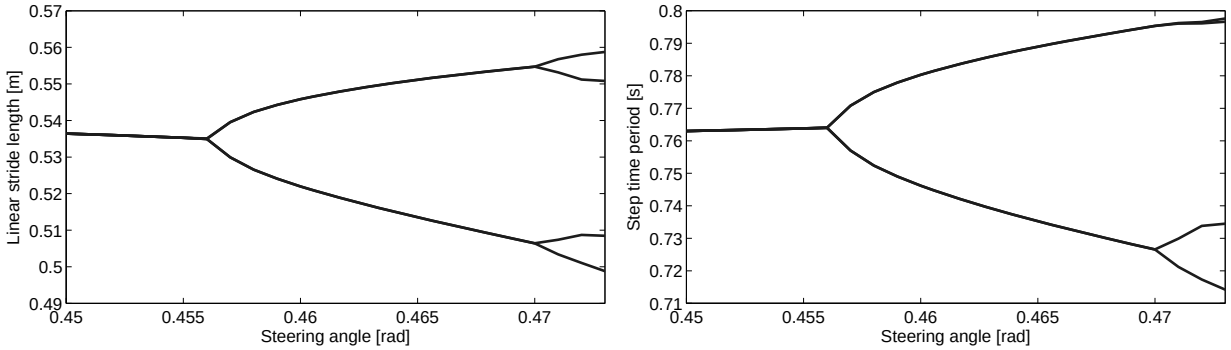

Figure 6.7: Bifurcation diagram of hipless 5-DOF biped's linear step length (left) and time period (right) over steering angle $s \in [0.45, 0.473]$.

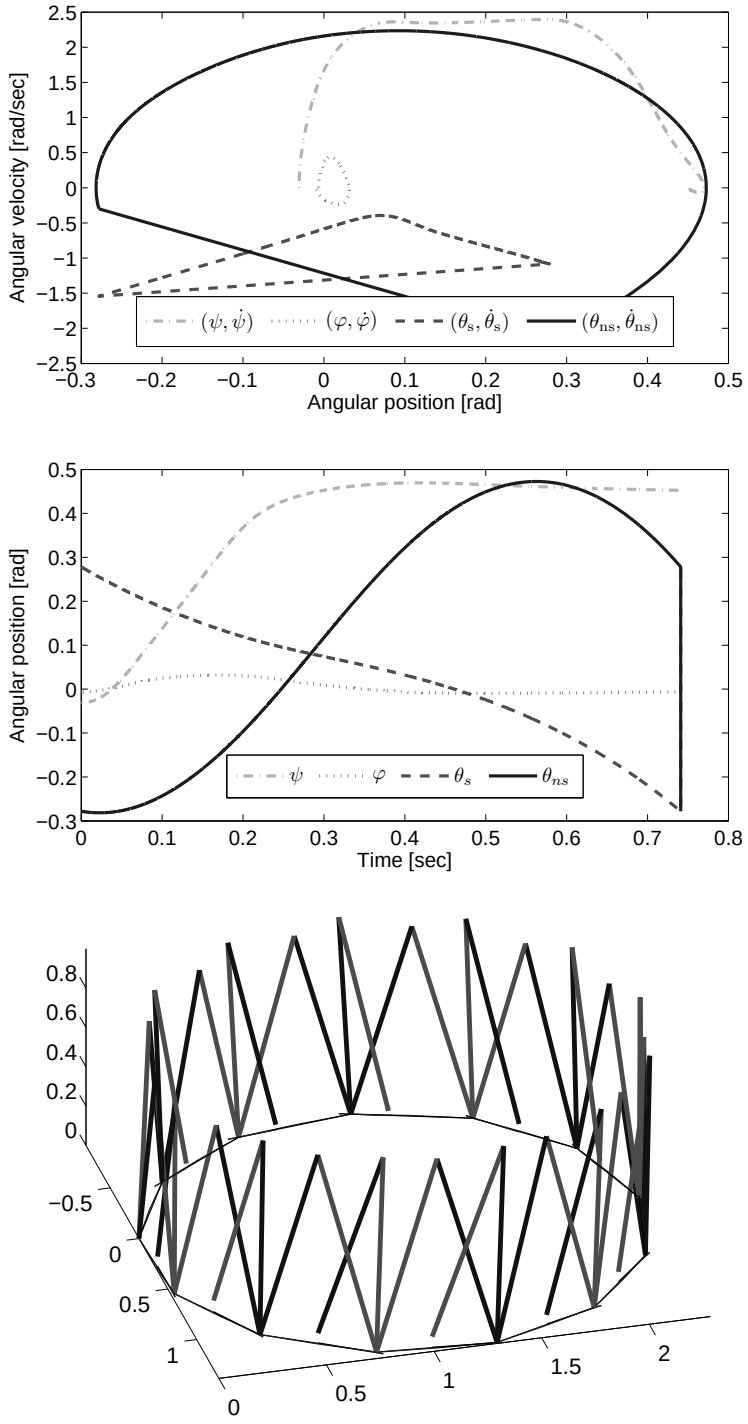

Figure 6.8: Hipless 4-DOF CW $\hat{s}$-turning 1-step gait: phase portrait (top), coordinate trajectories (middle), and 13-step 360°-turn animation (bottom).

Similarly, we demonstrate turning gaits for the 5-DOF biped by choosing $\tilde{s} = 0.32$:

$$\begin{aligned} x_{5\mathrm{D}}^{*\mathrm{tu}(\tilde{s})} &\approx (-0.1287, -0.019, -0.2701, 0.003, 0.2701, -0.109, 0.0172, -1.3391, 0.0659, -1.6091)^T \\ x_{5\mathrm{D}}^{*\mathrm{tu}(-\tilde{s})} &\approx (0.1287, 0.019, -0.2701, 0.003, 0.2701, 0.109, -0.0172, -1.3391, 0.0659, -1.6091)^T . \end{aligned}$$

The CW-turning gait is illustrated in Fig. 6.9 (and CCW by symmetry). We see in Fig. 6.6 that the nominal walking arc for this CW gait primitive is characterized by $\delta x_{\mathrm{pos}}^* = 0.1679$ m and $\delta y_{\mathrm{pos}}^* = 0.5066$ m.

Finally, we emphasize that these turning gaits naturally arise from our asymptotically stable straight-ahead systems, without changing any reference trajectories. Integrating $\dot{q}^T\tau$ to obtain net work per step, the specific mechanical cost of transport for each gait is $c_{\mathrm{mt}}(x_{4\mathrm{D}}^{*\mathrm{st}}) = 0.052$, $c_{\mathrm{mt}}(x_{4\mathrm{D}}^{*\mathrm{tu}(\pm\hat{s})}) = 0.06$, $c_{\mathrm{mt}}(x_{5\mathrm{D}}^{*\mathrm{st}}) = 0.038$, and $c_{\mathrm{mt}}(x_{5\mathrm{D}}^{*\mathrm{tu}(\pm\tilde{s})}) = 0.04$, which compare favorably with the costs of other mechanisms shown in Fig. 5.13. We now must numerically derive the switching rules discussed in Section 6.3 for these primitive sets.

6.5.3 Computing the switching rules

Although it is computationally difficult to find the exact region $[-\bar{S}, \bar{S}]$, we can easily verify containment of a particular s through simulation. Therefore, we can confirm the conditions of Lemma 7 starting with 4-DOF primitive set $\mathcal{P}_{4\mathrm{D}}^{\hat{s}} = \{\mathcal{G}_{4\mathrm{D}}^{\mathrm{st}}, \mathcal{G}_{4\mathrm{D}}^{\mathrm{tu}(\hat{s})}, \mathcal{G}_{4\mathrm{D}}^{\mathrm{tu}(-\hat{s})}\}$, i.e., $\hat{s} = 0.4833 \in [-\bar{S}_{4\mathrm{D}}, \bar{S}_{4\mathrm{D}}]$. This corresponds to

$$x_{4\mathrm{D}}^{*\mathrm{st}}, x_{4\mathrm{D}}^{*\mathrm{tu}(\hat{s})}, x_{4\mathrm{D}}^{*\mathrm{tu}(-\hat{s})} \in BoA\left(x_{4\mathrm{D}}^{*\mathrm{st}}\right) \bigcap BoA\left(x_{4\mathrm{D}}^{*\mathrm{tu}(\hat{s})}\right) \bigcap BoA\left(x_{4\mathrm{D}}^{*\mathrm{tu}(-\hat{s})}\right).$$

This overlapping attractive region influences the minimum dwell time N along primitives for Theorem 13. We simulate worst-case gait switching tests to estimate N for this primitive set.

Based on the intuition provided by Theorem 13, worst-case walking scenarios are those with high frequencies of switching gait transitions (i.e., dwell time $k < N$). The more often a biped switches between gait primitives, the more likely it will accumulate transient perturbations that cannot be attenuated during the short duration of each gait transition. Eventually, the impact-event state from one gait primitive will be outside the basin of attraction of the next.

We first simulate switching between two fixed primitives at every step (i.e., $k = 1$). Both the CW-to-CCW and CW-to-Straight cases eventually converge to 2- and 4-periodic cycles, respectively,

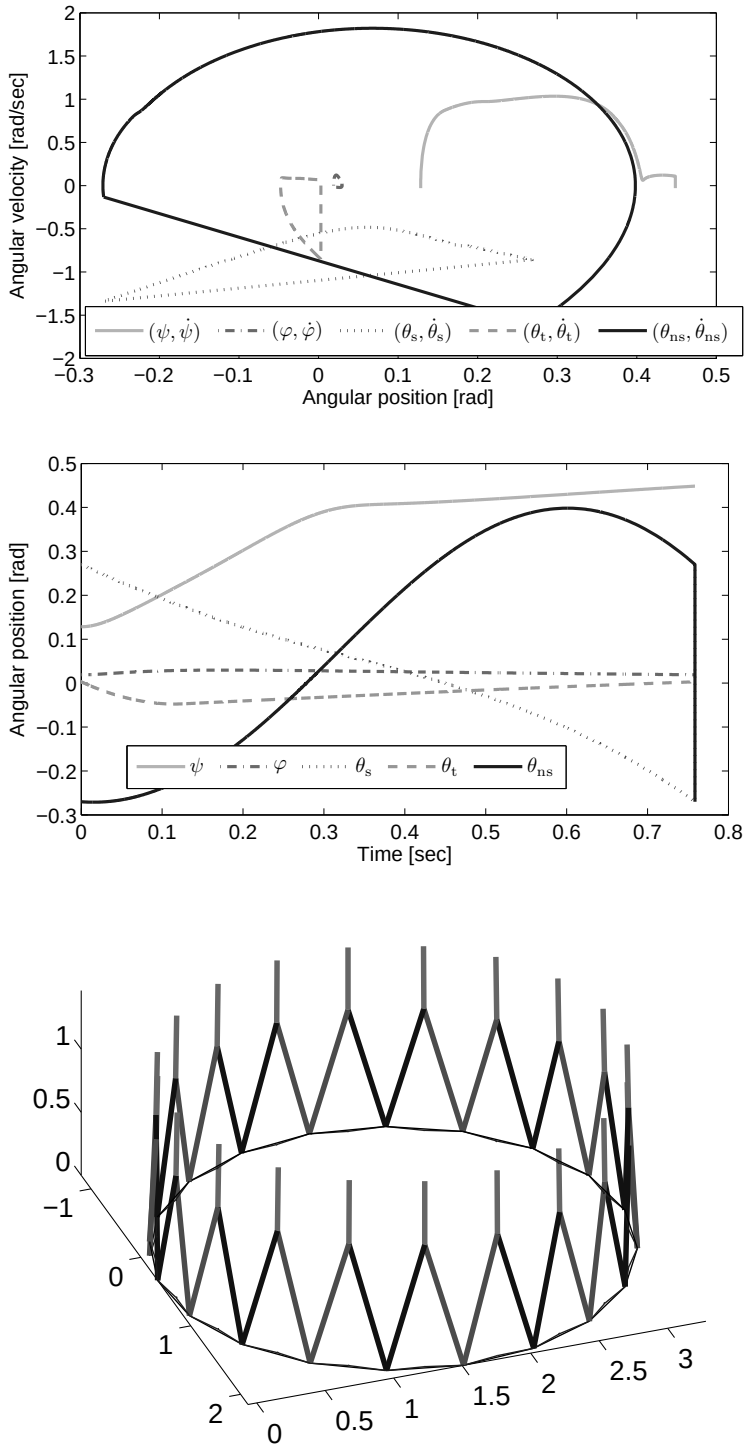

Figure 6.9: Hipless 5-DOF CW $\tilde{s}$-turning 1-step gait: phase portrait (top), coordinate trajectories (middle), and 13-step 360°-turn animation (bottom).

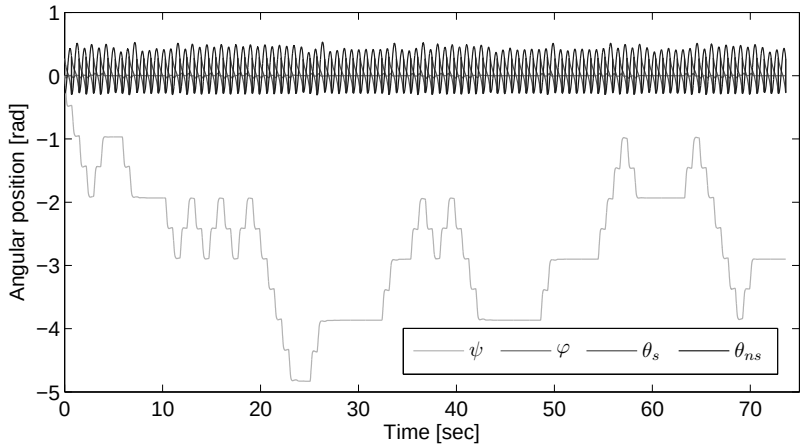

Figure 6.10: Hipless 4-DOF biped's random walk with gait dwell time $k = 2$ over 100 steps.

showing that the biped is robust for periodic switching transitions. This convergent behavior of k-step steering patterns to mk-periodic gaits, for some positive integer m, demonstrates another strength of asymptotically stable walking.

We next try a "random walk," picking a gait primitive at every step from a uniform random distribution. Here, we observe occasional falls, e.g., the sequence $\mathcal{S} = (\hat{s}, 0, 0, 0, \hat{s}, 0, 0, 0)$, implying that $N > 1$. Setting $k = 2$ (switching allowed every other step), we are unable to produce falls after several lengthy simulations (400+ steps, e.g., Fig. 6.10), suggesting that minimum dwell time $N = 2$. This is evidence that the overlapping attractive region of our primitive set is large, presumably due to the close proximity of the set's fixed-points, e.g., $d(x_{4\mathrm{D}}^{*\mathrm{tu}(\hat{s})}, x_{4\mathrm{D}}^{*\mathrm{tu}(-\hat{s})}) < 0.064$, as well as the large size of each gait's basin of attraction. Hence, the 4-DOF primitive set is capable of building a large class of robust walking paths through 3-D space.

The same process is performed for the 5-DOF primitive set $\mathcal{P}_{5\mathrm{D}}^{\tilde{s}} = \{\mathcal{G}_{5\mathrm{D}}^{\mathrm{st}}, \mathcal{G}_{5\mathrm{D}}^{\mathrm{tu}(\tilde{s})}, \mathcal{G}_{5\mathrm{D}}^{\mathrm{tu}(-\tilde{s})}\}$, confirming that $\tilde{s} = 0.32 \in [-\bar{S}_{5\mathrm{D}}, \bar{S}_{5\mathrm{D}}]$ and that $N = 2$. We now present planned walking results using a tree search algorithm to provide open-loop supervisory control of each model's switched system.

6.6 Planned Walking Results

These gait primitives and their associated switching rules enable path planning (e.g., Fig. 6.11) by exploring the action space of primitive arcs. The set of feasible action sequences, characterizing robust paths not in collision with the environment, forms a discrete tree of walking arcs with branching factor $b = 3$, the cardinality of the primitive set. This tree expands exponentially with

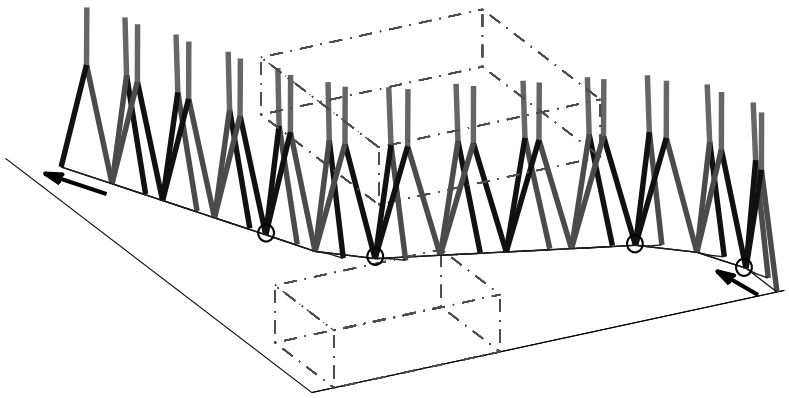

Figure 6.11: Example of a planned path using gait primitives for hipless 5-DOF biped. The sequence of primitives is (S, CCW, CCW, S, S, S, S, CW, CW, S, S, S, S), where switching transitions are signified by circles at the impact events.

$O(b^d)$, where d is the tree depth in number of steps. We must use a heuristic to prune less promising branches (i.e., a biased sampling of the action space) in order to find paths of high depth in the tree, which will almost always be the case when navigating a complex environment. However, *any* tree search heuristic can be chosen for this planning framework, and many suitable methods exist (e.g., the $A*$ algorithm [111, 112], applied to humanoid planning in [113]).

To simplify our planning problem, we define a goal region $R_{\mathrm{f}} \subset \mathrm{SE}(2)$ so that any robust walking path execution $\mathcal{E}_{c_0}^{c_w}(x_0^{\mathrm{e}})$ ending at world configuration $c_w \in R_{\mathrm{f}}$ is considered admissible. In most cases, this greatly enlarges the class $\mathcal{C}_{c_0}^{R_{\mathrm{f}}}$ of robust walking paths between c_0 and R_{f}, allowing us to ignore issues of reachability. We now adopt the tree search algorithm developed in [99] specifically for this application, which performs a cell decomposition of the environment to bias tree growth toward the desired goal region R_{f}. This planner outputs a sequence $\mathcal{S}\left(\mathcal{E}_{c_0}^{c_w}(x_0^{\mathrm{e}})\right) \in \{s, 0, -s\}^w$ of steering angles parameterizing the gait primitive at each step in the walking execution $\mathcal{E}_{c_0}^{c_w}(x_0^{\mathrm{e}})$.

The search algorithm plans candidate paths through the example obstacle environment of Fig. 6.12 using 4-DOF primitive set $\mathcal{P}_{4\mathrm{D}}^{\hat{s}}$, parameterized by $\hat{s} = 0.4833$, and 5-DOF primitive set $\mathcal{P}_{5\mathrm{D}}^{\tilde{s}}$, parameterized by $\tilde{s} = 0.32$. In each case, we choose the candidate path that best approximates the optimal path with respect to a cost function that equally penalizes the number of steps and the number of switching transitions:

$$J\left\{\mathcal{S}\left(\mathcal{E}_{c_0}^{c_w}(x_0^{\mathrm{e}})\right)\right\} = \begin{cases} w + \sum_{i=1}^{w-1} \mathbb{1}\{\mathcal{G}^i \neq \mathcal{G}^{i+1}\} & , \quad c_w \in R_{\mathrm{f}} \\ \infty & , \quad c_w \notin R_{\mathrm{f}} \end{cases} \tag{6.2}$$

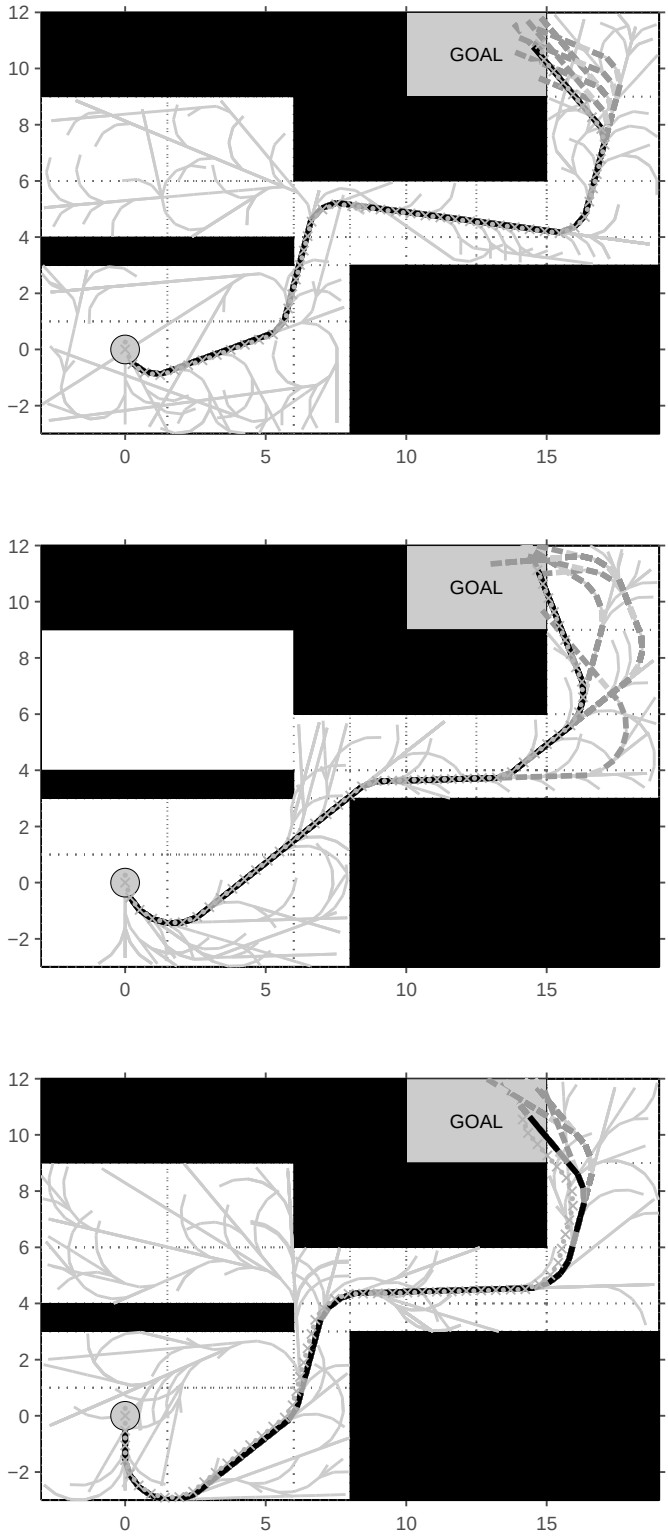

Figure 6.12: Planned walking for the hipless 4-DOF biped, with $\hat{s} = 0.4833$ (top) and $\tilde{s} = 0.32$ (middle), and the hipless 5-DOF biped with $\tilde{s} = 0.32$ (bottom). The suboptimal path is plotted in black, other candidate paths are plotted in gray, and switching transitions are indicated by lighter segments. Simulated step placements are given by circles (left foot) and X's (right foot).

where w is the number of steps in the path execution and $\mathbb{1}$ is an indicator function that determines whether a switching transition occurs at step i. By minimizing cost function J, the planner will output a shorter and smoother (consequently more stable) walking path.

The example cases of Fig. 6.12 show the planned walking path (in black) and simulated walking execution (in gray circles and X's). Since the 4-DOF biped is more maneuverable, we also simulate a planned execution of this model using the lower-curvature primitive set $\mathcal{P}_{4\mathrm{D}}^{\tilde{s}}$ for the purpose of comparison (note that $\tilde{s} \in [-\bar{S}_{4\mathrm{D}}, \bar{S}_{4\mathrm{D}}]$ since $\tilde{s} < \hat{s}$). We see that the 4-DOF biped using both primitive sets traces the pre-planned path without any noticeable drift, whereas the 5-DOF biped using its low-curvature set (parameterized by $\tilde{s}$) has minor drift near the end of the path execution.

Recall that the bipeds do not explicitly track these planned paths, but rather the gait primitives accurately predict the walking path execution using the nominal walking arcs. This is noteworthy given the transient effects after each switching transition. The minor drift observed may indeed accumulate over longer paths, but occasional re-planning, taking a couple seconds or less, can easily compensate for this. In more practical applications, such an iterative planner would already be necessary to incorporate information obtained while navigating through new environments.

6.7 Remarks

The planning framework of dynamic gait primitives can be used with any control method that produces asymptotically stable gaits (e.g., walking [35,43,50,51,80], climbing [114], running [6,115], or swimming [79]). Gait primitives and their switching rules might also be pre-computed using the feedback motion planning method of randomized LQR trees [116].

Each gait primitive is characterized by its hybrid system dynamics and stable fixed-point, thus corresponding to a nominal hybrid periodic orbit. In our compass-gait examples, these orbits are naturally attractive by the (pseudo-passive) robot dynamics after controlled reduction. This motion is not prescribed by full-state trajectories [106] or subjected to any postural constraints to ensure stability [17, 20, 21], yet we have robustness over a *large* class of paths composed of gait primitives.

This allows decomposed tree search planning for *fast* and *efficient* bipedal locomotion based on human-like passive walking principles, which is fundamentally different from ZMP methods. In other words, the walking paths can be planned much like trivial Dubins curves [100]. Although ZMP biped planners often use Dubins curves as a local planning heuristic [17], our results may reaffirm this choice from the perspective of *stability*.

If this control/planning framework were to be applied to a practical real-world environment, we could integrate a suite of other feedback motion planning tools, such as step-level planning over rough terrain [41, 42] and time-scaling for variable walking speeds [38]. Experimental results have been achieved for planar limit cycle walking (cf. [6,28]), and 3-D results may soon be possible with advances in actuator and biped mechanical design. For example, the preliminary investigation of [80] aims to implement controlled reduction on the highly-redundant Sarcos humanoid robot [117].

CHAPTER 7

EXTENSIONS TO LOCOMOTOR REHABILITATION

The field of therapeutic robotics has shown great promise in treating neuromotor disorders and alleviating the intensive labor required by physical therapists. However, significant challenges still remain with the design of control strategies for robot-assisted locomotor rehabilitation. In this section, we propose extensions of our energy-shaping feedback control paradigm to address some of these challenges. We speculate on the utility of these robot-assist strategies based on evidence from the literature that would suggest similarities between our robot walking results and human biomechanics.

7.1 Connections to Human Biomechanics

We first review the biomechanics literature to establish several connections to the autonomous robot walking material presented in the previous chapters.

7.1.1 Modeling assumptions

To begin, we must consider the effect of our modeling assumptions in comparing our results to human walking. A human gait has a substantial double-support phase including a pushoff period (positive CoM work) followed by collision/weight-acceptance (negative CoM work) [98]. However, the compass-gait biped has instantaneous double-support due to perfectly plastic impact events (negative work) and immediate replenishment of potential energy (positive work) if walking on a decline slope. For this reason, the vertical GRF plot of Fig. 5.5 lacks the extra "hump" observed in human walking during double support [118].

The compass-gait model is therefore most useful for characterizing the midstance behavior of human walking, which begins with "rebounding" during the upward pendular arc (positive CoM work) and ends with "preloading" during the downward pendular arc (negative CoM work) [98].

Nontrivial double-support phases for the compass-gait walker have recently been considered in [26], which might prove helpful in future analysis. Moreover, non-trivial feet are considered in the controlled reduction work of [90], showing that these results can be extended to more anthropomorphic models.

7.1.2 Turning strategies

The turning gaits of Chapters 5 and 6 exhibit the fundamental sagittal-plane periodicity of straight-ahead gaits with slight step length and velocity adjustments. This behavior resembles the constant-curvature human turning experiments of [95,96], in which healthy subjects walked 4 m (i.e., 6 steps) along a constant-curvature path with radius of curvature 1.2 m. The resulting body trajectories were segmented by three complete two-step gait cycles, each consisting of a straight-ahead trajectory with steering every other step (which we reproduced in Chapter 5). Electromyography (EMG) analysis showed that the legs propagated the same rhythm (and similar muscle activity) despite differences in stride length and velocity between the inner and outer legs [96]. This led the authors to suggest that human turning exploits the same "basic mechanisms of the spinal locomotor generator" as straight-ahead walking, i.e., turning gaits are built from one periodic rhythm/motion as in our control theoretic results. We certainly do not believe that humans use a sophisticated geometric approach like controlled reduction, but this observation could be explained by a locomotor control strategy that employs some form of sagittal-plane decoupling, where the out-of-plane (i.e., transverse and frontal) modes synchronize to the basic sagittal-plane rhythm (with modulation for turning).

More specifically, three distinct strategies for sharp turns have been observed in healthy human subjects [101]. Instructed to perform a 90° turn over two steps, subjects induced steering motion about the stance leg ("spin" turns) or stepped into the turn by appropriately placing the swing leg ("step" turns). The former category is further decomposed into an "ipsilateral pivot," where the ipsilateral (i.e., stance) foot pivots into the new heading at approximately midstance, or an "ipsilateral crossover," where the hip swings the contralateral (i.e., swing) leg around the ipsilateral limb into the new direction of travel. The majority of subjects employed the step turn, but our simple 3-D models do not have the hip abduction/adduction DOFs necessary to implement this strategy (see [35] for models that are capable of this motion).

Instead, the bipeds in Chapter 5 employ spin turns, which cannot be further distinguished due

to the point-foot assumption (i.e., there is no difference between rotation at the stance ankle or foot). We were unable to successfully simulate two-step 90° turns due to the destabilizing effect of the increased range of motion (RoM) in the transverse plane. However, [101] found that the RoM outside the sagittal plane was smaller for step turns, suggesting that this strategy might be more robust to sharp maneuvers than our spin turns.

7.1.3 Gait primitives and switching

Although we constructed the gait primitive framework of Chapter 6 for robot motion planning, evidence exists for human gait primitives in the biomechanics literature. Recall that the curved walking paths from the human trials of [95] are distinctly segmented by two-step arcs, suggesting the composition of period-2 gait primitives. This is further supported by the study [119], in which healthy subjects were instructed to alter their walking direction when visually cued at random. The investigators offer three important observations from these experiments [119]:

1. *Subjects were unable to alter the direction in the ongoing step, with the major constraint being the inability to rotate the body in the appropriate direction within a step duration.*
2. *The majority of the subjects were unable to alter their direction of locomotion when the cue was given one step duration ahead.*
3. *The success rate for a change in direction was very high (70%) when the cue was given two step durations ahead.*

This behavior could indeed be explained by planned switching between two-step gait primitives to achieve the heading change after the unanticipated cue.

We also find evidence for locomotor primitives in studies unrelated to turning. In the plantar flexor stretch reflex experiments of [120], an EMG-controlled powered ankle exoskeleton was used to amplify the ankle torque of one leg during treadmill walking. Subjects completed 30 minute training sessions with this asymmetric assistance, after which the assistance was unexpectedly decreased during steady-state walking. Although subjects initially took several minutes to reach steady-state with the exoskeleton assistance, they adapted to the decreased assistance by increasing soleus muscle activity with a delay of about 60 ms. Similarly, subjects were able to quickly adapt to reactivated assistance after the initial learning phase.

This suggests that humans with robotic assistance can learn multiple gaits involving different neuromotor patterns, and effectively switch among the set of acquired gaits (i.e., the gait primitives).

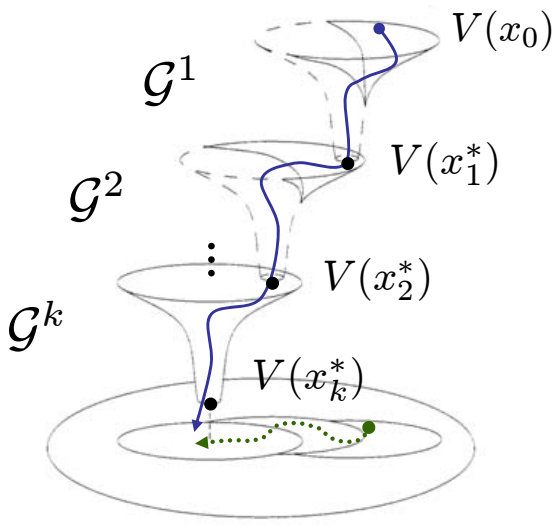

Figure 7.1: Sequential composition of Lyapunov funnels, corresponding to intermediate training gaits, toward some nominal (healthy) gait with fixed-point x_k^*. The funneled state trajectory (dotted green) corresponds to the trajectory of the funneled Lyapunov functions (solid blue). Original figure from [52] reproduced with permission of the publisher.

This may motivate progressive gait therapies based on sequential composition of intermediate training gaits (Fig. 7.1), which can be designed *a priori* as in Chapter 6.

7.2 Challenges in Robot-Assisted Therapy

Recent studies with the Lokomat lower-extremity exoskeleton suggest that strategies imposing reference gait patterns (i.e., joint position trajectories) are less effective than manual therapy in terms of recovered walking speed and endurance for chronic stroke patients [121, 122]. Based on similar control principles, this quasi-static form of locomotor training may indeed suffer from the same fundamental flaws as quasi-static robot walking.

Other challenges exist in the control design for robotic ankle-foot orthosis (AFO), where control patterns are typically tuned in an ad hoc manner based on how a healthy walking gait *should* look. This requires active estimation of the intended modality (e.g., walking or standing) as well as the phase of a gait cycle, which are prone to errors that risk life-threatening falls. Costly attention must also be given to adapting these control sequences to individual morphology and impairment. The impetus to address these control challenges is eloquently stated in [123]:

> *Robotics has the opportunity to make a quantum leap by systematically implementing and controlling therapies, and by enabling systematic adjustment of treatment parameters.*

Future work must consider novel feedback control paradigms for locomotor therapy, where control theories from robot locomotion are translated into strategies for functional human assistance.

Recall that the potential energy provided by gravity at every step is fundamental to efficient dynamic locomotion, particularly passive downhill walking. These stable gaits do not track reference patterns, but naturally appear from the system nonlinearities. The metabolic energetic cost of human walking is minimized on shallow downhill slopes [124] by similarly exploiting the potential energy provided by gravity. This suggests that passive walking models may relate fundamental principles behind human dynamics to guide our design and analysis of robot-assisted therapies. It is also known that speed-intensive training, which effectively encourages dynamic walking, improves gait efficiency and muscle activation for hemiparetic[1] patients [125]. This demonstrates the importance of compliance to passive dynamics in locomotor therapy, so control strategies should be designed to enable and encourage this motion.

7.3 Control Design Methodology

We can now use these control theoretic principles to develop assistive strategies for personalized therapeutic benefit. The theory of Lagrangian mechanics allows direct examination of functional characteristics of mechanical system dynamics and therefore will be useful in control design.

The configuration of an n-DOF human-machine system is given by the vector q of generalized coordinates in configuration space $\mathcal{Q}$. Given Lagrangian function $\mathcal{L}$, we consider the dynamical equations $\mathscr{EL}_q\{\mathcal{L}\} = \tau$ of (2.2), where n-dimensional torque vector $\tau = Bu+v$ is composed of robot control input u and *unknown* human input v. Since the assistive robot input is m-dimensional with $m < n$, we define $n \times m$-matrix B as the map from control u to the n-dimensional joint torques. Therefore, the 2nd-order system of ordinary differential equations (2.2) has the dynamical structure

$$M(q)\ddot{q} + C(q,\dot{q})\dot{q} + N(q) \quad = \quad Bu + v, \tag{7.1}$$

where C is the $n \times n$ Coriolis/centrifugal matrix and $N = \nabla_q \mathcal{V}$ is the potential torque vector.

Recalling that gravitational potential energy is fundamental to dynamic walking, we can use robot input u to shape the human's potential energy, i.e., replace known $\mathcal{V}$ with some $\widetilde{\mathcal{V}}$ that has beneficial properties. Since this control is underactuated ($m < n$), matrix B is not invertible, so

[1] Weakness in one side of the body, often caused by stroke.

only a particular set of energies are achievable from the range space of B. This has been well studied in the literature (e.g., [58]) in terms of energy *matching conditions*. Given continuous dynamics (7.1) and desired potential vector $\widetilde{N} = \nabla_q \widetilde{\mathcal{V}}$, we want to enforce the equality

$$\begin{aligned} v &= M(q)\ddot{q} + C(q,\dot{q})\dot{q} + N(q) - Bu \\ &= M(q)\ddot{q} + C(q,\dot{q})\dot{q} + \widetilde{N}(q), \end{aligned} \tag{7.2}$$

which is equivalent to the necessary condition

$$Bu = N(q) - \widetilde{N}(q). \tag{7.3}$$

We must characterize the null space of B, so we define the full rank *left-annihilator* $B^{\perp}$ such that $B^{\perp}B = 0$. The right-hand side of (7.3) is in the range space of B if

$$B^{\perp}\{N(q) - \widetilde{N}(q)\} = 0, \ \forall \ q \in \mathcal{Q}. \tag{7.4}$$

We can then derive the underactuated control law that exactly achieves desired potential $\widetilde{V}$:

$$u = (B^T B)^{-1} B^T \{N(q) - \widetilde{N}(q)\}. \tag{7.5}$$

In order to develop a strategy for personalized locomotor therapy, we propose three guiding principles for selecting virtual potential energy $\widetilde{\mathcal{V}}$ for the patient:

1. Satisfy energy matching condition (7.4).
2. Preserve the natural limit cycle known to exist in the human dynamics.
3. Alter specific dynamical characteristics based on impairment.

Preliminary work in [126] designs such a strategy for the portable-powered AFO of [127], using one actuated DOF to reduce the perceived weight of a patient's center of mass. In other words, virtual $\widetilde{\mathcal{V}}$ can be chosen as the original potential energy with a smaller hip mass to mimic the body-weight support/stability provided by conventional harnesses. Computer simulations of passive walkers demonstrate that increased body-weight support reduces stride length, velocity, and human work, while improving energy regulation and stability. This suggests that slow walking can be enabled at the onset of therapy for stroke-induced paresis, in order to encourage progressively

faster, more natural gaits as the assistance is gradually decreased. Moreover, the simple feedback control architecture is independent of gait modality and defined in terms of physical parameters that can be easily tuned to individual need.

7.4 Potential Impact

The need for accessible and personalized locomotor therapy after stroke continues to grow with the aging population in the United States. In order for assistive robotics to meet this demand, a systematic approach for functional control design must be developed to address current challenges in automated therapy. This will yield control strategies that modify meaningful characteristics of impaired gaits through feedback loops *without* reference patterns. Passive walking simulations may then allow "rapid prototyping" of personalized strategies by predicting effects on specific impairments, helping clinicians prescribe sequential locomotor therapies based on intermediate training gaits (designed *a priori*).

The therapeutic value of control theories such as kinetic-energy shaping and passivity-based control could also be studied, in order to determine the most effective control paradigms for locomotor training. This will enable therapies to be widely automated with active AFO or lower-extremity exoskeletons such as Lokomat. Moreover, this could be applied to portable-powered AFO devices (e.g., [127]) for long-term use at home. This will assist elders with decreased mobility and increased risk for life-threatening falls (especially after stroke). This also offers a simple alternative to exoskeletal performance augmentation (cf. [128]) for carrying heavy equipment near the body's center of mass, where the virtual mass can be tuned to the human's mass without payload.

Likewise, potential-energy shaping has promise for assisted control of neuroprosthetic lower limbs. Control theoretic strategies could serve as autonomous components to lower-extremity neural control systems, counteracting the destabilizing effect of gravity at high speeds to enable natural walking without canes or crutches. This is particularly relevant in the United States, where lower-extremity amputation rates are higher than other developed countries.

CHAPTER 8

CONCLUSIONS

This thesis has shown that reduction-based control enables fully 3-D bipedal robots to walk dynamically based on human-like passivity principles. The energy-shaping control paradigm, and controlled reduction in particular, aim by construction to minimally cancel system nonlinearities and thus achieve energetic efficiency with natural swaying motion. In fact, we saw that reduction-based control is fundamentally related to passive feedback and thus inverse-optimality.

Our results require only the existence of stable limit cycles in the sagittal subsystem, thus simplifying the search for full-order stable limit cycles and expanding the class of walking robots that can stably exploit passive dynamics to a subset of 3-D open kinematic chains. We have a reasonable understanding of limit cycle stability, since the high-dimensional basin of attraction depends primarily on the sagittal-plane subsystem, for which locally stable behavior is guaranteed from anywhere on the conserved quantity surface. And because we do not enforce a particular trajectory, overall walking gaits need not be known a priori, suggesting a natural robustness to perturbations such as steering motions.

The sequential composition framework of dynamic gait primitives can be used with any control method that produces asymptotically stable gaits (e.g., walking [35, 43, 50, 51, 80], climbing [114], running [6,115], or swimming [79]). This framework reduces dynamically stable motion planning for *fast* and *efficient* dynamic locomotion to a simple tree search, enabling motion planning applications similar to what is readily possible for inefficient quasi-static walkers. Using the developing theory of [104,105], the basin of attraction of each gait's hybrid limit cycle can be conservatively estimated to derive switching rules. Future work such as [99] will detail high-level planning algorithms that can integrate a suite of other motion control tools, such as step-level planning over rough terrain [41,42,129] and time-scaling for variable walking speeds [38,39]. Gait primitives and their switching rules might also be pre-computed using the feedback motion planning method of randomized LQR trees [116].

These results motivate two main thrusts of future work, one attempting to achieve dynamic walking on practical humanoid robots, and the other investigating the value of energy-shaping control in robot-assisted locomotor rehabilitation.

8.1 Autonomous Robot Walking

Experimental results have been achieved for planar limit cycle walking (cf. [6, 28]), and 3-D results may soon be possible with advances in actuator and biped design. As discussed in Section 5.6, this will likely require the degree-one underactuated implementation of our reduction-based control method, where the ankles have passive damping in the yaw DOF and torque control in lean and pitch (like that of a human). High power-density ankle actuators (i.e., small size with high power output) are becoming more common, but comparable spherical actuators for roll, pitch, *and* yaw remain a significant challenge in mechanical design.

We presented the general k-stage case of reduction-based control for n-DOF open kinematic chains, so this method extends to higher-dimensional robotic systems. This could potentially be applied to highly-redundant humanoids with articulated arms that can interact with the environment. However, we have seen that energy-shaping control laws require $n \times n$ matrix inverses, often making these control theories difficult to scale to high-dimensional systems (in terms of computation time and modeling error amplified by inversion).

The recent work [80] presents a first step towards the application of energy-shaping methods on real humanoid robots by casting controlled reduction into a framework of acceleration-based inverse dynamics. Representing the momentum conservation laws as constraints in acceleration space, a general expression can be constructed for desired joint accelerations that render the constraint surface invariant. The unconstrained (reduced) dynamics can then be decoupled from the constrained dynamics by appropriately choosing an orthogonal projection. This planar subsystem (a double-integrator) can be stabilized by any acceleration-based controller, including passivity-based/energy-shaping methods. The overall control law is surprisingly simple, requiring only a $k \times k$ matrix inverse, and represents a practical way for robotic platforms to employ control theoretic stability results. This line of work has reproduced the 5-DOF bipedal walking results of Section 5.4 to show correspondence between the new and original controllers, and preliminary balancing results for a 16-DOF lower-extremity Sarcos humanoid [117] demonstrate the future applicability of this method.

After addressing such implementation challenges, gait primitive theory could allow complex robots with active control to embrace passive dynamics for dynamic walking between desired locations. Such robots could perform tasks while having great autonomy from base stations, as the efficient and natural walking gaits would allow significant locomotion range and long battery life (arguably superior to related characteristics of quadrupedal and treaded robots [13]). These are absolute necessities if robotic technologies are to be implemented on intelligent prosthetic legs or assisted walking devices for the elderly or disabled. There are similar applications in the manufacturing industry, where versatile and long-lasting robots are desirable for the varying demands of lean manufacturing environments. This raises interesting questions about biped coordination, such as synchronizing robot marching given differing initial conditions and asynchronous parameters.

8.2 Robot-Assisted Locomotor Rehabilitation

Evidence from the biomechanics literature in Chapter 7 suggests that feedback control paradigms such as energy shaping may have value as novel strategies for robot-assisted locomotor rehabilitation. This future work aims to establish systematic design methods for personalized control strategies that provably modify meaningful characteristics of the human gait. This must also address challenges related to the underactuated nature of the robot control authority in the human-machine system, where the human control policy is unknown.

Preliminary applications of these ideas include portable-powered ankle-foot orthosis (AFO) with one actuated DOF such as [127]. The paper [126] proposes a control theoretic strategy for this device based on the methodology discussed in Section 7.3, *underactuated potential energy shaping*. This yields a simple control law that lessens the perceived weight of the patient's center of mass, and simulations indicate this will provide energy regulation and improved stability through progressive training regiments designed with Lyapunov funneling in mind. Given current challenges in developing effective robotic locomotor therapies for stroke patients [121–123], this line of work can potentially offer novel systematic approaches to control strategy design.

The discussion of Section 7.1.3 also begs deeper questions about the building blocks of human locomotion: is our motion based on a set of gait primitives in the form of neuromuscular memory and periodic rhythms from the spinal cord's central pattern-generator? The relevance of these questions and our motivating results will continue to grow as the medical, industrial, and military sectors become increasingly interested in legged robotics.

APPENDIX A

PROPERTIES OF ALMOST-CYCLIC LAGRANGIAN SYSTEMS

Since reduction-based control shapes the kinetic and potential characteristics of robots, we must consider whether the well-known properties of general robotic systems still hold. To begin, almost-cyclic systems do not preserve the linearity-in-the-parameters property, which provides that the E-L equations can be "linearly" expressed by

$$\frac{d}{dt}\nabla_{\dot{q}}\mathcal{L} - \nabla_q\mathcal{L} = Y(q,\dot{q},\ddot{q})\Theta,$$

where $\Theta \in \mathbb{R}^p$ is the *parameter vector* of constants, in terms of link masses, inertias, and lengths, and $Y \in \mathbb{R}^{n\times p}$ is the *regressor* matrix of nonlinear functions of $(q,\dot{q},\ddot{q})$, as discussed in [55]. This property does not hold because reduction-based control laws require matrix inversion (demonstrated in Section 4.3), introducing rational dependencies on q in the system dynamics and thus breaking linearity in the parameters. This can explicitly be seen in the almost-cyclic matrix $M_{\lambda_1^k}$ of (4.4).

On the other hand, several important properties of robotic systems do hold for k-ACL systems. After shaping a standard robot's Lagrangian to a k-ACL through reduction-based control law (4.8), we prove the following properties are preserved:

1. Symmetry of the inertia matrix
2. Positive definiteness of the inertia matrix
3. Skew-symmetry of the inertia matrix minus twice the Coriolis matrix

These properties are used in Theorem 7 to show that passivity is also preserved.

A.1 Inertia Matrix

Theorem 14. Given a k-almost-cyclic Lagrangian, its inertia matrix $M_{\lambda_1^k}(q_2^n)$ is symmetric and positive definite.

Proof. Recall that k-almost-cyclic inertia matrix $M_{\lambda_1^k}(q_2^n)$ is defined in (4.4) by

$$M_{\lambda_1^k}(q_2^n) = M(q_2^n) + \sum_{i=1}^{k} \begin{pmatrix} 0 & 0 \\ 0 & \frac{M^T_{q_i,q^n_{i+1}}(q^n_{i+1}) M_{q_i,q^n_{i+1}}(q^n_{i+1})}{m_{q_i}(q^n_{i+1})} \end{pmatrix}.$$

First, we know that inertia matrix $M(q_2^n)$ is symmetric and positive definite. Also, each summation term

$$\begin{pmatrix} 0 & 0 \\ 0 & \frac{M^T_{q_i,q^n_{i+1}}(q^n_{i+1}) M_{q_i,q^n_{i+1}}(q^n_{i+1})}{m_{q_i}(q^n_{i+1})} \end{pmatrix}, \quad i \in \{1, k\},$$

is symmetric since the zero terms are trivially symmetric and since $m_{q_i}(q^n_{i+1})$ is scalar/symmetric and

$$\left(M^T_{q_i,q^n_{i+1}}(q^n_{i+1}) M_{q_i,q^n_{i+1}}(q^n_{i+1})\right)^T = M^T_{q_i,q^n_{i+1}}(q^n_{i+1}) M_{q_i,q^n_{i+1}}(q^n_{i+1}).$$

Each summation term is positive semidefinite since there are i zero-eigenvalues and since $m_{q_i}(q^n_{i+1})$ is positive definite by the positive definiteness of $M(q_2^n)$ and $M^T_{q_i,q^n_{i+1}}(q^n_{i+1}) M_{q_i,q^n_{i+1}}(q^n_{i+1})$ is trivially positive definite. Finally, the sum of symmetric matrices is symmetric, and the sum of a positive definite matrix with positive semidefinite matrices is positive definite. □

A.2 Skew-Symmetry

Given a k-almost-cyclic Lagrangian, its Coriolis-gyroscopic matrix is

$$C_{\lambda_1^k}(q, \dot{q}) = C_{M_{\lambda_1^k}}(q_2^n, \dot{q}) + C_{Q_{\lambda_1}}(q) + \ldots + C_{Q_{\lambda_k}}(q_k^n), \tag{A.1}$$

where $C_{M_{\lambda_1^k}}(q_2^n, \dot{q}) \in \mathbb{R}^{n \times n}$ is derived from $M_{\lambda_1^k}(q_2^n)$ and $C_{Q_{\lambda_i}}(q_i^n) \in \mathbb{R}^{n \times n}$ is derived from

$$Q_{\lambda_i}(q_i^n) = \begin{pmatrix} 0 & -\lambda_i(q_i) m_{q_i}^{-1}(q^n_{i+1}) M_{q_i,q^n_{i+1}}(q^n_{i+1}) \end{pmatrix}^T, \quad i \in \{1, k\}.$$

Lemma 8. Matrix $C_{Q_{\lambda_i}}(q_i^n)$ is skew-symmetric $\forall i \in \{1, k\}$.

Proof. This is proven by calculation for any fixed $i \in \{1, k\}$:

$$C_{Q_{\lambda_i}}(q_i^n)\dot{q} = \frac{d}{dt} \nabla_{\dot{q}} [Q^T_{\lambda_i}(q_i^n)\dot{q}] - \nabla_q [Q^T_{\lambda_i}(q_i^n)\dot{q}],$$

where

$$\nabla_{\dot{q}}[Q_{\lambda_i}^T(q_i^n)\dot{q}] = \begin{pmatrix} 0_{i\times 1} \\ \frac{\lambda_i(q_i)}{m_{q_i}(q_{i+1}^n)} M_{q_i,q_{i+1}^n}^T(q_{i+1}^n) \end{pmatrix},$$

implying that

$$\frac{d}{dt}\nabla_{\dot{q}}[Q_{\lambda_i}^T(q_i^n)\dot{q}] = \begin{pmatrix} 0_{i\times 1} \\ \frac{\dot{\lambda}_i(q_i)}{m_{q_i}(q_{i+1}^n)} M_{q_i,q_{i+1}^n}^T(q_{i+1}^n) - \lambda_i(q_i)\frac{\dot{m}_{q_i}(q_{i+1}^n)}{m_{q_i}^2(q_{i+1}^n)} M_{q_i,q_{i+1}^n}^T(q_{i+1}^n) + \frac{\lambda_i(q_i)}{m_{q_i}(q_{i+1}^n)}\dot{M}_{q_i,q_{i+1}^n}^T(q_{i+1}^n) \end{pmatrix}.$$

Also, the second term of $C_{Q_{\lambda_i}}(q_i^n)\dot{q}$ is given by

$$\nabla_q[Q_{\lambda_i}^T(q_i^n)\dot{q}] = \begin{pmatrix} 0_{(i-1)\times 1} \\ \frac{\partial\lambda_i(q_i)}{\partial q_i}\frac{1}{m_{q_i}(q_{i+1}^n)} M_{q_i,q_{i+1}^n}(q_{i+1}^n)\dot{q}_{i+1}^n \\ \frac{\lambda_i(q_i)}{m_{q_i}(q_{i+1}^n)}\frac{\partial M_{q_i,q_{i+1}^n}(q_{i+1}^n)}{\partial q_{i+1}^n}^T \dot{q}_{i+1}^n - \frac{\lambda_i(q_i)}{m_{q_i}^2(q_{i+1}^n)} M_{q_i,q_{i+1}^n}^T(q_{i+1}^n)\frac{\partial m_{q_i}(q_{i+1}^n)}{\partial q_{i+1}^n}^T \dot{q}_{i+1}^n \end{pmatrix}.$$

In this context, we have (note that $\frac{dy}{dt} := (\frac{\partial y}{\partial t})^T$ and $\frac{\partial(y^T)}{\partial x} = (\frac{\partial y}{\partial x})^T$ for all vectors x, y [130]):

$$\begin{aligned} \dot{\lambda}_i(q_i) &= \frac{\partial\lambda_i(q_i)}{\partial q_i}\dot{q}_i \\ \dot{m}_{q_i}(q_{i+1}^n) &= \dot{m}_{q_i}^T(q_{i+1}^n) = \frac{\partial m_{q_i}(q_{i+1}^n)}{\partial q_{i+1}^n}^T \dot{q}_{i+1}^n \\ \dot{M}_{q_i,q_{i+1}^n}^T(q_{i+1}^n) &= \frac{\partial M_{q_i,q_{i+1}^n}(q_{i+1}^n)}{\partial q_{i+1}^n}^T \dot{q}_{i+1}^n, \end{aligned}$$

so after canceling terms we get

$$C_{Q_{\lambda_i}}(q_i^n)\dot{q} = \begin{pmatrix} 0_{(i-1)\times 1} \\ -\frac{\partial\lambda_i(q_i)}{\partial q_i}\frac{1}{m_{q_i}(q_{i+1}^n)} M_{q_i,q_{i+1}^n}(q_{i+1}^n)\dot{q}_{i+1}^n \\ \frac{\partial\lambda_i(q_i)}{\partial q_i}\frac{1}{m_{q_i}(q_{i+1}^n)} M_{q_i,q_{i+1}^n}^T(q_{i+1}^n)\dot{q}_i \end{pmatrix},$$

implying that

$$C_{Q_{\lambda_i}}(q_i^n) = \begin{pmatrix} 0_{(i-1)\times(i-1)} & 0_{(i-1)\times 1} & 0_{(i-1)\times(n-i)} \\ 0_{1\times(i-1)} & 0 & -\frac{\partial\lambda_i(q_i)}{\partial q_i}\frac{1}{m_{q_i}(q_{i+1}^n)} M_{q_i,q_{i+1}^n}(q_{i+1}^n) \\ 0_{(n-i)\times(i-1)} & \frac{\partial\lambda_i(q_i)}{\partial q_i}\frac{1}{m_{q_i}(q_{i+1}^n)} M_{q_i,q_{i+1}^n}^T(q_{i+1}^n) & 0_{(n-i)\times(n-i)} \end{pmatrix}.$$

Hence, $C_{Q_{\lambda_i}}$ is skew-symmetric. □

Theorem 15. The skew-symmetry property holds for a k-almost-cyclic Lagrangian system, i.e., matrix $(\dot{M}_{\lambda_1^k} - 2C_{\lambda_1^k})$ is skew-symmetric.

Proof. According to Equation (A.1),

$$\dot{M}_{\lambda_1^k} - 2C_{\lambda_1^k} = (\dot{M}_{\lambda_1^k} - 2C_{M_{\lambda_1^k}}) - 2C_{Q_{\lambda_1}} - \ldots - 2C_{Q_{\lambda_k}}.$$

Since $M_{\lambda_1^k}$ is symmetric by Theorem 14, and $C_{M_{\lambda_1^k}}$ is derived from $M_{\lambda_1^k}$, it follows that $(\dot{M}_{\lambda_1^k} - 2C_{M_{\lambda_1^k}})$ is skew-symmetric (see the original skew-symmetry property in [55]). Moreover, the additional $C_{Q_{\lambda_i}}$ terms are skew-symmetric by Lemma 8. Finally, the summation of skew-symmetric terms is skew-symmetric. □

APPENDIX B

PROOF OF CONTROLLED REDUCTION THEOREM

We now revisit [49] to prove Theorem 10 from Section 4.3 (note that this proof is based on the construction from [131]).

Proof. We begin this proof by inductively relating the v_{k+1}^n-controlled E-L equations of $\mathcal{L}_{\lambda_1^k}$ to the k-reduced controlled E-L equations of $\mathcal{R}_\lambda$. We will then be able to show the direct correspondence of solutions based on the uniqueness of solutions to well-behaved differential equations.

For the general case of reduction stage-j, where $j \in \{1, k-1\}$, we consider the generalized ACL[1] $\mathcal{L}_{\lambda_j^k}$ in terms of its nested ACL and remaining term:

$$\mathcal{L}_{\lambda_j^k}(q_j, q_{j+1}^n, \dot{q}_j, \dot{q}_{j+1}^n) = \mathcal{L}_{\lambda_{j+1}^k}(q_{j+1}^n, \dot{q}_{j+1}^n) + \mathrm{Rem}_j(q_j, q_{j+1}^n, \dot{q}_j, \dot{q}_{j+1}^n),$$

and similarly for the base case of stage-k, we have

$$\mathcal{L}_{\lambda_k^k}(q_k, q_{k+1}^n, \dot{q}_k, \dot{q}_{k+1}^n) = \mathcal{R}_\lambda(q_{k+1}^n, \dot{q}_{k+1}^n) + \mathrm{Rem}_k(q_k, q_{k+1}^n, \dot{q}_k, \dot{q}_{k+1}^n),$$

where, for $l \in \{1, k\}$, the remaining term is apparent from (4.7):

$$\begin{aligned}
\mathrm{Rem}_l(q_l^n, \dot{q}_l^n) \;=\; & \frac{1}{2} m_{q_l}(q_{l+1}^n)(\dot{q}_l)^2 + \dot{q}_l M_{q_l, q_{l+1}^n}(q_{l+1}^n)\dot{q}_{l+1}^n \\
& + \frac{1}{2} \dot{q}_{l+1}^{n\,T} \frac{M_{q_l, q_{l+1}^n}^T(q_{l+1}^n) M_{q_l, q_{l+1}^n}(q_{l+1}^n)}{m_{q_l}(q_{l+1}^n)} \dot{q}_{l+1}^n \\
& - \frac{\lambda_l(q_l)}{m_{q_l}(q_{l+1}^n)} M_{q_l, q_{l+1}^n}(q_{l+1}^n)\dot{q}_{l+1}^n + \frac{1}{2} \frac{\lambda_l(q_l)^2}{m_{q_l}(q_{l+1}^n)}.
\end{aligned}$$

[1] This generalized almost-cyclic Lagrangian is the parent of the j^{th} stage of reduction, as opposed to the target Routhian of the stage-j projection.

Therefore, the controlled E-L equations for the general case are

$$\begin{aligned}
\frac{d}{dt}\frac{\partial \mathcal{L}_{\lambda_j^k}}{\partial \dot{q}_j} - \frac{\partial \mathcal{L}_{\lambda_j^k}}{\partial q_j} &= \frac{d}{dt}\frac{\partial \mathrm{Rem}_j}{\partial \dot{q}_j} - \frac{\partial \mathrm{Rem}_j}{\partial q_j} = 0 && \text{(B.1)}\\
\frac{d}{dt}\frac{\partial \mathcal{L}_{\lambda_j^k}}{\partial \dot{q}_i} - \frac{\partial \mathcal{L}_{\lambda_j^k}}{\partial q_i} &= \frac{d}{dt}\frac{\partial \mathcal{L}_{\lambda_{j+1}^k}}{\partial \dot{q}_i} - \frac{\partial \mathcal{L}_{\lambda_{j+1}^k}}{\partial q_i} + \frac{d}{dt}\frac{\partial \mathrm{Rem}_j}{\partial \dot{q}_i} - \frac{\partial \mathrm{Rem}_j}{\partial q_i} && \text{(B.2)}\\
&= \begin{pmatrix} 0_{(k-j)\times 1} \\ B_{q_{k+1}^n} v_{k+1}^n \end{pmatrix} e_{i-j}
\end{aligned}$$

for $i \in \{j+1, n\}$, where e_{i-j} is the $(i-j)^{\text{th}}$ standard basis vector for $\mathbb{R}^{n-j}$. As for the base case, we have

$$\begin{aligned}
\frac{d}{dt}\frac{\partial \mathcal{L}_{\lambda_k^k}}{\partial \dot{q}_k} - \frac{\partial \mathcal{L}_{\lambda_k^k}}{\partial q_k} &= \frac{d}{dt}\frac{\partial \mathrm{Rem}_k}{\partial \dot{q}_k} - \frac{\partial \mathrm{Rem}_k}{\partial q_k} = 0 && \text{(B.3)}\\
\frac{d}{dt}\frac{\partial \mathcal{L}_{\lambda_k^k}}{\partial \dot{q}_i} - \frac{\partial \mathcal{L}_{\lambda_k^k}}{\partial q_i} &= \frac{d}{dt}\frac{\partial \mathcal{R}_\lambda}{\partial \dot{q}_i} - \frac{\partial \mathcal{R}_\lambda}{\partial q_i} + \frac{d}{dt}\frac{\partial \mathrm{Rem}_k}{\partial \dot{q}_i} - \frac{\partial \mathrm{Rem}_k}{\partial q_i} = B_{q_{k+1}^n} v_{k+1}^n e_{i-k} && \text{(B.4)}
\end{aligned}$$

for $i \in \{k+1, n\}$, where e_{i-k} is the $(i-k)^{\text{th}}$ standard basis vector for $\mathbb{R}^{n-k}$.

It is now necessary to calculate the derivatives of $\mathrm{Rem}_l(q_l^n, \dot{q}_l^n)$, for $l \in \{1, k\}$:

$$\begin{aligned}
\frac{d}{dt}\frac{\partial \mathrm{Rem}_l}{\partial \dot{q}_l} &= \frac{d}{dt}(M_{q_l, q_{l+1}^n}(q_{l+1}^n))\dot{q}_{l+1}^n + M_{q_l, q_{l+1}^n}(q_{l+1}^n))\ddot{q}_{l+1}^n + m_{q_l}(q_{l+1}^n)\ddot{q}_l && \text{(B.5)}\\
&\quad + \frac{d}{dt}(m_{q_l}(q_{l+1}^n))\dot{q}_l\\
\frac{\partial \mathrm{Rem}_l}{\partial q_l} &= -\frac{\frac{\partial}{\partial q_l}(\lambda_l(q_l))}{m_{q_l}(q_{l+1}^n)} M_{q_l, q_{l+1}^n}(q_{l+1}^n))\dot{q}_{l+1}^n + \frac{\lambda_l(q_l)\frac{\partial}{\partial q_1}(\lambda_l(q_l))}{m_{q_l}(q_{l+1}^n)} && \text{(B.6)}
\end{aligned}$$

$$
\begin{aligned}
\frac{d}{dt}\frac{\partial \mathrm{Rem}_l}{\partial \dot{q}_i} &= \ddot{q}_{l+1}^{n^T}\frac{M_{q_l,q_{l+1}^n}(q_{l+1}^n)^T M_{q_l,q_{l+1}^n}(q_{l+1}^n)}{m_{q_l}(q_{l+1}^n)}e_{i-1} \\
&\quad + \dot{q}_{l+1}^{n^T}\frac{\frac{d}{dt}(M_{q_l,q_{l+1}^n}(q_{l+1}^n))^T M_{q_l,q_{l+1}^n}(q_{l+1}^n)}{m_{q_l}(q_{l+1}^n)}e_{i-1} \\
&\quad + \dot{q}_{l+1}^{n^T}\frac{M_{q_l,q_{l+1}^n}(q_{l+1}^n)^T \frac{d}{dt}(M_{q_l,q_{l+1}^n}(q_{l+1}^n))}{m_{q_l}(q_{l+1}^n)}e_{i-1} \\
&\quad - \frac{d}{dt}(m_{q_l}(q_{l+1}^n))\dot{q}_{l+1}^{n^T}\frac{M_{q_l,q_{l+1}^n}(q_{l+1}^n)^T M_{q_l,q_{l+1}^n}(q_{l+1}^n)}{m_{q_l}(q_{l+1}^n)^2}e_{i-1} \\
&\quad + \ddot{q}_l M_{q_l,q_{l+1}^n}(q_{l+1}^n)e_{i-1} + \dot{q}_l\frac{d}{dt}(M_{q_l,q_{l+1}^n}(q_{l+1}^n))e_{i-1} \\
&\quad + \frac{\lambda_l(q_l)\frac{d}{dt}(m_{q_l}(q_{l+1}^n))}{m_{q_l}(q_{l+1}^n)^2}M_{q_l,q_{l+1}^n}(q_{l+1}^n)e_{i-1} \\
&\quad - \frac{\frac{d}{dt}(\lambda_l(q_l))}{m_{q_l}(q_{l+1}^n)}M_{q_l,q_{l+1}^n}(q_{l+1}^n)e_{i-1} - \frac{\lambda_l(q_l)}{m_{q_l}(q_{l+1}^n)}\frac{d}{dt}(M_{q_l,q_{l+1}^n}(q_{l+1}^n))e_{i-1}
\end{aligned} \tag{B.7}
$$

$$
\begin{aligned}
\frac{\partial \mathrm{Rem}_l}{\partial q_i} &= 2\dot{q}_{l+1}^{n^T}\frac{\frac{\partial}{\partial q_i}(M_{q_l,q_{l+1}^n}(q_{l+1}^n))^T M_{q_l,q_{l+1}^n}(q_{l+1}^n)}{2m_{q_l}(q_{l+1}^n)}\dot{q}_{l+1}^n \\
&\quad - \dot{q}_{l+1}^{n^T}\frac{\frac{\partial}{\partial q_i}(m_{q_l}(q_{l+1}^n))M_{q_l,q_{l+1}^n}(q_{l+1}^n)^T M_{q_l,q_{l+1}^n}(q_{l+1}^n)}{2m_{q_l}(q_{l+1}^n)^2}\dot{q}_{l+1}^n \\
&\quad + \frac{1}{2}\frac{\partial}{\partial q_i}(m_{q_l}(q_{l+1}^n))(\dot{q}_{l+1})^2 + \dot{q}_l\frac{\partial}{\partial q_i}(M_{q_l,q_{l+1}^n}(q_{l+1}^n))\dot{q}_{l+1}^n \\
&\quad + \frac{\frac{\partial}{\partial q_i}(m_{q_l}(q_{l+1}^n))\lambda_l(q_l)}{m_{q_l}(q_{l+1}^n)^2}M_{q_l,q_{l+1}^n}(q_{l+1}^n)\dot{q}_{l+1}^n \\
&\quad - \frac{\lambda_l(q_l)}{m_{q_l}(q_{l+1}^n)}\frac{\partial}{\partial q_i}(M_{q_l,q_{l+1}^n}(q_{l+1}^n))\dot{q}_{l+1}^n - \frac{1}{2}\frac{\frac{\partial}{\partial q_i}(m_{q_l}(q_{l+1}^n))\lambda_l(q_l)^2}{m_{q_l}(q_{l+1}^n)^2},
\end{aligned} \tag{B.8}
$$

where $i \in \{l+1, n\}$. Given these expressions, we can prove that the E-L equations for Rem_l hold when restricted to the constrained surface defined by (4.2). In particular, this constraint implies the following derivative of $\lambda_l(q_l)$ and second derivative of q_l:

$$
\frac{d}{dt}(\lambda_l(q_l)) = \frac{\partial}{\partial q_l}(\lambda_l(q_l))\dot{q}_l = \frac{\partial \mathrm{Rem}_l}{\partial q_l}, \tag{B.9}
$$

$$
\begin{aligned}
\ddot{q}_l &= \frac{\frac{d}{dt}(m_{q_l}(q_{l+1}^n))}{m_{q_l}(q_{l+1}^n)^2}M_{q_l,q_{l+1}^n}(q_{l+1}^n)\dot{q}_{l+1}^n - \frac{\frac{d}{dt}(m_{q_l}(q_{l+1}^n))}{m_{q_l}(q_{l+1}^n)^2}\lambda_l(q_l) \\
&\quad + \frac{\frac{d}{dt}(\lambda_l(q_l))}{m_{q_l}(q_{l+1}^n)} - \frac{\frac{d}{dt}(M_{q_l,q_{l+1}^n}(q_{l+1}^n))}{m_{q_l}(q_{l+1}^n)}\dot{q}_{l+1}^n - \frac{M_{q_l,q_{l+1}^n}(q_{l+1}^n)}{m_{q_l}(q_{l+1}^n)}\ddot{q}_{l+1}^n.
\end{aligned} \tag{B.10}
$$

Then, (B.5) and (B.6) given (4.2), (B.9), (B.10) implies

$$\left[\frac{d}{dt}\frac{\partial \mathrm{Rem}_l}{\partial \dot{q}_l} - \frac{\partial \mathrm{Rem}_l}{\partial q_l}\right]\Bigg|_{J_l(q_l^n,\dot{q}_l^n)=\lambda_l(q_l)} = 0. \tag{B.11}$$

And, (B.7) given (4.2) and (B.10) implies

$$\frac{d}{dt}\frac{\partial \mathrm{Rem}_l}{\partial \dot{q}_i}\Bigg|_{J_l(q_l^n,\dot{q}_l^n)=\lambda_l(q_l)} = 0.$$

And, (B.8) given (4.2) implies

$$\frac{\partial \mathrm{Rem}_l}{\partial q_i}\Bigg|_{J_l(q_l^n,\dot{q}_l^n)=\lambda_l(q_l)} = 0.$$

Hence, we have

$$\left[\frac{d}{dt}\frac{\partial \mathrm{Rem}_l}{\partial \dot{q}_i} - \frac{\partial \mathrm{Rem}_l}{\partial q_i}\right]\Bigg|_{J_l(q_l^n,\dot{q}_l^n)=\lambda_l(q_l)} = 0, \tag{B.12}$$

for $i = l+1, \ldots, n$, showing that the E-L equations for Rem_l hold given that the functional quantities are conserved.

Then, by the single-stage reduction proof of [46], based on the uniqueness of solutions to well-behaved differential equations, we know that solutions can be related through the single-stage reduction of both the general case and the base case. Hence, the multistage theorem follows by induction, proving the relationship between solutions of full-order vector field $\hat{f}_{\lambda_1^k}$ and solutions of k-reduced vector field $\hat{f}_{\mathcal{R}_\lambda}$. □

APPENDIX C

BIPED INERTIA MATRIX TERMS

Recall that the inertia matrix of an n-DOF biped has the form

$$M(\varphi,\theta) \;=\; \begin{pmatrix} m_\psi(\varphi,\theta) & \text{---} & M_{\psi\varphi\theta}(\varphi,\theta) \\ | & m_\varphi(\theta) & M_{\varphi\theta}(\theta) \\ M_{\psi\varphi\theta}^T(\varphi,\theta) & M_{\varphi\theta}^T(\theta) & M_\theta(\theta) \end{pmatrix}.$$

We now give expressions for these symbolic modeling terms corresponding to the two biped models in Section 5.1. To obtain the analogous hipless models from Section 6.5, set hip width $w = 0$ and leg splay angle $\rho = 0$ in the expressions below.

C.1 4-DOF Hipped Biped

In the 4-DOF model, the submatrix of $M_{4\mathrm{D}}$ corresponding to the sagittal subsystem is given by

$$M_\theta(\theta) \;=\; \begin{pmatrix} \frac{l^2}{4}(5m+4M)\cos(\rho)^2 & -\frac{l^2 m}{2}\cos(\theta_{\mathrm{s}}-\theta_{\mathrm{ns}})\cos(\rho)^2 \\ -\frac{l^2 m}{2}\cos(\theta_{\mathrm{s}}-\theta_{\mathrm{ns}})\cos(\rho)^2 & \frac{l^2 m}{4}\cos(\rho)^2 \end{pmatrix}.$$

The lean DOF terms in the 3×3 inertia submatrix are given by

$$\begin{aligned} m_\varphi(\theta) \;=\; & \frac{1}{32}(4l^2(13m+6M)+8(4m+M)w^2 \\ & +l(-4l(7m+2M)\cos(2\rho)+lm\cos(2(\rho-\theta_{\mathrm{ns}}))+2lm\cos(2\theta_{\mathrm{ns}}) \\ & +lm\cos(2(\rho+\theta_{\mathrm{ns}})) \\ & +4(l\cos(\rho)^2(-8m\cos(\theta_{\mathrm{ns}})\cos(\theta_{\mathrm{s}})+(5m+4M)\cos(2\theta_{\mathrm{s}})) \\ & -8(3m+M)w\sin(\rho)))) \\ M_{\varphi\theta}(\theta) \;=\; & \begin{pmatrix} -\frac{l}{4}\cos(\rho)(-2(2m+M)w+l(7m+4M)\sin(\rho))\sin(\theta_{\mathrm{s}}) \\ \frac{lm}{4}\cos(\rho)(-2w+3l\sin(\rho))\sin(\theta_{\mathrm{ns}}) \end{pmatrix}^T. \end{aligned}$$

Finally, the yaw DOF terms in $M_{4\mathrm{D}}$ are given by

$$\begin{aligned}
m_\psi(\varphi,\theta) &= \frac{1}{16}(2l(4l\cos(\rho)^2(3m+2M-2m\cos(\theta_{\mathrm{ns}}-\theta_{\mathrm{s}}))\sin(\varphi)^2 \\
&\quad +4w\cos(\rho)(-m\cos(\theta_{\mathrm{ns}})+(2m+M)\cos(\theta_{\mathrm{s}}))\sin(2\varphi) \\
&\quad -l(-3m\cos(\theta_{\mathrm{ns}})+(7m+4M)\cos(\theta_{\mathrm{s}}))\sin(2\rho)\sin(2\varphi)) \\
&\quad -\cos(\varphi)^2(-2(l^2(13m+6M)+2(4m+M)w^2) \\
&\quad +l^2\cos(2\rho)(14m+4M+m\cos(2\theta_{\mathrm{ns}}) \\
&\quad +(5m+4M)\cos(2\theta_{\mathrm{s}})+8m\sin(\theta_{\mathrm{ns}})\sin(\theta_{\mathrm{s}})) \\
&\quad +l(lm\cos(2\theta_{\mathrm{ns}})+l(5m+4M)\cos(2\theta_{\mathrm{s}}) \\
&\quad +8(2(3m+M)w\sin(\rho)+lm\sin(\theta_{\mathrm{ns}})\sin(\theta_{\mathrm{s}}))))).
\end{aligned}$$

$$\begin{aligned}
M_{\psi\varphi\theta}(\varphi,\theta) &= \begin{pmatrix} m_{\psi,\varphi}(\varphi,\theta) & m_{\psi,\theta_{\mathrm{s}}}(\varphi,\theta) & m_{\psi,\theta_{\mathrm{ns}}}(\varphi,\theta) \end{pmatrix}, \\
m_{\psi,\varphi}(\varphi,\theta) &= \frac{1}{8}l(4w\cos(\rho)\sin(\varphi)(-m\sin(\theta_{\mathrm{ns}})+(2m+M)\sin(\theta_{\mathrm{s}})) \\
&\quad -l\sin(2\rho)\sin(\varphi)(-3m\sin(\theta_{\mathrm{ns}})+(7m+4M)\sin(\theta_{\mathrm{s}})) \\
&\quad -l\cos(\rho)^2\cos(\varphi)(m\sin(2\theta_{\mathrm{ns}})+(5m+4M)\sin(2\theta_{\mathrm{s}})-4m\sin(\theta_{\mathrm{ns}}+\theta_{\mathrm{s}}))), \\
m_{\psi,\theta_{\mathrm{s}}}(\varphi,\theta) &= \frac{1}{8}l(4(2m+M)w\cos(\rho)\cos(\varphi)\cos(\theta_{\mathrm{s}})-l(7m+4M)\cos(\varphi)\cos(\theta_{\mathrm{s}})\sin(2\rho) \\
&\quad +2l\cos(\rho)^2(5m+4M-2m\cos(\theta_{\mathrm{ns}}-\theta_{\mathrm{s}}))\sin(\varphi)), \\
m_{\psi,\theta_{\mathrm{ns}}}(\varphi,\theta) &= -\frac{1}{4}lm\cos(\rho)(\cos(\varphi)\cos(\theta_{\mathrm{ns}})(2w-3l\sin(\rho)) \\
&\quad +l\cos(\rho)(-1+2\cos(\theta_{\mathrm{ns}}-\theta_{\mathrm{s}}))\sin(\varphi)).
\end{aligned}$$

C.2 5-DOF Hipped Biped

In the 5-DOF model, the submatrix of $M_{5\mathrm{D}}$ corresponding to the sagittal subsystem is given by

$$M_\theta(\theta) = \begin{pmatrix} \frac{1}{4}l^2(5m+4(M_{\mathrm{h}}+M_{\mathrm{t}}))\cos(\rho)^2 & l_{\mathrm{t}}lM_{\mathrm{t}}\cos(\rho)\cos(\theta_{\mathrm{s}}-\theta_{\mathrm{t}}) & -\frac{1}{2}l^2m\cos(\rho)^2\cos(\theta_{\mathrm{ns}}-\theta_{\mathrm{s}}) \\ l_{\mathrm{t}}lM_{\mathrm{t}}\cos(\rho)\cos(\theta_{\mathrm{s}}-\theta_{\mathrm{t}}) & l_{\mathrm{t}}^2M_{\mathrm{t}} & 0 \\ -\frac{1}{2}l^2m\cos(\rho)^2\cos(\theta_{\mathrm{ns}}-\theta_{\mathrm{s}}) & 0 & \frac{1}{4}l^2m\cos(\rho)^2 \end{pmatrix}.$$

The lean DOF terms in the 4×4 inertia submatrix are given by

$$
\begin{aligned}
m_{\varphi}(\theta) \;=\; & \frac{1}{4}(-4l^2 m\cos(\rho)^2\cos(\theta_{\mathrm{ns}})\cos(\theta_{\mathrm{s}}) + 8l_{\mathrm{t}} l M_{\mathrm{t}}\cos(\rho)\cos(\theta_{\mathrm{s}})\cos(\theta_{\mathrm{t}}) \\
& + m\cos(\theta_{\mathrm{ns}})^2(5l^2 + 4w^2 - 4l^2\cos(2\rho) + 12lw\sin(\rho)) \\
& + \cos(\theta_{\mathrm{s}})^2(l^2(3m + 4M_{\mathrm{h}} + 2M_{\mathrm{t}}) + M_{\mathrm{h}}w^2 \\
& + 2l^2(m + M_{\mathrm{t}})\cos(2\rho) + 4lM_{\mathrm{h}}w\sin(\rho)) \\
& + M_{\mathrm{t}}\cos(\theta_{\mathrm{t}})^2(4l_{\mathrm{t}}^2 + w^2 + 4l\sin(\rho)(w + l\sin(\rho))) \\
& + m(2w + 3l\sin(\rho))^2\sin(\theta_{\mathrm{ns}})^2 + M_{\mathrm{h}}w^2\sin(\theta_{\mathrm{s}})^2 \\
& + 4lM_{\mathrm{h}}w\sin(\rho)\sin(\theta_{\mathrm{s}})^2 + l^2 m\sin(\rho)^2\sin(\theta_{\mathrm{s}})^2 \\
& + 4l^2 M_{\mathrm{h}}\sin(\rho)^2\sin(\theta_{\mathrm{s}})^2 M_{\mathrm{t}}(w + 2l\sin(\rho))^2\sin(\theta_{\mathrm{t}})^2).
\end{aligned}
$$

$$
M_{\varphi\theta}(\theta) \;=\; \begin{pmatrix} \frac{1}{4}l\cos(\rho)(2(2m + M_{\mathrm{h}} + M_{\mathrm{t}})w + l(7m + 4(M_{\mathrm{h}} + M_{\mathrm{t}}))\sin(\rho))\sin(\theta_{\mathrm{s}}) \\ \frac{1}{2}l_{\mathrm{t}}M_{\mathrm{t}}(w + 2l\sin(\rho))\sin(\theta_{\mathrm{t}}) \\ -\frac{1}{4}lm\cos(\rho)(2w + 3l\sin(\rho))\sin(\theta_{\mathrm{ns}}) \end{pmatrix}^T .
$$

Finally, the yaw DOF terms in $M_{5\mathrm{D}}$ are given by

$$
\begin{aligned}
m_{\psi}(\varphi,\theta) \;=\; & \frac{1}{8}(\cos(\theta_{\mathrm{s}})^2\cos(\varphi)^2(l^2(m+4M_{\mathrm{h}})+2M_{\mathrm{h}}w^2 \\
& +l(-l(m+4M_{\mathrm{h}})\cos(2\rho)+8M_{\mathrm{h}}w\sin(\rho))) \\
& +2m\cos(\theta_{\mathrm{ns}})^2(2w+3l\sin(\rho))(\cos(\varphi)^2(2w+3l\sin(\rho)) \\
& +2l\cos(\rho)\cos(\theta_{\mathrm{s}})\sin(2\varphi))+2(M_{\mathrm{t}}\cos(\theta_{\mathrm{t}})^2\cos(\varphi)^2(w+2l\sin(\rho))^2 \\
& +\cos(\varphi)^2(m(5l^2+4w^2-4l^2\cos(2\rho)+12lw\sin(\rho))\sin(\theta_{\mathrm{ns}})^2 \\
& -4l^2m\cos(\rho)^2\sin(\theta_{\mathrm{ns}})\sin(\theta_{\mathrm{s}})+(l^2(3m+4M_{\mathrm{h}}+2M_{\mathrm{t}}) \\
& +M_{\mathrm{h}}w^2+2l(l(m+M_{\mathrm{t}})\cos(2\rho)+2M_{\mathrm{h}}w\sin(\rho)))\sin(\theta_{\mathrm{s}})^2 \\
& +8l_{\mathrm{t}}lM_{\mathrm{t}}\cos(\rho)\sin(\theta_{\mathrm{s}})\sin(\theta_{\mathrm{t}})+M_{\mathrm{t}}(4l_{\mathrm{t}}^2+w^2 \\
& +4l\sin(\rho)(w+l\sin(\rho)))\sin(\theta_{\mathrm{t}})^2)+2(2l_{\mathrm{t}}^2M_{\mathrm{t}} \\
& +l\cos(\rho)(l\cos(\rho)(3m+2(M_{\mathrm{h}}+M_{\mathrm{t}}) \\
& -2m\sin(\theta_{\mathrm{ns}})\sin(\theta_{\mathrm{s}}))+4l_{\mathrm{t}}M_{\mathrm{t}}\sin(\theta_{\mathrm{s}})\sin(\theta_{\mathrm{t}})))\sin(\varphi)^2 \\
& +2l_{\mathrm{t}}M_{\mathrm{t}}\cos(\theta_{\mathrm{t}})(w+2l\sin(\rho))\sin(2\varphi)) \\
& -2lm\cos(\rho)\cos(\theta_{\mathrm{ns}})(4l\cos(\rho)\cos(\theta_{\mathrm{s}})\sin(\varphi)^2+(2w+3l\sin(\rho))\sin(2\varphi)) \\
& +l\cos(\theta_{\mathrm{s}})(l(4(m+M_{\mathrm{h}}+M_{\mathrm{t}})-3m\cos(2\theta_{\mathrm{ns}}))\sin(2\rho)\sin(2\varphi) \\
& +4\cos(\rho)(4l_{\mathrm{t}}M_{\mathrm{t}}\cos(\theta_{\mathrm{t}})\sin(\varphi)^2 \\
& +w(m+M_{\mathrm{h}}+M_{\mathrm{t}}-m\cos(2\theta_{\mathrm{ns}}))\sin(2\varphi)))).
\end{aligned}
$$

$$
\begin{aligned}
M_{\psi\varphi\theta}(\varphi,\theta) &= \left(\begin{array}{cccc} m_{\psi,\varphi}(\varphi,\theta) & m_{\psi,\theta_{\mathrm{s}}}(\varphi,\theta) & m_{\psi,\theta_{\mathrm{t}}}(\varphi,\theta) & m_{\psi,\theta_{\mathrm{ns}}}(\varphi,\theta) \end{array} \right), \\
m_{\psi,\varphi}(\varphi,\theta) &= \frac{1}{8}(-l^2\cos(\rho)^2\cos(\varphi)(m\sin(2\theta_{\mathrm{ns}}) + (5m + 4(M_{\mathrm{h}} + M_{\mathrm{t}}))\sin(2\theta_{\mathrm{s}}) \\
&\quad -4m\sin(\theta_{\mathrm{ns}} + \theta_{\mathrm{s}})) - 4l_{\mathrm{t}}^2 M_{\mathrm{t}}\cos(\varphi)\sin(2\theta_{\mathrm{t}}) + (7l^2 m\sin(2\rho)\sin(\theta_{\mathrm{s}}) \\
&\quad +4l_{\mathrm{t}}M_{\mathrm{t}}(w + 2l\sin(\rho))\sin(\theta_{\mathrm{t}}))\sin(\varphi) \\
&\quad +2l\cos(\rho)(-4l_{\mathrm{t}}M_{\mathrm{t}}\cos(\theta_{\mathrm{t}})\cos(\varphi)\sin(\theta_{\mathrm{s}}) - 4l_{\mathrm{t}}M_{\mathrm{t}}\cos(\theta_{\mathrm{s}})\cos(\varphi)\sin(\theta_{\mathrm{t}}) \\
&\quad +(-m(2w + 3l\sin(\rho))\sin(\theta_{\mathrm{ns}}) + 2((2m + M_{\mathrm{h}} + M_{\mathrm{t}})w \\
&\quad +2l(M_{\mathrm{h}} + M_{\mathrm{t}})\sin(\rho))\sin(\theta_{\mathrm{s}}))\sin(\varphi))), \\
m_{\psi,\theta_{\mathrm{s}}}(\varphi,\theta) &= \frac{1}{8}l(7lm\cos(\theta_{\mathrm{s}})\cos(\varphi)\sin(2\rho) \\
&\quad +2l\cos(\rho)^2(5m + 4(M_{\mathrm{h}} + M_{\mathrm{t}}) - 2m\cos(\theta_{\mathrm{ns}} - \theta_{\mathrm{s}}))\sin(\varphi) \\
&\quad +4\cos(\rho)(\cos(\theta_{\mathrm{s}})\cos(\varphi)((2m + M_{\mathrm{h}} + M_{\mathrm{t}})w + 2l(M_{\mathrm{h}} + M_{\mathrm{t}})\sin(\rho)) \\
&\quad +2l_{\mathrm{t}}M_{\mathrm{t}}\cos(\theta_{\mathrm{s}} - \theta_{\mathrm{t}})\sin(\varphi))), \\
m_{\psi,\theta_{\mathrm{t}}}(\varphi,\theta) &= \frac{1}{2}l_{\mathrm{t}}M_{\mathrm{t}}(\cos(\theta_{\mathrm{t}})\cos(\varphi)(w + 2l\sin(\rho)) \\
&\quad +2(l_{\mathrm{t}} + l\cos(\rho)\cos(\theta_{\mathrm{s}} - \theta_{\mathrm{t}}))\sin(\varphi)), \\
m_{\psi,\theta_{\mathrm{ns}}}(\varphi,\theta) &= -\frac{1}{4}lm\cos(\rho)(\cos(\theta_{\mathrm{ns}})\cos(\varphi)(2w + 3l\sin(\rho)) \\
&\quad +l\cos(\rho)(-1 + 2\cos(\theta_{\mathrm{ns}} - \theta_{\mathrm{s}}))\sin(\varphi)).
\end{aligned}
$$

REFERENCES

[1] W. R. Leonard and M. L. Robertson, "Energetic efficiency of human bipedality," *American Journal of Physical Anthropology*, vol. 97, pp. 335–338, 1995.

[2] M. D. Sockol, D. A. Raichlen, and H. Pontzer, "Chimpanzee locomotor energetics and the origin of human bipedalism," *Proceedings of the National Academy of Sciences*, vol. 104, no. 30, pp. 12 265–12 269, 2007.

[3] T. McGeer, "Passive dynamic walking," *International Journal of Robotics Research*, vol. 9, no. 2, pp. 62–82, 1990.

[4] A. Goswami, B. Thuilot, and B. Espiau, "Compass-like biped robot part I: Stability and bifurcation of passive gaits," Institut National de Recherche en Informatique et en Automatique (INRIA), Grenoble, France, Tech. Rep. 2996, 1996.

[5] E. R. Westervelt, J. W. Grizzle, and D. E. Koditschek, "Hybrid zero dynamics of planar biped walkers," *IEEE Transactions on Automatic Control*, vol. 48, no. 1, pp. 42–56, 2003.

[6] E. R. Westervelt, J. W. Grizzle, C. Chevallereau, J. H. Choi, and B. Morris, *Feedback Control of Dynamic Bipedal Robot Locomotion*. New York, NY: CRC Press, 2007.

[7] Wikipedia, "Sagittal plane," 2006. [Online]. Available: http://en.wikipedia.org/wiki/Sagittal_plane.

[8] H. K. Khalil, *Nonlinear Systems*, 3rd ed. Upper Saddle River, NJ: Prentice Hall, 2002.

[9] L. B. Freidovich, U. Mettin, A. S. Shiriaev, and M. W. Spong, "A passive 2-DOF walker: Hunting for gaits using virtual holonomic constraints," *IEEE Transactions on Robotics*, vol. 25, no. 5, pp. 1202–1208, 2009.

[10] K. Kaneko, F. Kanehiro, S. Kajita, H. Hirukawa, T. Kawasaki, M. Hirata, K. Akachi, and T. Isozumi, "Humanoid robot HRP-2," in *IEEE International Conference on Robotics and Automation*, New Orleans, LA, 2004, pp. 1083–1090.

[11] Honda Worldwide, "Asimo walking technology," 2009. [Online]. Available: http://world.honda.com/ASIMO/technology/walking.html.

[12] M. Vukobratovic and B. Borovac, "Zero-moment point - thirty years of its life," *International Journal on Humanoid Robotics*, vol. 1, no. 1, pp. 157–174, 2004.

[13] A. D. Kuo, "Choosing your steps carefully: Walking and running robots," *IEEE Robotics and Automation Magazine*, vol. 14, no. 2, pp. 18–29, 2007.

[14] D. Hobbelen and M. Wisse, "Limit cycle walking," in *Humanoid Robots: Human-Like Machines*, M. Hackel, Ed. Vienna, Austria: I-TECH, 2007, pp. 277–294.

[15] S. H. Collins and A. Ruina, "A bipedal walking robot with efficient and human-like gait," in *IEEE International Conference on Robotics and Automation*, Barcelona, Spain, 2005, pp. 1983–1988.

[16] K. Steudel, "Limb morphology, bipedal gait, and the energetics of hominid locomotion," *American Journal of Physical Anthropology*, vol. 99, pp. 345–355, 1996.

[17] E. Yoshida, C. Esteves, I. Belousov, J.-P. Laumond, T. Sakaguchi, and K. Yokoi, "Planning 3-D collision-free dynamic robotic motion through iterative reshaping," *IEEE Transactions on Robotics*, vol. 24, no. 5, pp. 1186–1198, 2008.

[18] O. Brock and O. Khatib, "Elastic strips: A framework for motion generation in human environments," *International Journal of Robotics Research*, vol. 21, no. 12, pp. 1031–1052, 2002.

[19] J. J. Kuffner Jr., S. Kagami, K. Nishiwaki, M. Inaba, and H. Inoue, "Dynamically-stable motion planning for humanoid robots," *Autonomous Robots*, vol. 1, no. 12, pp. 105–118, 2002.

[20] J. J. Kuffner Jr., K. Nishiwaki, S. Kagami, M. Inaba, and H. Inoue, "Motion planning for humanoid robots," in *Robotics Research*. New York, NY: Springer, 2005, pp. 365–374.

[21] K. Hauser, T. Bretl, J.-C. Latombe, K. Harada, and B. Wilcox, "Motion planning for legged robots on varied terrain," *International Journal of Robotics Research*, vol. 27, no. 11-12, pp. 1325–1349, 2008.

[22] P. Michel, J. Chestnutt, S. Kagami, K. Nishiwaki, J. J. Kuffner Jr., and T. Kanade, "GPU-accelerated real-time 3D tracking for humanoid locomotion and stair climbing," in *IEEE International Conference on Intelligent Robots and Systems*, San Diego, CA, 2007, pp. 463–469.

[23] M. W. Spong, "Passivity based control of the compass gait biped," in *IFAC World Congress*, Beijing, China, 1999.

[24] M. W. Spong and F. Bullo, "Controlled symmetries and passive walking," *IEEE Transactions on Automatic Control*, vol. 50, no. 7, pp. 1025–1031, 2005.

[25] B. Morris and J. W. Grizzle, "A restricted Poincaré map for determining exponentially stable periodic orbits in systems with impulse effects: Application to bipedal robots," in *IEEE Conference on Decision and Control*, Seville, Spain, 2005, pp. 4199–4206.

[26] M. Scheint, M. Sobotka, and M. Buss, "Virtual holonomic constraint approach for planar bipedal walking robots extended to double support," in *IEEE Conference on Decision and Control*, Shanghai, China, 2009, pp. 8180–8185.

[27] C. Chevallereau, G. Abba, Y. Aoustin, F. Plestan, E. R. Westervelt, C. Canudas-de-Wit, and J. W. Grizzle, "Rabbit: A testbed for advanced control theory," *IEEE Control Systems Magazine*, vol. 23, no. 5, pp. 57–79, 2003.

[28] K. Sreenath, H. W. Park, I. Poulakakis, and J. W. Grizzle, "A compliant hybrid zero dynamics controller for stable, efficient and fast bipedal walking on MABEL," *International Journal of Robotics Research*, 2010, submitted for publication.

[29] K. Byl and R. Tedrake, "Metastable walking machines," *International Journal of Robotics Research*, vol. 28, no. 8, pp. 1040–1064, 2009.

[30] A. D. Kuo, "Stabilization of lateral motion in passive dynamic walking," *International Journal of Robotics Research*, vol. 18, no. 9, pp. 917–930, 1999.

[31] S. H. Collins, M. Wisse, and A. Ruina, "A 3-D passive dynamic walking robot with two legs and knees," *International Journal of Robotics Research*, vol. 20, pp. 607–615, 2001.

[32] R. Tedrake, T. W. Zhang, and H. S. Seung, "Stochastic policy gradient reinforcement learning on a simple 3D biped," in *IEEE International Conference on Intelligent Robots and Systems*, vol. 3, Sendai, Japan, 2004, pp. 2849–2854.

[33] T. Fukuda, M. Doi, Y. Hasegawa, and H. Kajima, "Multi-locomotion control of biped locomotion and brachiation robot," in *Fast Motions in Biomechanics and Robotics*, ser. Lecture Notes in Control and Information Sciences. Heidelberg, Allemagne, Germany: Springer, 2006, pp. 121–145.

[34] C. Chevallereau, J. W. Grizzle, and C. Shih, "Asymptotically stable walking of a five-link underactuated 3D bipedal robot," *IEEE Transactions on Robotics*, vol. 25, no. 1, pp. 37–50, 2008.

[35] C. Shih, J. W. Grizzle, and C. Chevallereau, "From stable walking to steering of a 3D bipedal robot with passive point feet," *Robotica*, 2010, submitted for publication.

[36] M. W. Spong, "The passivity paradigm in bipedal locomotion," in *International Conference on Climbing and Walking Robots*, Madrid, Spain, 2004.

[37] M. W. Spong, J. K. Holm, and D. Lee, "Passivity-based control of bipedal locomotion," *IEEE Robotics and Automation Magazine*, vol. 12, no. 2, pp. 30–40, 2007.

[38] J. K. Holm, D. Lee, and M. W. Spong, "Time-scaling trajectories of passive-dynamic bipedal robots," in *IEEE International Conference on Robotics and Automation*, Roma, Italy, 2007, pp. 3603–3608.

[39] Y. Hu, G. Yan, and Z. Lin, "Time-scaling control and passive walking of bipeds with underactuation degree one," in *IEEE Conference on Decision and Control*, Atlanta, GA, 2010.

[40] J. W. Grizzle, C. H. Moog, and C. Chevallereau, "Nonlinear control of mechanical systems with an unactuated cyclic variable," *IEEE Transactions on Automatic Control*, vol. 50, no. 5, pp. 559–576, 2005.

[41] S. Ramamoorthy and B. Kuipers, "Trajectory generation for dynamic bipedal walking through qualitative model based manifold learning," in *IEEE International Conference on Robotics and Automation*, Pasadena, CA, 2008, pp. 359–366.

[42] I. R. Manchester, U. Mettin, F. Iida, and R. Tedrake, "Stable dynamic walking over rough terrain: Theory and experiment," in *14th International Symposium on Robotics Research*, Lucerne, Switzerland, 2009.

[43] R. D. Gregg, T. W. Bretl, and M. W. Spong, "Asymptotically stable gait primitives for planning dynamic bipedal locomotion in three dimensions," in *IEEE International Conference on Robotics and Automation*, Anchorage, AK, 2010, pp. 1695–1702.

[44] A. D. Ames, R. D. Gregg, E. D. B. Wendel, and S. Sastry, "On the geometric reduction of controlled three-dimensional bipedal robotic walkers," in *Lagrangian and Hamiltonian Methods for Nonlinear Control*, ser. Lecture Notes in Control and Information Sciences, vol. 366. Nagoya, Japan: Springer, 2007, pp. 183–196.

[45] A. D. Ames and R. D. Gregg, "Stably extending two-dimensional bipedal walking to three dimensions," in *American Control Conference*, New York, NY, 2007, pp. 2848–2854.

[46] A. D. Ames, R. D. Gregg, and M. W. Spong, "A geometric approach to three-dimensional hipped bipedal robotic walking," in *IEEE Conference on Decision and Control*, New Orleans, LA, 2007, pp. 5123–5130.

[47] M. Krstic, I. Kanellakopoulos, and P. V. Kokotovic, *Nonlinear and Adaptive Control Design*. New York, NY: John Wiley and Sons, Inc., 1995.

[48] R. D. Gregg and M. W. Spong, "Reduction-based control with application to three-dimensional bipedal walking robots," in *American Control Conference*, Seattle, WA, 2008, pp. 880–887.

[49] R. D. Gregg and M. W. Spong, "Reduction-based control of three-dimensional bipedal walking robots," *International Journal of Robotics Research*, vol. 26, no. 6, pp. 680–702, 2010.

[50] R. D. Gregg and M. W. Spong, "Reduction-based control of branched chains: Application to three-dimensional bipedal torso robots," in *IEEE Conference on Decision and Control*, Shanghai, China, 2009, pp. 8166–8173.

[51] R. D. Gregg and M. W. Spong, "Bringing the compass-gait bipedal walker to three dimensions," in *IEEE International Conference on Intelligent Robots and Systems*, St. Louis, MO, 2009, pp. 4469–4474.

[52] R. Burridge, A. Rizzi, and D. Koditschek, "Sequential composition of dynamically dexterous robot behaviors," *International Journal of Robotics Research*, vol. 18, no. 6, pp. 534–555, 1999.

[53] R. Ortega, A. Loria, P. J. Nicklasson, and H. Sira-Ramirez, *Passivity-Based Control of Euler-Lagrange Systems: Mechanical, Electrical, and Electromechanical Applications*. New York, NY: Springer-Verlag, 1998.

[54] R. Sepulchre, M. Janković, and P. V. Kokotović, *Constructive Nonlinear Control*. New York, NY: Springer-Verlag, 1997.

[55] M. W. Spong, S. Hutchinson, and M. Vidyasagar, *Robot Modeling and Control*. Hoboken, NJ: John Wiley and Sons, Inc., 2006.

[56] M. W. Spong and M. Vidyasagar, "Robust linear compensator design for nonlinear robotic control," *IEEE Journal of Robotics and Automation*, vol. 3, no. 4, pp. 345–351, 1987.

[57] R. Ortega and M. W. Spong, "Adaptive motion control of rigid robots: A tutorial," in *IEEE Conference on Decision and Control*, San Antonio, TX, 1988, pp. 1575–1584.

[58] R. Ortega, M. W. Spong, F. Gomez-Estern, and G. Blankenstein, "Stabilization of a class of underactuated mechanical systems via interconnection and damping assignment," *IEEE Transactions on Automatic Control*, vol. 47, no. 8, pp. 1218–1233, 2002.

[59] G. Blankenstein, R. Ortega, and A. J. Van Der Schaft, "The matching conditions of controlled Lagrangians and IDA-passivity based control," *International Journal of Control*, vol. 75, no. 9, pp. 645–665, 2002.

[60] N. Chopra and M. W. Spong, "Passivity-based control of multi-agent systems," in *Advances in Robot Control*. New York, NY: Springer-Verlag, 2007, pp. 107–134.

[61] P. Moylan, "Implications of passivity in a class of nonlinear systems," *IEEE Transactions on Automatic Control*, vol. 19, no. 4, pp. 373–381, 1974.

[62] J. E. Marsden and T. S. Ratiu, *Introduction to Mechanics and Symmetry*, 2nd ed. New York, NY: Springer, 2002.

[63] H. Cendra, J. E. Marsden, and T. S. Ratiu, *Lagrangian Reduction by Stages*, ser. Memoirs of the AMS. Providence, RI: AMS Bookstore, 2001.

[64] J. E. Marsden, J.-P. Ortega, T. S. Ratiu, G. Misiolek, and M. Perlmutter, *Hamiltonian Reduction by Stages*, ser. Lecture Notes in Mathematics. New York, NY: Springer, 2007.

[65] E. Gu, "Configuration manifolds and their applications to robot dynamic modeling and control," *IEEE Transactions on Robotics and Automation*, vol. 16, no. 5, pp. 517–527, 2000.

[66] M. Fliess, J. Levine, P. Martin, and P. Rouchon, "Flatness and defect of non-linear systems: Introductory theory and examples," *International Journal of Control*, vol. 61, no. 6, pp. 1327–1361, 1995.

[67] M. Rathinam, "Differentially flat nonlinear control systems," Ph.D. dissertation, California Institute of Technology, Pasadena, CA, 1997.

[68] F. Lamiraux and J.-P. Laumond, "Flatness and small-time controllability of multibody mobile robots: Application to motion planning," *IEEE Transactions on Automatic Control*, vol. 45, no. 10, pp. 1878–1880, 2000.

[69] R. M. Murray, Z. Li, and S. S. Sastry, *A Mathematical Introduction to Robotic Manipulation*. Boca Raton, FL: CRC Press, 1994.

[70] P. J. Olver, *Applications of Lie Groups to Differential Equations*. New York, NY: Springer-Verlag, 2000.

[71] B. O'Neill, *Elementary Differential Geometry*, 2nd ed. San Diego, CA: Elsevier Academic Press, 2006.

[72] P. G. Mehta, G. Hagen, and A. Banaszuk, "Symmetry and symmetry-breaking for a wave equation with feedback," *SIAM Journal of Applied Dynamical Systems*, vol. 6, no. 3, pp. 549–575, 2007.

[73] N. E. Leonard, "Stabilization of underwater vehicle dynamics with symmetry-breaking potentials," *Systems and Control Letters*, vol. 32, pp. 35–42, 1997.

[74] E. A. Shammas, H. Choset, and A. A. Rizzi, "Geometric motion planning analysis for two classes of underactuated mechanical systems," *International Journal of Robotics Research*, vol. 26, no. 10, pp. 1043–1073, 2007.

[75] E. A. Shammas, H. Choset, and A. A. Rizzi, "Towards a unified approach to motion planning for dynamic underactuated mechanical systems with non-holonomic constraints," *International Journal of Robotics Research*, vol. 26, no. 10, pp. 1075–1124, 2007.

[76] A. M. Bloch, N. E. Leonard, and J. E. Marsden, "Controlled Lagrangians and the stabilization of mechanical systems. I: The first matching theorem," *IEEE Transactions on Automatic Control*, vol. 45, no. 12, pp. 2253–2270, 2000.

[77] D. E. Chang and J. E. Marsden, "Reduction of controlled Lagrangian and Hamiltonian systems with symmetry," *SIAM Journal on Control and Optimization*, vol. 43, no. 1, pp. 277–300, 2005.

[78] A. M. Bloch, D. E. Chang, N. E. Leonard, and J. E. Marsden, "Controlled Lagrangians and the stabilization of mechanical systems. II: Potential shaping," *IEEE Transactions on Automatic Control*, vol. 46, no. 10, pp. 1556–1571, 2001.

[79] R. D. Gregg and M. W. Spong, "Passivity and symmetry-breaking in the controlled geometric reduction of mechanical systems," *IEEE Transactions on Automatic Control*, 2010, submitted for publication.

[80] R. D. Gregg, L. Righetti, J. Buchli, and S. Schaal, "Acceleration-based inverse dynamics for controlled reduction: Sagittal-plane decoupling in biped locomotion," in *IEEE International Conference on Humanoid Robots*, Nashville, TN, 2010.

[81] M. W. Spong, "The swing up control problem for the Acrobot," *IEEE Control Systems Magazine*, vol. 15, no. 1, pp. 49–55, 1995.

[82] M. D. Berkemeier and R. S. Fearing, "Tracking fast inverted trajectories of the underactuated acrobot," *IEEE Transactions on Robotics and Automation*, vol. 15, no. 4, pp. 740–750, 1999.

[83] G. Marmo, E. Saletan, A. Simoni, and B. Vitale, *Dynamical Systems: A Differential Geometric Approach to Symmetry and Reduction.* New York, NY: John Wiley & Sons Inc, 1985.

[84] V. A. Yakubovich and V. M. Starzhinskii, *Linear Differential Equations with Periodic Coefficients.* New York, NY: Wiley, 1975.

[85] S. P. Boyd and L. Vandenberghe, *Convex Optimization.* New York, NY: Cambridge University Press, 2004.

[86] M. W. Spong and F. Bullo, "Controlled symmetries and passive walking," in *IFAC World Congress*, Barcelona, Spain, 2002.

[87] J. Wittenburg, *Dynamics of Multibody Systems*, 2nd ed. New York, NY: Springer, 2007.

[88] D. Agahi and K. Kreutz-Delgado, "A star-topology dynamic model for multipedal locomotion," in *IEEE Conference on Decision and Control*, vol. 5, San Diego, CA, 1997, pp. 4868–4873.

[89] S. S. Sastry, *Nonlinear Systems: Analysis, Stability and Control*. New York, NY: Springer-Verlag, 1999.

[90] R. Sinnet and A. D. Ames, "3D bipedal walking with knees and feet: A hybrid geometric approach," in *IEEE Conference on Decision and Control*, Shanghai, China, 2009, pp. 3208–3213.

[91] J. W. Grizzle, G. Abba, and F. Plestan, "Asymptotically stable walking for biped robots: Analysis via systems with impulse effects," *IEEE Transactions on Automatic Control*, vol. 46, no. 1, pp. 51–64, 2001.

[92] G. Bhatia, "Passivity based control of biped robots," M.S. thesis, University of Illinois at Urbana-Champaign, Urbana, IL, December 2002.

[93] R. D. Gregg, "Subrobots: Reduction-based control with application to three-dimensional bipedal walking robots," M.S. thesis, University of Illinois at Urbana-Champaign, Urbana, IL, December 2007.

[94] Y. Hurmuzlu and D. Marghitu, "Rigid body collisions of planar kinematic chains with multiple contact points," *International Journal of Robotics Research*, vol. 13, no. 1, pp. 82–92, 1994.

[95] G. Courtine and M. Schieppati, "Human walking along a curved path. I. Body trajectory, segment orientation and the effect of vision," *European Journal of Neuroscience*, vol. 18, no. 1, pp. 177–190, 2003.

[96] G. Courtine and M. Schieppati, "Human walking along a curved path. II. Gait features and EMG patterns," *European Journal of Neuroscience*, vol. 18, no. 1, pp. 191–205, 2003.

[97] S. Collins, A. Ruina, R. Tedrake, and M. Wisse, "Efficient bipedal robots based on passive-dynamic walkers," *Science*, vol. 307, no. 5712, pp. 1082–1085, 2005.

[98] A. D. Kuo, J. M. Donelan, and A. Ruina, "Energetic consequences of walking like an inverted pendulum: Step-to-step transitions," *Exercise and Sport Sciences Reviews*, vol. 33, no. 2, pp. 88–97, 2005.

[99] R. D. Gregg, A. K. Tilton, S. Candido, T. Bretl, and M. W. Spong, "Control and planning of 3D bipedal dynamic walking with asymptotically stable gait primitives," *IEEE Transactions on Robotics*, 2010, in preparation.

[100] L. E. Dubins, "On curves of minimal length with a constraint on average curvature, and with prescribed initial and terminal positions and tangents," *American Journal of Mathematics*, vol. 79, no. 3, pp. 497–516, 1957.

[101] M. J. D. Taylor, P. Dabnichki, and S. Strike, "A 3-D biomechanical comparison between turning strategies during the stance phase of walking," *Human Movement Science*, vol. 24, no. 4, pp. 558–573, 2005.

[102] D. Liberzon, *Switching in Systems and Control*. New York, NY: Springer, 2003.

[103] T. Alpcan and T. Basar, "A stability result for switched systems with multiple equilibria," *Dynamics of Continuous, Discrete and Impulsive Systems*, 2009, submitted for publication.

[104] I. R. Manchester, "Tranverse dynamics and regions of stability for nonlinear hybrid limit cycles," presented at Dynamic Walking, Cambridge, MA, 2010.

[105] U. Topcu, A. Packard, and P. Seiler, "Local stability analysis using simulations and sum-of-squares programming," *Automatica*, vol. 44, no. 10, pp. 2669–2675, 2008.

[106] E. Frazzoli, M. A. Dahleh, and E. Feron, "Maneuver-based motion planning for nonlinear systems with symmetries," *IEEE Transactions on Robotics*, vol. 21, no. 6, pp. 1077–1091, 2005.

[107] D. C. Conner, H. Kress-Gazit, H. Choset, A. A. Rizzi, and G. J. Pappas, "Valet parking without a valet," in *IEEE International Conference on Intelligent Robots and Systems*, San Diego, CA, 2007, pp. 572–577.

[108] S. M. LaValle and J. J. Kuffner Jr., "Randomized kinodynamic planning," *International Journal of Robotics Research*, vol. 20, no. 5, pp. 378–400, 2001.

[109] D. Hsu, R. Kindel, J.-C. Latombe, and S. Rock, "Kinodynamic motion planning amidst moving obstacles," *International Journal of Robotics Research*, vol. 21, no. 3, pp. 233–255, 2002.

[110] E. Frazzoli, M. A. Dahleh, and E. Feron, "Real-time motion planning for agile autonomous vehicles," *AIAA Journal of Guidance, Control, and Dynamics*, vol. 25, no. 1, pp. 116–129, 2002.

[111] S. M. LaValle, *Planning Algorithms*. New York, NY: Cambridge University Press, 2006.

[112] H. M. Choset, K. M. Lynch, S. Hutchinson, G. Kantor, W. Burgard, L. E. Kavraki, and S. Thrun, *Principles of Robot Motion*. Cambridge, MA: MIT Press, 2005.

[113] S. Candido, Y. T. Kim, and S. Hutchinson, "An improved hierarchical motion planner for humanoid robots," in *IEEE International Conference on Humanoid Robots*, Daejeon, Korea, 2008, pp. 654–661.

[114] A. Degani, H. Choset, and M. T. Mason, "DSAC – dynamic, single actuated climber: Local stability and bifurcations," in *IEEE International Conference on Robotics and Automation*, Anchorage, AK, 2010, pp. 2803–2809.

[115] J. Shill, B. Miller, J. Schmitt, and J. E. Clark, "Design of a dynamically stable horizontal plane runner," in *IEEE International Conference on Robotics and Automation*, Anchorage, AK, 2010, pp. 4749–4754.

[116] R. Tedrake, I. R. Manchester, M. M. Tobenkin, and J. W. Roberts, "LQR-Trees: Feedback motion planning via sums-of-squares verification," *International Journal of Robotics Research*, vol. 29, no. 8, pp. 1038–1052, 2010.

[117] G. Cheng, S.-H. Hyon, A. Ude, J. Morimoto, J. Hale, J. Hart, J. Nakanishi, D. Bentivegna, J. Hodgins, C. Atkeson, M. Mistry, S. Schaal, and M. Kawato, "CB: Exploring neuroscience with a humanoid research platform," in *IEEE International Conference on Robotics and Automation*, Pasadena, CA, 2008, pp. 1772–1773.

[118] D. A. Winter, *Biomechanics and Motor Control of Human Movement*. New York, NY: Wiley, 2009.

[119] A. E. Patla, S. D. Prentice, C. Robinson, and J. Neufeld, "Visual control of locomotion: Strategies for changing direction and for going over obstacles," *Journal of Experimental Psychology: Human Perception and Performance*, vol. 17, no. 3, pp. 603–634, 1991.

[120] P. C. Kao, C. L. Lewis, and D. P. Ferris, "Joint kinetic response during unexpectedly reduced plantar flexor torque provided by a robotic ankle exoskeleton during walking," *Journal of Biomechanics*, vol. 43, no. 7, pp. 1401–1407, 2010.

[121] T. G. Hornby, D. Campbell, J. H. Kahn, T. Demott, J. L. Moore, and H. R. Roth, "Enhanced gait-related improvements after therapist-versus robotic-assisted locomotor training in subjects with chronic stroke: A randomized controlled study," *Stroke*, vol. 39, no. 6, pp. 1786–1792, 2008.

[122] J. Hidler, D. Nichols, M. Pelliccio, K. Brady, D. D. Campbell, J. H. Kahn, and T. G. Hornby, "Multicenter randomized clinical trial evaluating the effectiveness of the lokomat in subacute stroke," *Neurorehabilitation and Neural Repair*, vol. 23, no. 1, p. 5, 2009.

[123] L. Marchal-Crespo and D. Reinkensmeyer, "Review of control strategies for robotic movement training after neurologic injury," *Journal of NeuroEngineering and Rehabilitation*, vol. 6, no. 1, p. 20, 2009.

[124] A. Minetti, C. Moia, G. Roi, D. Susta, and G. Ferretti, "Energy cost of walking and running at extreme uphill and downhill slopes," *Journal of Applied Physiology*, vol. 93, no. 3, pp. 1039–1046, 2002.

[125] S. Hesse, C. Werner, T. Paul, A. Bardeleben, and J. Chaler, "Influence of walking speed on lower limb muscle activity and energy consumption during treadmill walking of hemiparetic patients," *Archive of Physical Medicine and Rehabilitation*, vol. 82, no. 11, pp. 1547–1550, 2001.

[126] R. D. Gregg, T. W. Bretl, and M. W. Spong, "A control theoretic approach to robot-assisted locomotor therapy," in *IEEE Conference on Decision and Control*, Atlanta, GA, 2010.

[127] R. Chin, E. T. Hsiao-Wecksler, E. Loth, G. Kogler, S. D. Manwaring, S. N. Tyson, K. A. Shorter, and J. N. Gilmer, "A pneumatic power harvesting ankle-foot orthosis to prevent foot-drop," *Journal of NeuroEngineering and Rehabilitation*, vol. 6, no. 1, p. 19, 2009.

[128] H. Kazerooni, "Exoskeletons for human performance augmentation," in *Handbook of Robotics*. New York, NY: Springer, 2008, pp. 773–793.

[129] A. S. Shiriaev, L. B. Freidovich, and I. R. Manchester, "Can we make a robot ballerina perform a pirouette? Orbital stabilization of periodic motions of underactuated mechanical systems," *Annual Reviews in Control*, vol. 32, no. 2, pp. 200–211, 2008.

[130] C. A. Felippa, *Introduction to Finite Element Methods*. Boulder, CO: University of Colorado at Boulder, 2004, ch. Appendix D: Matrix Calculus.

[131] A. D. Ames, "A categorical theory of hybrid systems," Ph.D. dissertation, University of California, Berkeley, Berkeley, CA, 2006.

AUTHOR'S BIOGRAPHY

Robert D. Gregg IV was born in Long Beach, California, in 1984. He received the B.S. in Electrical Engineering and Computer Sciences from the University of California, Berkeley, in May 2006 and the M.S. in Electrical and Computer Engineering from the University of Illinois at Urbana-Champaign in December 2007. He is currently a Ph.D. candidate in the Department of Electrical and Computer Engineering and the Coordinated Science Laboratory at the University of Illinois, under the direction of Mark W. Spong. His main research is in the geometric control of complex robotic systems, particularly dynamic bipedal walking in three-dimensional space. Robert was awarded the 2010 Engineering into Medicine Postdoctoral Fellowship from the Northwestern University Clinical and Translational Sciences Institute. He also received the 2009 O. Hugo Schuck Award from the IFAC American Automatic Control Council, and the Best Student Paper Award of the 2008 American Control Conference in Seattle, WA. Robert is a member of the IEEE Control Systems Society and Robotics and Automation Society, and he was co-chair of the 2010 Symposium on Control and Modeling of Biomedical Systems.